Title

Invoking Halogen Bonding: An Investigation of Halogenation Reactions Promoted By the Halogen Bonding Phenomenon Between Commercially Available Halogenating Reagents And Lewis Basic Additives

Permalink

https://escholarship.org/uc/item/4nm1116r

Author

Baker, Sarah Irene

Publication Date

2023

Peer reviewed|Thesis/dissertation

UNIVERSITY *of* CALIFORNIA, MERCED

Invoking Halogen Bonding:
An Investigation of Halogenation Reactions Promoted
By the Halogen Bonding Phenomenon Between
Commercially Available Halogenating Reagents
And Lewis Basic Additives

by,

Sarah Irene Baker

A dissertation submitted in partial fulfillment of the
requirements for the degree of Doctor of Philosophy

in

Chemistry and Chemical Biology

Doctoral Committee:

Hrant P. Hratchian, Chair

Ryan D. Baxter, PI

Rebeca Arevalo

Peter de Lijser

The Dissertation of Sarah Irene Baker is approved, and is acceptable in quality and form for publication on microfilm and electronically:

_____

Ryan D. Baxter, PI

_____

Rebeca Arevalo

_____

Peter de Lijser

_____

Hrant P. Hratchian, Chair

University of California, Merced

2023

DEDICATION

To my parents, Macaria Guadalupe and Phillip Norman, for always believing in meand being the little voice in my head to keep going. Thank you for your endless love and support through all of my education.

To my siblings, Joseph E. Baker, Jessica M. Burk, Joshua M. Baker and Phillip N. Beaton III, for always encouraging me to continue my education.

To my nieces and nephews, thank you for your endless love and support. Thank you for being so understanding when I missed special events.

To my husband, Nickalaus R. Bartoli, I could not have done this without you. I love you, like a 45.

To my fur babies, thank you for your endless amount of cuddles and cheering up.

TABLE *of* CONTENT

List *of* ABBREVIATIONS

ACN	acetonitrile
Ag	silver
AgNO$_3$	silver nitrate
BDE	bond dissociation energy
Boc	*tert*-butyloxycarbonyl
ºC	degrees Celsius
DCM	dichloromethane
DMSO	dimethyl sulfoxide
EtOAc	ethyl acetate
GC-MS	gas chromatography mass spectroscopy
H	hour
HAT	hydrogen atom transfer
HMBC	heteronuclear multiple bond correlation
HR-MS	high resolution mass spectroscopy
iPr	isopropyl
IR	infrared spectroscopy
equiv	Equivalent
Me	methyl
Mins	minutes
MeCN	acetonitrile

NBSa	*N*-bromosaccharin
NBS	*N*-bromosuccinimide
NMR	nuclear magnetic resonance
OMe	methoxy
PET	positron emission tomography
Ph	phenyl
pyr	pyridine
rt	room temperature
TEMPO	2, 2, 6, 6-Tetramethyl-1-piperidinyloxy
TBDPS	tert-Butyldiphenylsilyl
THF	tetrahydrofuran
TLC	thin layer chromatography
4-CF$_3$	4-(trifluoromethyl)

List *of* Figures

List *of* Schemes

List *of* Tables

ACKNOWLEDGEMENTS

CURRICULUM VITA

Education

Aug. 2017 – May 2023   M.S. in Chemistry
Ph.D. in Organic Chemistry
University of California, Merced

Aug 2013 – July 2017   B.S. in Biochemistry
California State University, Fullerton

Publication(s)

1. **Baker, S. I.;** Yaghoubi, M.; Bidwell, S. L.; Pierce, S. L.; Hratchian, H. P.; Baxter, R. D. *J. Org. Chem.* **2022**, 87, 8492-8502. "Enhanced Reactivity for Aromatic Bromination via Halogen Bonding with Lactic Acid Derivatives"

2. Hua, A. M.; Bidwell, S. L.; **Baker, S. I.;** Hratchian, H. P.; Baxter, R. D. *ACS Catal.,* **2019**, 9, 3322-3326. "Experimental and Theoretical Evidence for Nitrogen–Fluorine Halogen Bonding in Silver-Initiated Radical Fluorinations"

ABSTRACT

Halogenation has become of great interest. Recent studies show the biological advantages when pharmaceuticals contain various halogen-carbon bonds. Halogenated compounds are used in metal-catalyzed cross-coupling reactions, pesticides, and natural products. Previously, our lab has reported radical benzylic C-H fluorination using Selectfluor, as a mild oxidant and fluorine source, in the presence of unprotected amino acids and Ag(I). In doing control reactions, we found that N-protected amino acids did not yield any product, suggesting free nitrogen was required. In contrast to the amino acid/Ag(I) method, we found that a carboxylate group was not required as long as a free nitrogen additive, such as pyridine. Herein, we report an effective method for C-H fluorination via halogen-bonding between Selectfluor and monosubstituted pyridine additives. Computational and NMR studies showed that the Lewis basicity of the pyridine additive must be optimum for halogen-bonding but not strong enough to promote unwanted side reactions.

Using this knowledge, we expanded this strategy to include C-H bromination using N-bromosuccinimide. During the initial investigation, we discovered aromatic bromination was favored over benzylic. While optimizing the reaction conditions, we determined lactic acid was an efficient catalyst for aromatic bromination. Several lactic acid derivatives were investigated and found to affect the efficiency of aromatic bromination via halogen-bonding interactions. This method gives access to a relatively less toxic procedure using catalytic mandelic acid under aqueous conditions at room temperature.

1

The last chapter of this dissertation depicts the development of an alternative method for halohydrin formation of alkenes. Several brominating reagents were assessed and the best for this reaction was *N*-bromosaccharin. Through experimental investigations, it was determined that the carbonyl in the substrate was essential for the halohydrin formation to occur. Future work will further explore the reactivity of the carbonyl oxygen.

Chapter 2 is an adapted article of *J. Org. Chem.* **2022**, 87, 8492-8502.

Chapter 1

Benzylic C–H Radical Fluorination promoted by [N–F–N]$^+$ Halogen Bonding

1.1 Introduction

1.1.1 Why fluorinated compounds are important

Only roughly 4000 halogenated products have been isolated from plants and natural products.[1] Halogens, especially fluorine, are used as substituents in medicinal chemistry.[2] Synthetically, fluorine is found in various substances such as pharmaceuticals, pesticides, fragrances, and repellents.[3] The strength of the carbon halogen bond increases with the electron-withdrawing ability of the halogen, making fluorine the strongest among them and most valuable when designing protein inhibitors and drugs.[4] Fluorine has been found to enhance the biological activity of pharmaceuticals, given its relatively small size, the ability to alter pKa, and the ability for greater lipophilicity compared to that of a hydrogen atom.[5] Compounds containing monofluoromethyl groups on aromatics mimic oxygen molecules in nucleotides and various esters, which allows for the blocking of cytochrome P450 to improve target-binding affinity,[6] making fluorine the ideal halogen for the functionalization of pharmaceuticals.

Fluorine is known not only for its medicinal purposes but also for its use in medical procedures, including radioisotope labeling using ^{18}F for Positron Emission Tomography (PET) imaging. PET is commonly used for the early detection and treatment of cancer patients.[7] Fluorine has several short-lived isotopes, making it ideal for PET scans. The

system detects gamma rays emitted after the fluorine isotope has been injected into the body.[8] Although useful, unfortunately, not all types of cancers respond to the injected fluorine isotope, which has led to the development of late-stage functionalization.

1.1.2 Halogen Bonding

Halogen bonding is a noncovalent interaction between an electrophile and a nucleophile.[9] Although halogen bonding was first discovered in 1921 by Robert Milliken, scientists' interests in the subject have grown in the past decade. The halogen bonding interaction is driven by the σ-hole, the positively charged region of a halogen.[10] Recently, the Politizer group revealed that fluorine atoms possess the positively charged σ-hole, and fluorine atoms can form halogen bonding interactions in certain situations.[11] Halogen bonding has become of much interest in biological and medicinal sciences, given it helps promote protein-ligand bonding environments. Halogenated products, especially those containing fluorine, have increased lipophilicity, can alter pKa, and improve stability.
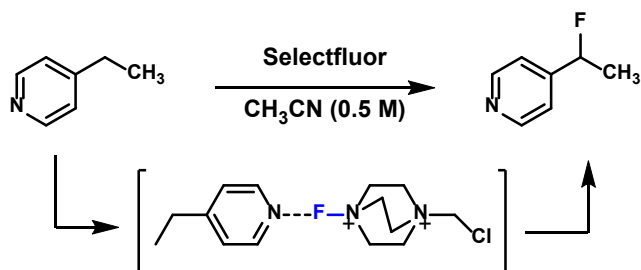
Scheme 1.1. Heterobenzylic radical fluorination

Concurrent to our study of halogen bonding, Van Humbeck and co-workers revealed UV/Vis data suggesting Selectfluor and pyridine interact (Scheme1.1).[12] The data presented shows an increase in absorbance at approximately the same wavelength and a slight broadening when pyridine is in the presence of Selectfluor. Suggesting that the Selectfluor and pyridine are interacting. This was the first Selectfluor–pyridine association report, although it does not fully explain what is occurring. Van Humbeck's findings are consistent with our of $[N–F–N]^+$ halogen bonding between the pyridine additives and Selectfluor.

1.1.3 Previous methods of fluorination

Benzylic fluorination has become of much interest, particularly for the biological properties it contributes to current pharmaceuticals and agrochemicals.[3] Traditional fluorinating methods require highly toxic chemicals, harsh reaction conditions, and expensive catalysts.[13] The search for a less aggressive, less toxic, stable, and easy-to-handle fluorinating reagent led to the development of Selectfluor (1-chloromethyl- 4-fluoro-1,4-diazoniabicyclo[2.2.2]octane bis(tetrafluoroborate)).[14] Increasing stability and handling also has downsides, like a decrease in reactivity. Recently, several groups, including ours, have set out to investigate alternative methodologies for increasing the reactivity of Selectfluor for benzylic fluorination.

Scheme 1.2. Benzylic radical fluorination using Fe(II) catalyst
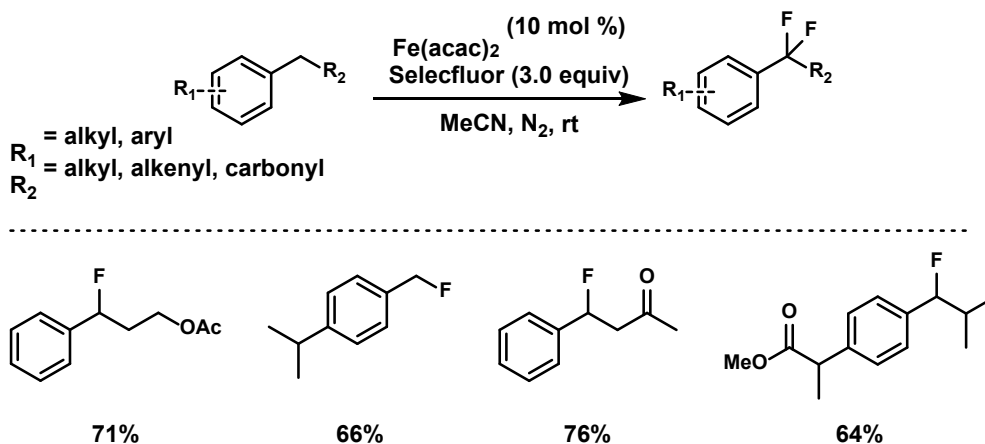
Lectka and co-workers reported a radical benzylic fluorination catalyzed by Fe(II) using Selectfluor as a mild fluorinating reagent[15] (Scheme 1.2), and several significant advances were made. For example, during this study, the Lectka group discovered the possibility of site-specific fluorination. Typically, fluorination of the α-position of ketones dominates in product distribution. This methodology discovered when using Fe(acac)$_2$ as a catalyst, benzylic fluorination (β-position of a ketone) is favored over the α-position. Although practical, this methodology had several limitations. This methodology was unable to fluorinate electron-withdrawing substrates, nitrogen-containing substrates were problematic, and the reaction preferred aromatic fluorination if the substrate contained strong electron-donating groups.

Scheme 1.3. First example of silver-catalyzed fluorination using Selectfluor
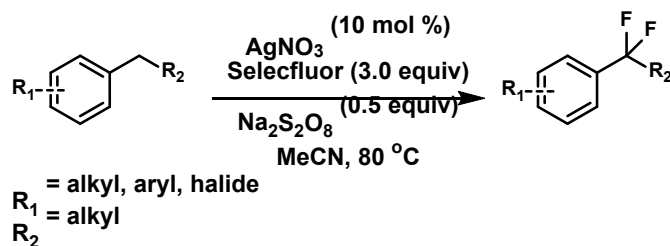
The first example of a silver-catalyzed oxidative activation of C–H bonds using Selectfluor was discovered by Tang and co-workers (Scheme 1.3).[16] The reaction proved sensitive to $Na_2S_2O_8$, where the bisfluorination increased in the presence of this strong oxidizer. This reaction likely proceeded through a single-electron transfer (SET) or a radical-chain mechanism. The reaction proceeds under relatively mild conditions and tolerates various substituents. Since the initial discovery of Selectfluor and its ability to fluorinate using less toxic reaction conditions, several groups, including ours, have set out to utilize its synthetic capabilities.

1.1.4 Amino Acid-Mediated Benzylic fluorination

In a recent study, our lab established a radical C–H fluorination strategy using Selectfluor as the fluorinating source and α-amino acids as stable radical precursors (Scheme 1.4). This methodology utilizes α-aminoalkyl radicals for the initial hydrogen atom abstraction of benzylic sp^3 C–H bonds. During the initial investigation, various N-substituted amino acids were explored.[17]

Scheme 1.4. Benzylic radical fluorination using amino acids as radical precursors

0.2 mmol	2.0 equiv	35 °C
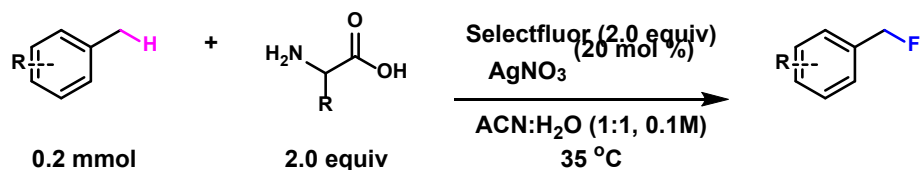
Studies involving ReactIR, electrochemistry, and deuterium labeling ^{1}H-NMR were used to establish the reaction mechanism. Deuterium-labeling experiments using ^{13}C-NMR provided initial evidence for the formation of the methylamine from the glycine additive. *In situ* reactIR experiments showed no significant change in the concentration of Selectfluor with the addition of AgNO₃. Interestingly, the concentration of Selectfluor drastically decreased upon the addition of glycine, suggesting that glycine does play an essential role in the reaction.

Cyclic voltammetry experiments further confirmed glycine lowered the onset oxidation potential of the Ag(I)/Ag(II) catalyst, while the onset oxidation potential change was negligible using N-Boc-glycine. Additionally, the results from the *in situ* reactIR and cyclic voltammetry experiments using *N*-Boc-glycine suggest the nucleophilicity of nitrogen is necessary to promote the ligation of the Ag(I) catalyst from the amino acid complex. The ligation results in the decarboxylation of the amino acid, leading to the formation of the α-aminoalkyl radical.
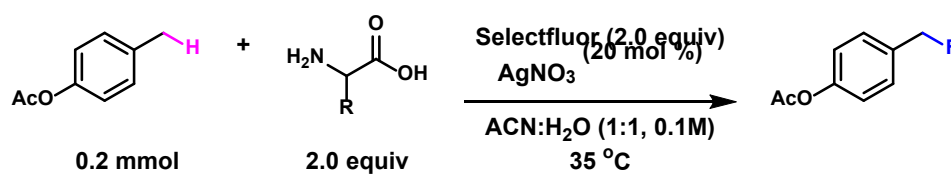
Trial	Deviation from standard conditions	Yield
1	glycine	70%
2	*N*-Boc-glycine	0%
3	*N*-Boc-glycine and 1.0 equiv of pyridine	67%

Table 1.1. Exploration of Lewis Basic Nitrogen

The reaction yielding no fluorinated product when glycine was replaced with the protected amino acid, *N*-Boc-glycine, further supports this (Table 1.1, entry 2). To further explore the Lewis basicity of nitrogen, the same reaction with *N*-Boc-glycine was run but with the addition of pyridine (entry 3). The results of this reaction yielded a fluorinated product, further supporting the theory that the identity of the Lewis basic atom matters.

1.2 Radical Benzylic fluorination via Pyridine–Selectfluor Halogen Bonding

1.2.1 Results and Discussion

1.2.1.1 Discovery of Pyridine additive

As discussed in section 1.1.5, our group had recently expanded upon the current methodology for radical fluorination promoted by unprotected amino acids. From this work, we questioned the Lewis basicity of the nitrogen in our amino acid additive. We began exploring the role of the Lewis basic nitrogen. Initially, we ran a reaction with *N*-Boc-glycine as the additive, and as suspected, the reaction yielded 0% of our desired product (Table 1.2, entry 2). Next, we ran the reaction with the addition of pyridine, which produced high quantities of the desired fluorinated product (entry 1). Before moving forward, we needed to assess what was essential for the reaction to produce the fluorinated product, and to do this, we ran control reactions (Table 1.2). Entries 2-3 yielded 0% of the product, meaning the reaction needs the catalyst and free Lewis basic nitrogen to proceed. Entry 4 was the most interesting, showing the reaction without *N*-Boc-glycine but with

pyridine yielded the desired product, suggesting an alternative reaction mechanism may occur when pyridine is the Lewis basic nitrogen additive. As expected, no fluorinated product was observed when adding the radical trap, TEMPO (entry 4). With these results in hand, we were eager to study the mechanism of our reaction, but first, we set out to establish the best reaction conditions.
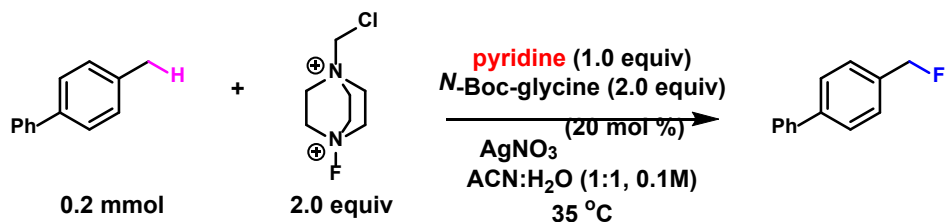
Trial	Deviation from standard conditions	Yield
1	none	70%
2	no pyridine	0%
3	no AgNO$_3$	0%
4	no N-Boc-glycine	51%
5	No N-Boc-glycine, TEMPO (2.0 equiv) added	trace

Table 1.2. Discovery of pyridine-mediated fluorination

1.2.1.2 Cyclic Voltammetry Studies

It was previously determined in our amino acid chemistry that when Ag(I) was in the presence of glycine, the onset oxidation potential drastically decreased. Using this knowledge, we ran cyclic voltammetry studies to see how the electronics of the different mono-substituted pyridine additives affect the oxidation potential of Ag(I). We believed the electronics of the various pyridine additives would interact with the Ag(I) catalyst.

Zangrando and co-workers previously determined that pyridine additives can form Ag(I)–Pyridine complexes. Zangrando also concluded the affinity of pyridine–silver complex in solution is typically governed by the solvent, and the greatest attraction is in the presence of water. [18] Combining our knowledge with Zangrando's findings, we anticipated the onset oxidation potential of Ag(I) to lower, resulting in higher product formation. Reducing the onset oxidation potential would also require less energy for the reaction to be initiated.
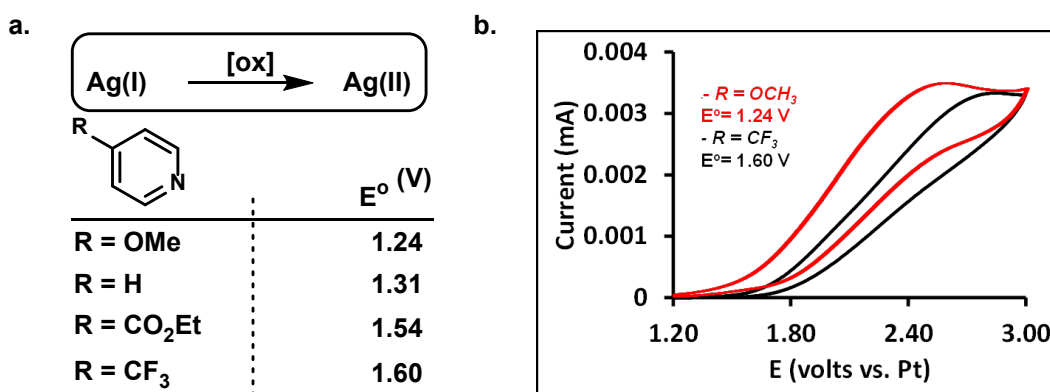
Figure 1.1. The oxidation potential of AgNO$_3$ in the presence of pyridine additives. **(a)** oxidation table of the various pyridine additives **(b)** direct comparison of 4-methoxypyridine and 4-(trifluoromethyl)pyridine.

We suspected the electron-rich pyridines would reduce the onset oxidation potential the most, similar to the amino acid chemistry. As anticipated, the pyridine additives with varying electron-rich substituents did lower the onset oxidation potential (**Figure 1, entries 1 – 2**). We found the electron-withdrawing pyridine additives increased the onset oxidation potential from 1.45 V to higher voltages (**Figure 1.1a**). Based on the CV data generated, we hypothesized 4-methoxypyridine would yield the highest amount of fluorinated product.

1.2.1.3 Optimization of reaction conditions

Before continuing the mechanistic investigation, we needed to establish optimal reaction conditions to promote difluorinated product (Table 1.3). At ambient and elevated temperatures, the reaction yielded lower product conversion (entries 2,3).
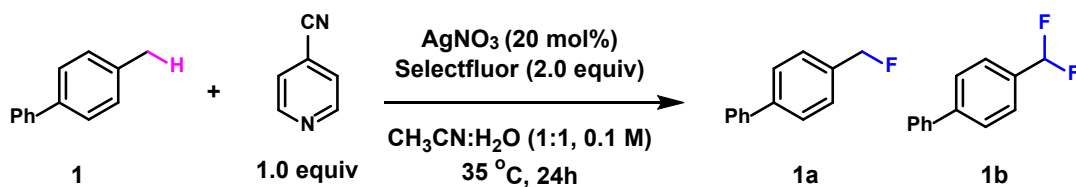
entry	deviation from standard conditions	NMR yield (%)	
		1a	1b
1	none	28	70
2	25 °C	37	49
3	50 °C	9	68

Table 1.3. Optimization – variation in reaction temperature

Pyridine additives with various electronic configurations were examined (Table 1.4). Electron-rich pyridines led to poor product conversion (entries 2 – 3), while electron-withdrawing pyridines afforded modest to excellent product conversions (entries 4-5). Next, the sterically hindered electron-withdrawing pyridine, ethyl 2,6-diisopropylnicotinate, was used. The steric hindrance dominated over the electron-withdrawing aspect resulting in no product (entry 6). Increasing the concentration of the pyridine additive caused the reaction to dwindle (entry 7) while decreasing the concentration produced similar yields to the standard reaction conditions (entry 8).
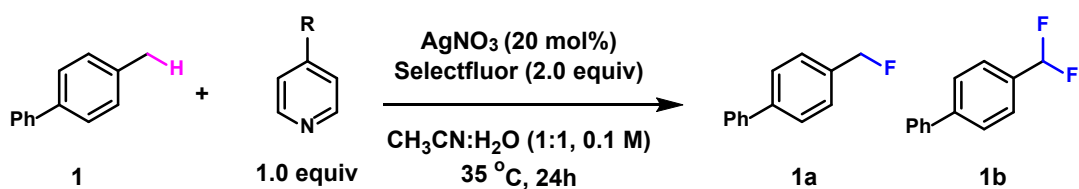
entry	deviation from standard conditions	NMR yield (%)	
1	none	28	70
2	pyridine instead of 4-cyanopyridine	52	trace
3	4-methoxypyridine instead of 4-cyanopyridine	35	0
4	4-(trifluoromethyl)pyridine instead of 4-cyanopyridine	12	85
5	ethyl isonicotinate instead of 4-cyanopyridine	25	49
6	ethyl 2,6-diisopropylnicotinate	0	0
7	2.0 equiv 4-cyanopyridine	23	31
8	0.5 equiv 4-cyanopyridine	7	76

Table 1.4. Optimization – variation in pyridine additive

Changes to the reaction's concentration influenced product distributions (Table 1.5). Diluting caused the reaction to favor the mono-fluorinated product, while increasing the concentration caused the reaction to favor the di-fluorinated product (entries 2 – 3). Acetonitrile was replaced with dichloromethane and acetone; these organic solvents caused the reaction to yield a reduced amount of fluorinated product (entries 4 – 5). AgNO₃ and the 4-cyanopyridine additive were found to be required for the reaction to proceed (entries 6 – 7). After completing the optimization, the best reaction conditions to produce the most bis-fluorinated product was table 1.4 entry 4.
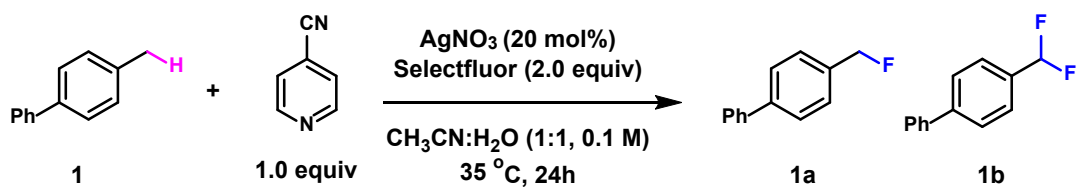
entry	deviation from standard conditions	NMR yield (%)	
1	none	28	70
2	CH$_3$CN:H$_2$O (1:1, 0.05 M)	70	30
3	CH$_3$CN:H$_2$O (1:1, 0.2 M)	15	77
4	CH$_2$Cl$_2$:H$_2$O (1:1)	50	0
5	acetone:H$_2$O (1:1)	54	0
6	no AgNO$_3$	0	0
7	no 4-cyanopyridine	0	0

Table 1.5. Optimization – variation in concentrations

1.2.1.4 Investigation of Pyridine Additives

One of the more significant findings to emerge from the optimization study is entry 4 from Table 1.4. Based on the cyclic voltammetry data, we hypothesized 4-methoxypyridine would yield the highest amount of fluorinated product because it drastically decreased the onset oxidation potential of Ag(I). To our surprise, 4-(trifluoromethyl)pyridine was the best pyridine additive. It was observed that the pyridine additives' electronics determine the reaction's effectiveness (scheme 1.5). These findings were opposite to what we had hypothesized and from what was seen in the amino acid chemistry.

Scheme 1.5. Pyridine-dependent product distribution
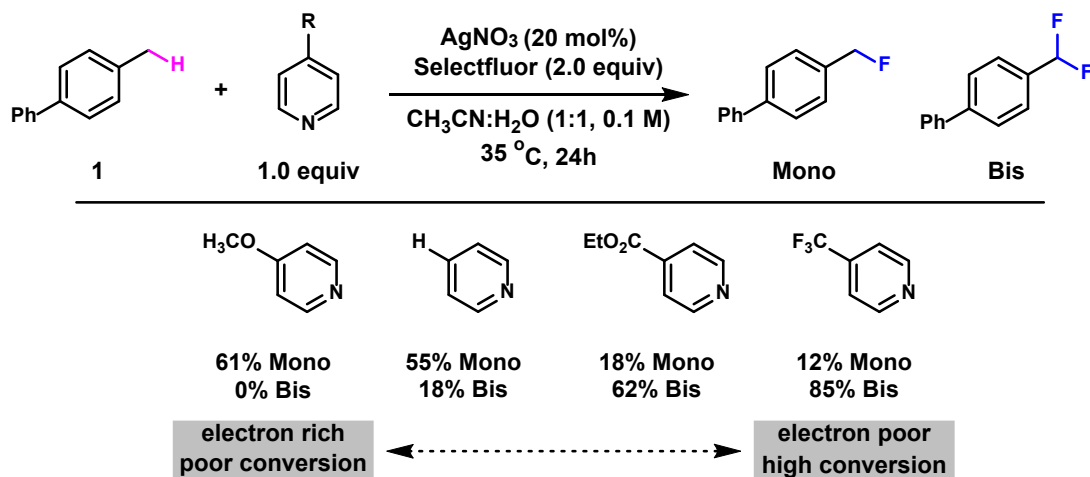
Based on the results illustrated in scheme 1.5 and figure 1.1 (CV), we set out to understand what was occurring in our reaction. Knowing that pyridine's electronics dictate the product distribution, we wondered what the role of our pyridine additive is and if it interacted with the Selectfluor. Using *in situ* reactIR, we hoped to see how and if the additive directly affected Selectfluor. The wavenumber relative to the N–F peak of Selectfluor was determined via a dosing experiment and was concluded to be 1008 cm^{-1}. By monitoring the peak at 1008 cm^{-1}, we could determine the concentration of Selectfluor and monitor it during experiments.

The results of this experiment revealed the order in which the reactants were added is essential for a productive reaction. If the pyridine additive was added before Ag(I), then an unproductive amount of Selectfluor is consumed (Figure 1.2, red). We believe this occurs because the Selectfluor and pyridine additives coordinate together, leaving trace amounts of unbound pyridine additive available for coordination with Ag(I)/Ag(II). This

reasoning would explain why the oxidation potential of Ag(I) remains consistent. It was evident from this data to conclude the pyridine additives played a crucial role in its interaction with Selectfluor. The next step was determining the role and how it varies on the pyridine additive.
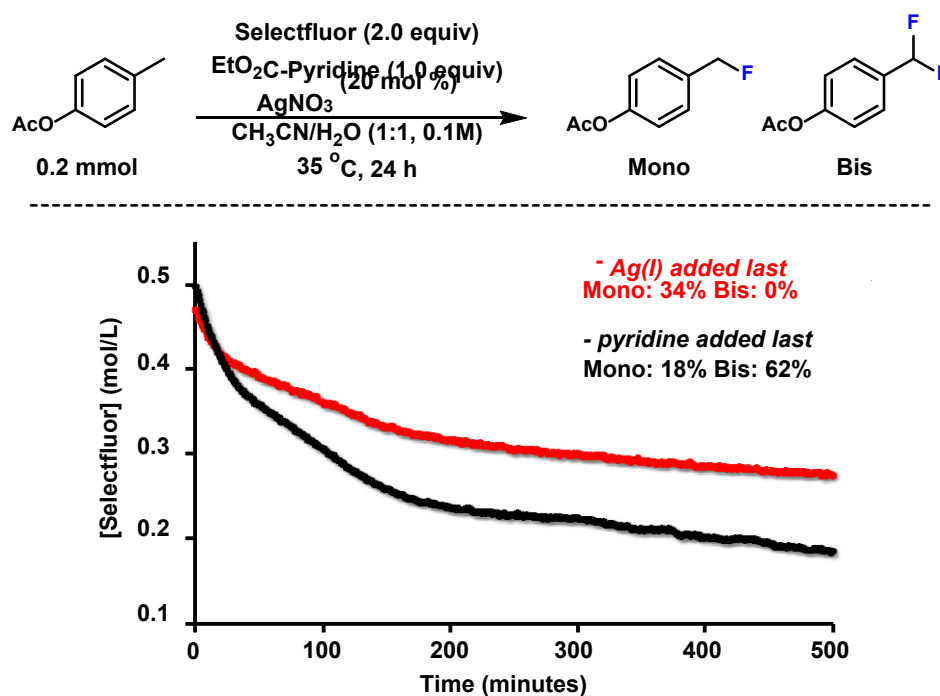
Figure 1.2. ReactIR Spectra of the order of addition reactions

After completing the initial screening of the order of addition experiments, the interaction between the pyridine additives and Selectfluor was monitored. The stair-like incline seen in Figure 1.3 occurs with each dose of pyridine added. The concentration of Selectfluor decreased in the presence of electron-donating pyridine additives (Figure 1.3 A &B). The additive 4-methoxypyridine consumed the Selectfluor more rapidly than

pyridine. In contrast, the dosing experiments with the electron-withdrawing pyridines showed no signs of consumption of the Selectfluor (Figure 1.3 C&D). The consumption of Selectfluor seen in the reactIR experiments could be a rational explanation for the lower product conversions when using electron-donating pyridines, 4-methoxypyridine, and pyridine. Suggesting a pyridinium like compound could be forming, causing the decrease in the N–F bond. This reasoning is also supported by the formation of the fluoride ion in our ^{19}F NMR experiments at -74 ppm, which matches the recorded literature chemical shift.[19]
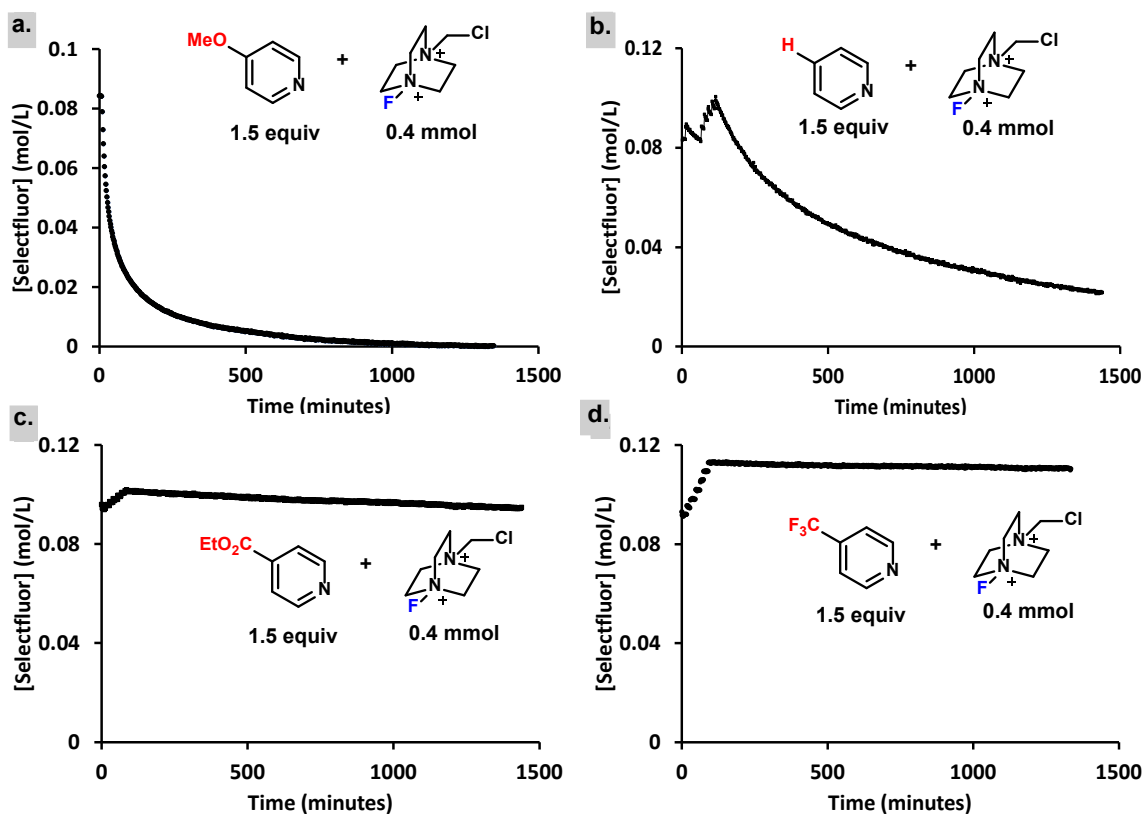
Figure 1.3. ReactIR Spectra of the dosing experiments

Once the order of addition and dosing experiments were complete, it was finally time to directly compare each reaction using the different pyridine additives (**Figure 1.4**). Unfortunately, we could not monitor the reaction using 4-(trifluoromethyl)pyridine as an additive since this pyridine additive forms oil droplets during a productive reaction that interferes with monitoring the reaction. Instead, ethyl isonicotinate was used as the electron-deficient pyridine additive. Figure 1.4 shows ethyl isonicotinate globally consumes more Selectfluor, while 4-methoxypyridine, the electron-rich pyridine, initially consumes Selectfluor more rapidly and then slows down. The results of these experiments lead us to consider the possibility of halogen bonding as the course of reactivity.
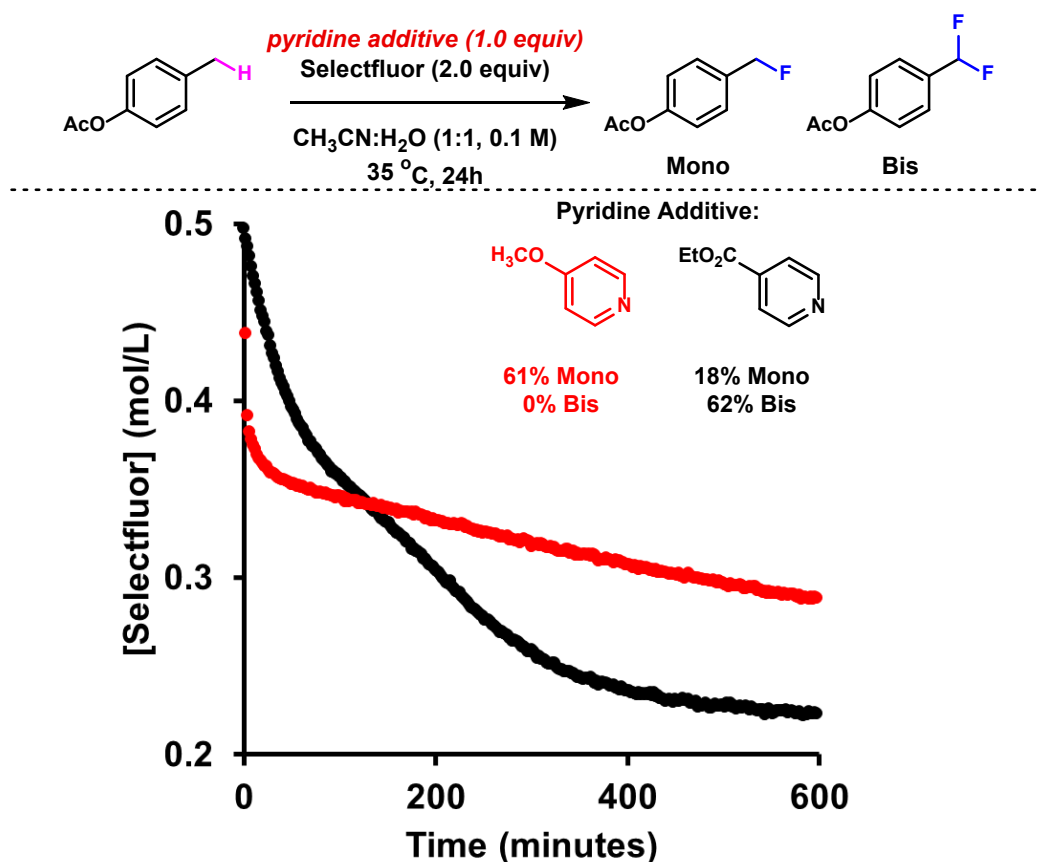
Figure 1.4. ReactIR reactions comparison. Standard conditions were used.

Based on the finding for Table 1.4, entry 6, if pyridine additives had substituents in the 2,6-position, the reaction failed. A brief investigation was conducted into how sterically hindered pyridine additives affect the reaction. It was observed that when the Lewis basic nitrogen of the pyridine additive was slightly blocked by one methyl substituent in the 2-C position, the yield decreased (Table 1.6, entry 2), and when two substituents blocked it in the 2–C and 6–C position, the reaction ultimately failed (Table 1.6, entries 3 and 6). The steric hindrance is likely affecting the coordination of the pyridine additive to the Selectfluor, which in turn is causing the reaction to fail. Studies have found the ideal bond idea to invoke halogen bonding complexes is 180°. Pyridine additives with a substituent in the 2-C position would disrupt the bond angle.[20] Further supporting the decrease in the fluorinated product and the possibility of halogen bonding. There is literature evidence of substituted pyridine additives coordinating with Ag(I).[18] This would lead us to believe the steric hindrance is not affecting pyridine's ability to coordinate with Ag(I) but the halogen–bonding interaction between the pyridine additive and Selectfluor. To investigate the possibility of halogen bonding in our reaction, we turned to our colleagues in the Hratchian theoretical group.
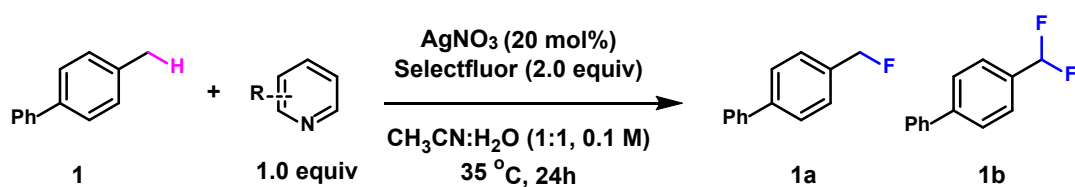
entry	deviation from standard conditions	NMR yield (%)	
1	pyridine	52	*trace*
2	2-methylpyridine	26	0
3	2,6-dimethylpyridine	0	0
4	4-methylpyridine	52	0
5	2,4-dimethylpyridine	19	0
6	2,4,6-trimethylpyridine	0	0

Table 1.6. Investigation of sterically hindered pyridine additives

1.2.1.5 Computational Investigation

Our colleagues in the Hratchian lab undertook a rigorous computation study to examine the feasibility of halogen bonding between Selectfluor and pyridine additives. Computational efforts initially involved determining the chemical properties of Ag(I)/pyridine complexes. Calculations were performed using the B3PW91/6-311G(d) model chemistry, which considered the implicit solvation by acetonitrile were carried out using a local development version of Gaussian.[21] This study showed that the calculated Ag(I) oxidation potentials resulted from a bis-pyridine Ag(I) complex species, and these

species are likely responsible for initiating radical fluorination reactions. The calculated oxidation potential of the bis-pyridine Ag(I) complexes was computed correlate to the experimental data collected, confirming the electron-donation pyridine additive, 4-methoxypyridine, lowered the onset oxidation potential of Ag(I) the most (Table 1.7).
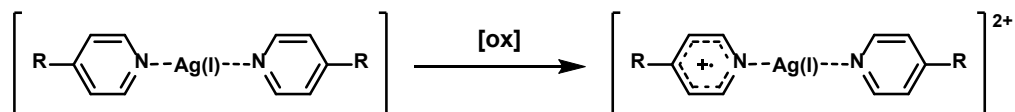
R Group	E^o_{exp} (V)	E_o calc
OCH$_3$	1.24	2.04
H	1.31	2.08
CO$_2$Et	1.54	2.20
CF$_3$	1.60	2.27

Table 1.7. Experimental and Computational oxidation potential of Ag in the presence of pyridine additives

With experimental and computational results in a consensus regarding Ag(I) oxidation, we explored the possibility of modeling the $[N–F–N]^+$ halogen bonding complex. The initial modeling investigation failed when using density functional theory (DFT) chemistries. Reports by Martin and Wong state only a minimal set of appropriate functionals can measure predicted halogen bonding strengths.[22] These findings led to using correlated wave function methods instead. Optimized geometries of the halogen-bound species were run using the MP2/6-311+G(d) theory, and single-point energies were evaluated using CCSD(T)/6-311+G(d) model.

$$\text{(1)}$$

$$\text{(2)}$$

Table 1.8. Computational calculations for Selectfluor–Pyridine halogen bonding
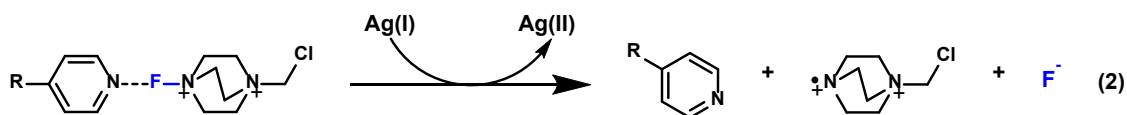
R Group	ΔH1 (kcal/mol)	ΔH2 (kcal/mol)
OCH₃	0.34	-31.42
H	0.74	-31.82
CO₂Et	3.63	-33.66
CF₃	2.57	-34.71

According to the calculated results, the energy of the coordinated species is higher than that of the unbound species, which means the coordinated Selecfluor–pyridine species dissociates quickly, and the coordination is reversible. These calculations also show that 4-methoxypyridine forms the Selectfluor–pyridine complex the easiest. The ΔH1 results in table 1.8 show the energy required to form the Selectfluor–pyridine complex (ΔH1). The ΔH1 data suggest that electron-rich pyridines require the least energy to create the complex with Selectfluor, making it more energetically favorable. The ΔH2 results in table 1.8 calculations show the reduction of the [N–F–N]⁺ complex is more energetical favorable in the presence of electron-withdrawing pyridines. These calculations suggest the 4-methoxypyridine–Selectfluor complex is stronger bound, causing the reduction of the [N–F–N]⁺ halogen bound complex to be decreased, leading to a lower yield. Additional

calculations were performed to determine if any other probable structures exist. These calculations determined that no other suitable geometries exist than the proposed [N–F–N]$^+$ linear complex. The results from the computational investigation suggest the reactivity trends in Scheme 5 effect from the pyridine's nitrogen interacting directly with the fluorine of Selectfluor.

1.2.1.6 Electrochemical Reduction of Selectfluor

With experimental and computational evidence in agreement, we experimentally investigated the reduction of the [N–F–N]$^+$ halogen bonding interaction and how the electronics of the pyridine additives affect it. The bond dissociation energy for the N–F bond of Selecfluor is calculated to be 64 kcal/mol, meaning the bond is relatively weak.[#] With computational data suggesting the reduction of the N–F bond is more favorable in the presence of pyridine additives, we then ran cyclic voltammetry studies focusing on the reduction of this bond. The cyclic voltammetry experiment determined Selectfluor produces an irreversible single-electron reduction of approximately -1.18 V (Scheme 1.6). The reduction of Selectfluor in the presence of pyridine additives is lowered. Experimental data in scheme 1.6 demonstrates that all pyridine additives cause a reduced potential than Selectfluor alone, but a more significant reduction is seen with electron-rich pyridine additives.
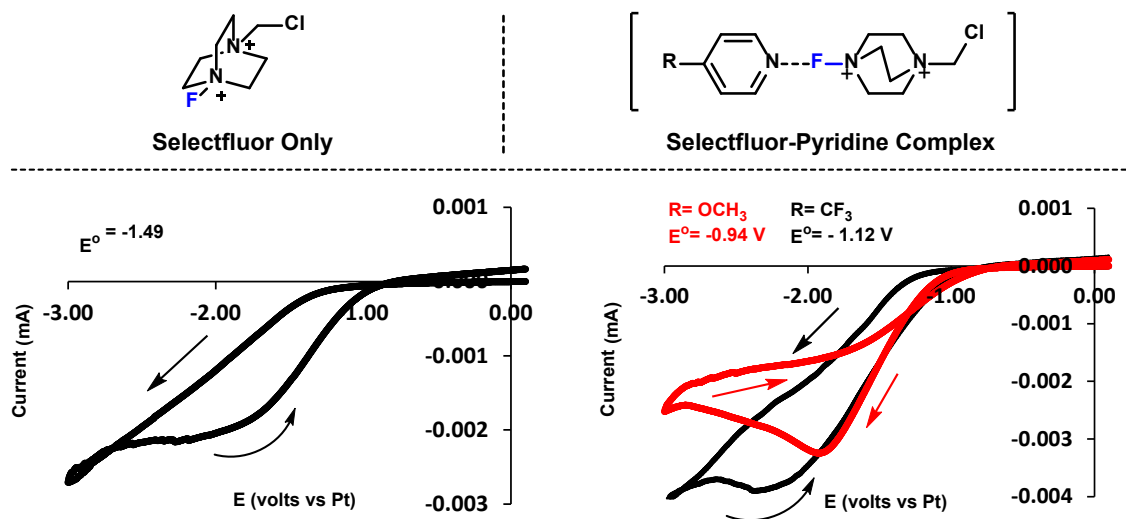
Scheme 1.6. Reduction of Selectfluor via cyclic voltammetry

1.2.1.7 Ag(I)[Pyridine]₂ Investigation

Based on the experimental and computational data, 4-methoxypyridine coordinated to Ag(I) should make the best catalyst. To test this theory, we synthesized the catalyst using a literature procedure.[23] The initial control reaction replacing the pyridine additive and AgNO₃ with the Ag(I)-4-methoxypyridine catalyst, ultimately failed. This result led us to investigate if the lack of pyridine additive resulted in the failed reaction or if the 4-methoxypyridine from the catalyst was unproductively consuming Selectfluor. To further understand what was occurring, we studied the reaction using *in situ* reactIR (Figure 1.5). The results show that Ag(I)–4-methoxypyridine interacts with the N – F of Selectfluor; the consumption slows down over time and does not consume all of the Selectfluor available.
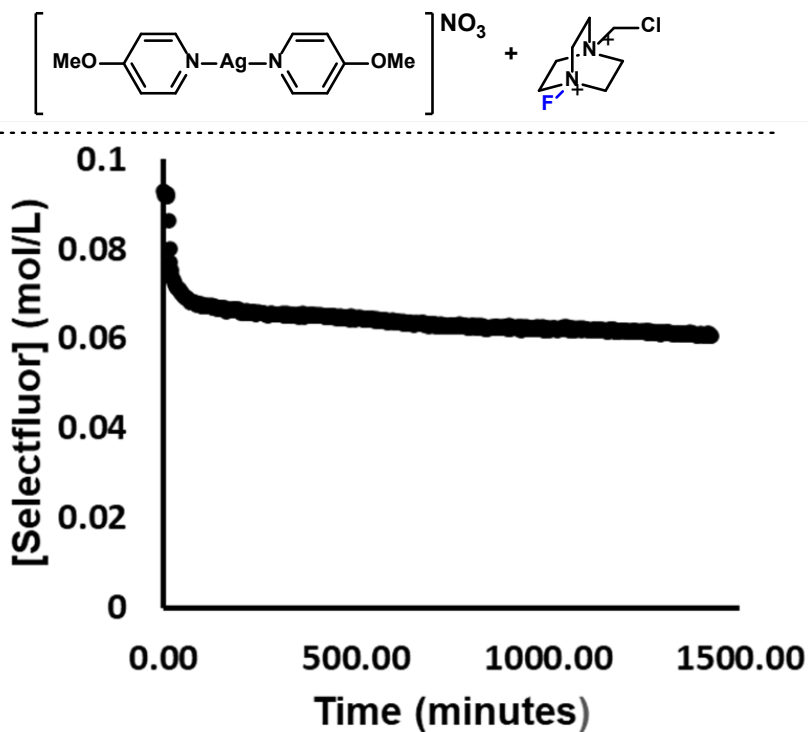
Figure 1.5. Ag(I)[4-methoxypyridine]₂ catalyst and Selectfluor. Ag(I)[4-methoxypyridine]₂ catalyst (40 mol %) and Selectfluor (0.2 mmol) in 2 mL CH₃CN/H₂O.

The Ag(I)[4-methoxypyridine]₂ catalyst was subjected to our reaction conditions in the presence of an additional pyridine additive, 4-(trifluoromethyl)pyridine, and monitored via *in situ* reactIR (Figure 1.6). The results show the consumption of Selectfluor globally increased as it produced the fluorinated product.
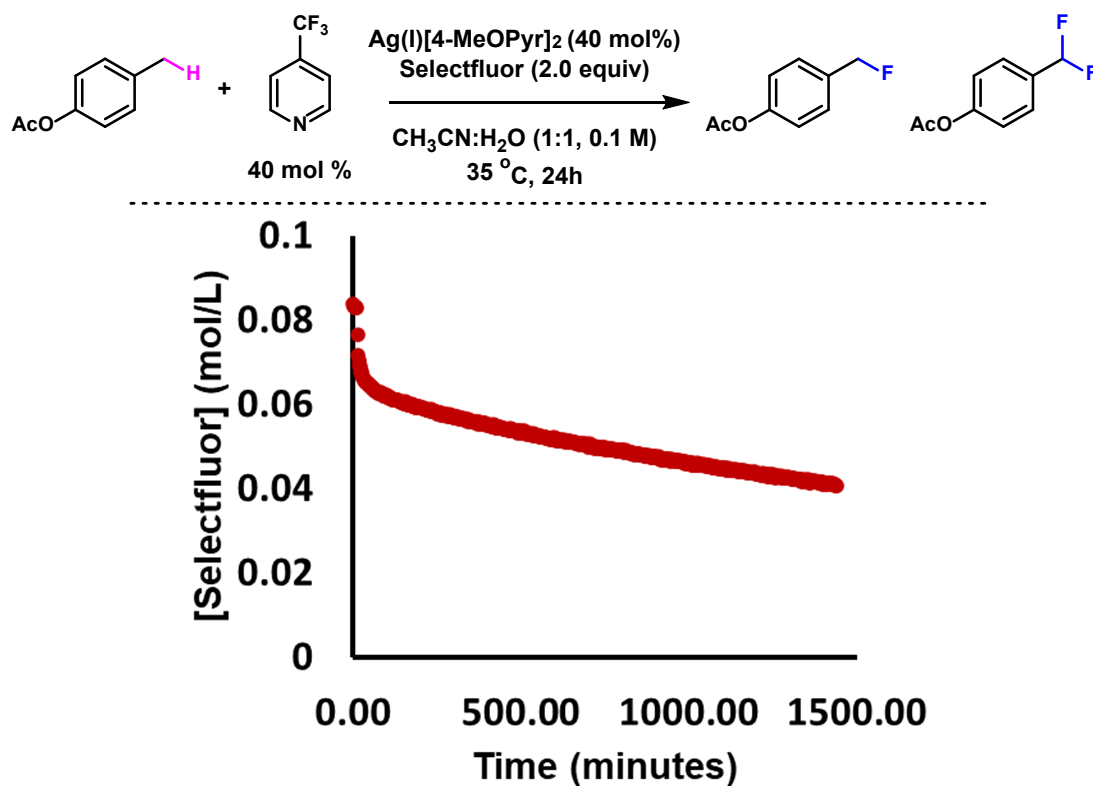
Figure 1.6. A productive reaction using the Ag(I)[4-methoxypyridine]$_2$ catalyst and 4-(trifluoromethyl)pyridine. p-tolylacetate (0.2 mmol), Selectfluor (0.2 mmol) Ag(I)[4-methoxypyridine]$_2$ catalyst (40 mol %), 4-(trifluoromethyl)pyridine (40 mol %) in CH$_3$CN/H$_2$O (1:1, 0.1M).

Once the initial investigation of Ag(I)[4-methoxypyridine]$_2$ catalyst was complete, we synthesized the catalyst using 4-(trifluoromethylpyridine). We tried various combinations of the catalysts and pyridine additives. The reaction that successfully yielded the most fluorinated product was using Ag(I)[4-(trifluoromethyl)pyridine]$_2$ catalyst as the catalyst and additive (Table 1.9). Although this yield was the most significant among the Ag(I)–pyridine catalysts, it was not as substantial as our standard reaction conditions.
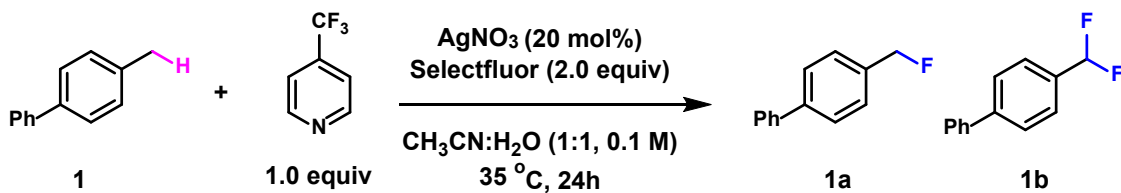
entry	deviation from standard conditions	NMR yield (%)	
1	none	12	85
2	Ag(OMe-Pyr)$_2$NO$_3$ (20 mol %), no pyridine	37	49
3	Ag(CF$_3$-Pyr)$_2$NO$_3$ (20 mol %), no pyridine	9	68
4	4-methoxypyridine (40 mol %)	0	0
5	4-(trifluoromethyl)pyridine (40 mol %)	63	26
6	Ag(OMe-Pyr)$_2$NO$_3$ (20 mol %), 4-(trifluoromethyl)pyridine (40 mol %)	60	24

Table 1.9. Ag(I)–pyridine catalysts as a catalyst in the reaction

1.2.1.8 NMR Study

After discovering the [N–F–N]$^+$ halogen bonding complex via reactIR, CV, and computational study, we began to wonder if it were possible to obtain more specific evidence using ^{19}F-NMR. Previously, Ergelyi found that [N–F]$^+$ halogen bonding only cause minor shifts in ^{19}F-NMR.[24] These findings are consistent with ours, as all the coordinated pyridine–Selectfluor intermediates had negligible shifts in ^{19}F ppm (table 1.10).

R	^{15}N		^{15}N	^{19}F
OCH$_3$	102.59		-153.76	50.00
H	-80.79		-92.64	50.01
CO$_2$Et	-66.76		-70.54	50.01
CF$_3$	-67.31		-68.21	50.01
(Selectfluor)	-122.39		—	50.02

Table 1.10. Chemical shifts of C–2 in Selectfluor–pyridine complexes

Ergelyi established pyridines' ability to halogen bond and showed how the pyridine's electronics affect the halogen-bonding intermediate by using ^{1}H,^{15}N HMBC experiments to monitor the ^{15}N NMR signal for each complex directly. Only minor chemical shifts were observed under several conditions. Our own ^{1}H,^{15}N HMBC investigation showed promising results. We observed considerable changes in our ^{1}H,^{15}N HMBC study using in situ reaction conditions by tracking the pyridine additive. All the pyridines ^{15}N chemical signals were shifted when combined with Selectfluor (Table 1.10). The signal's most significant shift and broadening was seen for 4-methoxypyridene, shifting the original signal from -102.59 ppm to -153.76 ppm (Figure 1.5). These results support the generation of a pyridinium-like intermediate, similar to Ergelyi's results, further supporting the evidence of [N–F–N]$^+$ halogen bonding complex.
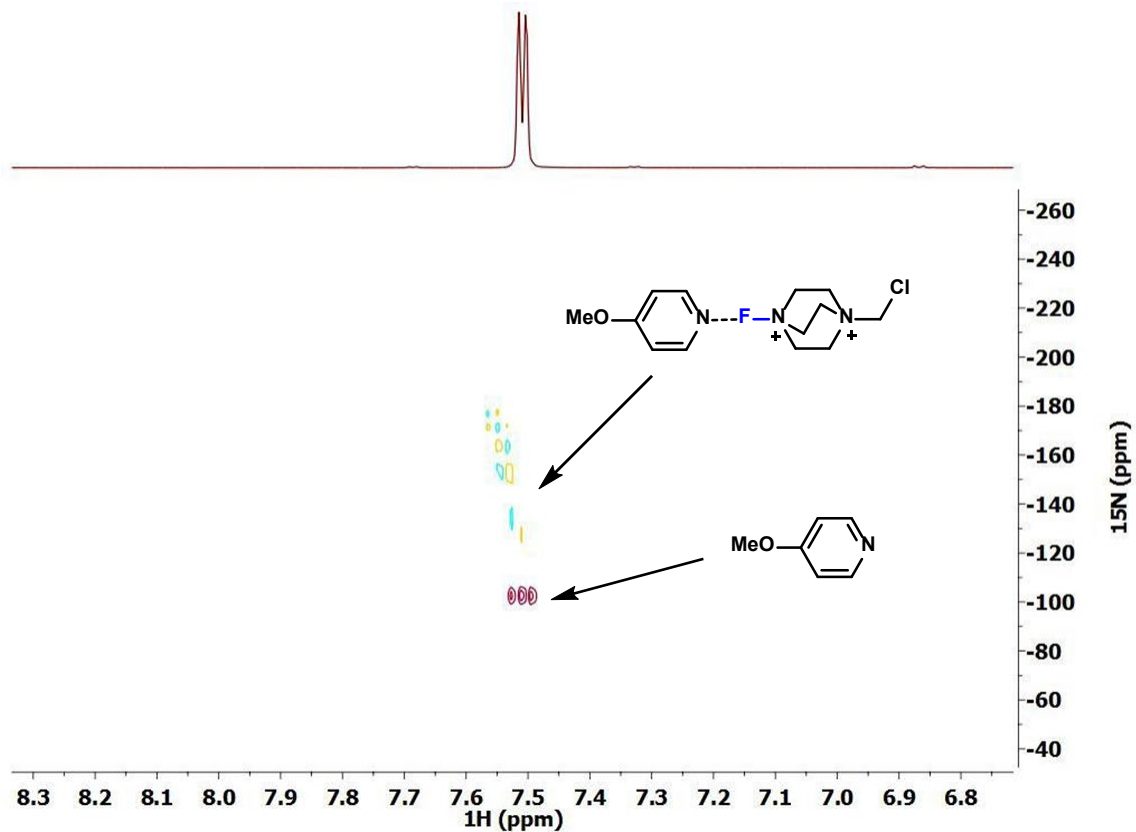
Figure 1.7. ^{1}H,^{15}N HMBC NMR of 4-methoxypyridine only (maroon), 4-methoxypyridine with Selectfluor (blue and yellow). Conditions: 4-methoxypyridine (0.1 mmol), Selectfluor (0.1 mmol), in 700 μL of CD$_3$CN/H$_2$O (1:1) with sealed capillary of nitromethane as internal standard at 25 °C

1.2.1.9 Mechanism

Based on our combined experimental and computational results, we propose the following radical C–H fluorination with Selectfluor – pyridine complex system and Ag (I) catalyst mechanism (Scheme 1.7).[25] We determined the pyridine additive must be present for the reaction to proceed. The pyridine additive plays two essential roles in the reaction to occur. The first role of the pyridine additives is to lower the onset oxidation potential of

Ag(I) to Ag(II). Experimental data collected using cyclic voltammetry and theoretical calculations support this conclusion (Table 1.7). The pyridine additive's second role is to bond with the Selectfluor to form the $[N–F–N]^+$ halogen bonding complex.

We propose the Ag(I)–pyridine catalyst initiates the single-electron reduction of the $[N–F–N]^+$ Selectfluor–pyridine halogen bonding complex to form the DABCO radical species, a fluoride ion, and Ag(II)–[pyr]$_2$ species. The DABCO radical abstracts a benzylic hydrogen atom from the substrate, generating the benzylic radical. The benzylic radical can then propagate with another equivalence of Selectfluor, leading to the mono-fluorinated product and regenerating the DABCO radical. The newly formed DABCO radical intermediate will then repeat the cycle to produce the bis-fluorinated product.
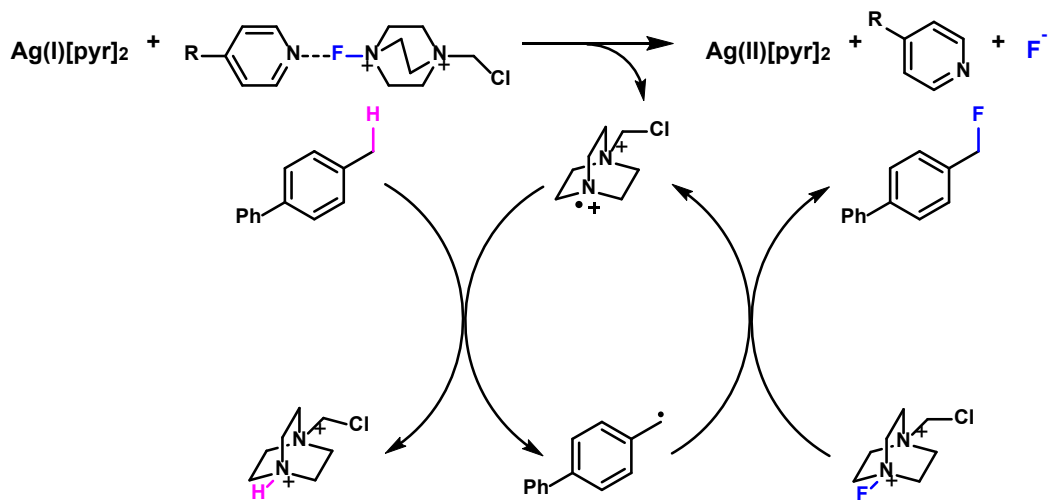
Scheme 1.7. Proposed mechanism for benzylic fluorination

1.2.1.10 Pfizer Collaboration

During the publication of this work, we began our collaboration with Pfizer. The collaboration consisted of using our new fluorination chemistry for the late-stage functionalization of Celecoxib. We provided Pfizer with a list of roughly 200 different additives to try in the reaction. Pfizer determined the best additive in the reaction was 3-cyanopyridine, which was opposite our findings. We found the best pyridine additive to produce the highest amount of bis-fluorinated Celecoxib is 4-(trifluoromethyl)pyridine (Scheme 1.8); this is the same result as our fluorination paper. We also attempted to boost bis-fluorination by resubjecting pure mono-fluorinated Celecoxib. Unfortunately, the reaction maxes out at 52% mono-fluorinated and 33% bis-fluorinated products. This is likely due to an increase in BDE after the first HAT to form the mono-fluorinated product, and this increase makes it unfavorable for the DABCO radical to break the C–H bond again.
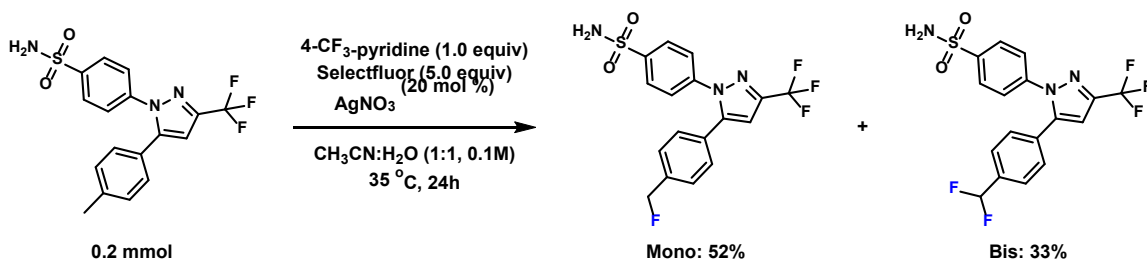
Scheme 1.8. Fluorination of Celecoxib

1.3 Summary

In summary, we have developed a methodology for promoting radical benzylic fluorination via halogen bonding interactions between Selectfluor and pyridine additives. We demonstrated how the electronics of the pyridine additives dictate the product distribution. Electron-donating pyridines caused a drastic decline in product conversion, while electron-withdrawing pyridine additives promoted bis-fluorination. Experimental and computational data both suggest the reduction of the $[N–F–N]^+$ Selectfluor–pyridine bond is more favorable in the presence of electron-withdrawing pyridine additives. Our data thoroughly supports our findings.

This work has also inspired our lab to investigate halogenation using commercially available reagents. Chapter two of this dissertation thoroughly explores our goal of using halogen bonding to invoke benzylic bromination.

1.4 References

(1) Gribble, G. W. Fujimori, *J. Chem. Ed.* **2004**, 81, 10, 99-109.
https://doi.org/10.1016/j.chembiol.2008.01.006

(2) Wilcken, R., Zimmerman, M. O., Lange, A., Joerger, A. C., Boeckler, F. M. *J. Med. Chem.* **2013**, 56, 1363–1388.

(3) (a) Jeschke, P. *Pest. Manag. Sci.* **2017**, 73, 1053 – 1066. (b) Neumann, C.S., Fujimori, D. G., Walsh, C.T. *Chem. & Bio.* **2008**, 15, 2, 99–109.

(4) Lu, Y., Liu, Y., Xu, Z., Li, H., Liu, H., Zhu, W. *Expert. Opin. Drug Discov.* **2012**, 7, 5, 375–383.

(5) Poonam, S., Westwell, A. D. *J. Of Enzyme Inhibition and Med. Chem.* **2007**, 22, 5, 527–520.

(6) Kita, Y., Shigetani, S., Kamata, K., Hara, M. *Mol. Cata.* **2019**, 475, 110463.

(7) Alauddin, M. *Am. J. Nucl. Med. And Mol Imaging.* **2012**, 2, 1, 55–76.

(8) Jacobson, O., Kiesewetter, D. O., Chen, X. *Bioconjugate Chem.***2015**, 26, 1, 1–18.

(9) Cavallo, G., Metrangolo, P., Milani, R., Pilati, T., Priimagi, A., Resnati, G., Terraneo, G. *Chem. Rev.* **2016**, 116, 2478–2601.

(10) Thorson, R. A., Woller, G. R., Driscoll, Z. L., Geiger, B. E., Moss, C. A., Schlapper, A. L., Speetzen, E. D., Bosch, E., Erdelyi, M., Bowling, N. P. *Eur. J. Org. Chem.* **2015**, 1685-1695.

(11) (a) Politzer, P., Murray, JS, Concha, M.C., *J. Mol. Model.* **2007**, 643–650. (b) Lu, X.Y., Zou, J. W., Yu, Q. S. *Chem. Phys. Lett.* **2007**, 449, 6–10.

(12) Danahy, K., Cooper, J., Humbeck, V. Angew. Chem. **2018**, 57, 5134- 5138.

(13) (a) Hull, K. L., Anani, W. Q., Sanford, M. S., *J. Am. Chem. Soc.* **2006**, 128, 22, 7134–7135. (b) Liu, W., Huang, X., Cheng, M. J., Nielsen, R. J., Goodard, W. A., Groves, J. T., *Science.* **2012**, 337, 6100, 1322–1325.

(14) (a) Banks, R. E., Besheesh, M. K., Mohialdin-Khaffaf, S. N., Sharif, I. *J. Chem. Soc.* **1992**, 595. (b) Banks, R.E. *US Patent.* **1992**, 5 086 178.

(15) S. Bloom, R. Pitts, R. Woltornist, A. Griswold, M. G. Holl, T. Lectka, *Org. Let.* **2013**, 17, 1722-1724.

(16) Xu, P., Guo, S., Wang, L., Tang, P. *Angew. Chem. Int. Ed.* **2014**, 53, 5955–5958.

(17) Hua, A. M., Mai, Martinez, R., Baxter, R. D. *Org. Lett.* **2017**, 19, 11, 2949–2952.

(18) Piero, S. D., Fedele, R., Melchior, A., Portanova, R., Tolazzi, M., Zangrando, E. *Inorg. Chem.* **2007**, 46, 4638–4691.

(19) (a) Christe, K. O., Wilson, W. W. *J. fluorine Chem.* **1990**, 46, 339–342. (b) Connick, R. E., Poulson, R. E. *J. Phys. Chem.* **1959**, 63, 4, 568–569.

(20) (a) Varadwaj, P. R., Varadwaj, A., Marques, H. M. *Inorganics.* **2019**, 7, 40. (b) Desiraju, G. R., Ho, P. S., Legon, A. C., Marquardt, R., Metrangolo, P., Politzer, P., Resnati, G., Rissanen, K. *Pure Appl. Chem.* **2013**, 85, 8, 1711–1713.

(21)(a) Becke, A.. *J. Chem. Phys.* **1993**, *98*, 5648. (b) Wang, Y.; Perdew J. P. *Phys. Rev. B.* **1991**, *43*, 8911. (c) Marenich, A.V.; Cramer, C.J.; Truhlar, D.G. *J. Phys. Chem. B.* **2009**, *113* (18), 6378–6396. (d) Hratchian, H.P.; Schlegel, H. B. Finding Minima, Transition States, and Following Reaction Pathways on Ab Initio Potential Energy Surfaces. In *Theory and applications of computational chemistry: The first forty years*, Dykstra, C. E.; Frenking, G.; Kin, K. S.; Scuseria,

G. E., Eds. Elsevier: Amsterdam, **2005**, 95. (5) Baik M.; Friesner, R. A. *J. Phys. Chem. A,* **2002**, *106*(32), 7407–7412.

(22) (a) Kozuch, S.; Martin, J. M. L. *J. Chem. Theory Comput.* 2013, 9, 1918−1931. (b) Anderson, L. N.; Aquino, F. W.; Raeber, A. E.; Chen, X.; Wong, B.M. *J. Chem. Theory Comput.* 2018, 14, 180−190.

(23) Wong, V. H. L.; White, A. J. P.; Hor, T. S. A.; Hii, K. K. *Adv. Synth. Catal.* **2015**, *357*, 2485–2491.

(24) A. Karim, M. Reitti, A. Carlsson, J. Grafenstein, M. Erdelyi, Chem. Sci. **2014**, 5, 3226. (F-NMR evidence)

(25) Hua, A. M., Bidwell, S. L., Baker, S. I., Hratchian, H. P, Baxter, R. D. *ACS Catal.* **2019**, 9, 3322–3326.

Chapter 2

Enhanced Reactivity for Aromatic Bromination via Halogen Bonding with Lactic acid Derivatives

2.1 Introduction

Halogenated arenes are important components of metal-catalyzed cross-coupling reactions, pesticides, pharmaceuticals, and natural products.[1] Seminal reports of aromatic bromination involving molecular bromine provided access to these useful structures, although harsh reaction conditions limited the scope of substrates that could participate.[2] N-bromosuccinimide (NBS) development provided a bench-stable alternative to molecular bromine, although at the cost of diminished reactivity.[3] Because of this, standard bromination reactions using NBS have traditionally been limited to primarily reactive electron-rich aromatics. Efforts to enhance the native reactivity of NBS have been of general interest to synthetic chemists, and several methods using catalytic activators or specialized reaction conditions have been developed.[4]

A common strategy for activating N-halosuccinimides involves the coordination of a Lewis acidic additive to the imide carbonyl, rendering the halogen more electrophilic via induction.[5] Alternatively, Lewis basic additives may enhance reactivity via halogen bonding or by the formation of a new halogenating reagent via direct halogen displacement.[6] Several methods have been developed using sulfur-based additives that interact nucleophilically with the halogens of N-halosuccinimides. Thioureas and thioacetamides have been shown to doubly activate N-halosuccinimides via a combination of hydrogen and halogen bonding to functionalize electron-rich arenes.[7] Phosphine sulfide

catalysts have shown promise for halogenating heteroarenes and electron-neutral aromatics, although air and moisture sensitivity diminishes their experimental utility.[8] Anionic sulfide catalysts promote regioselective halogenation at very low catalyst loadings but require anhydrous conditions for efficacy.[9] Although simple alkyl sulfides and disulfides are effective catalysts for halogenation,[10,11] sterically hindered triptycenyl methyl sulfide successfully promoted aromatic halogenation that was previously unachievable without the use of Br_2 or Cl_2. [12] Although an improvement over previous methods, triptycenyl methyl sulfide catalysts also suffer from air and moisture sensitivity and must be custom synthesized. Alternative strategies, such as using hexafluoroisopropanol as a solvent, may also rely on halogen bonding to NBS for efficacy[13] but are impractical for routine or large-scale use.[14] To complement these existing methods, our group has developed an operationally simple protocol for aromatic bromination using lactic acid derivatives as halogen bond acceptors from NBS (Figure 1).

A) Previous Methods for Electrophilic Aromatic Bromination of Arenes
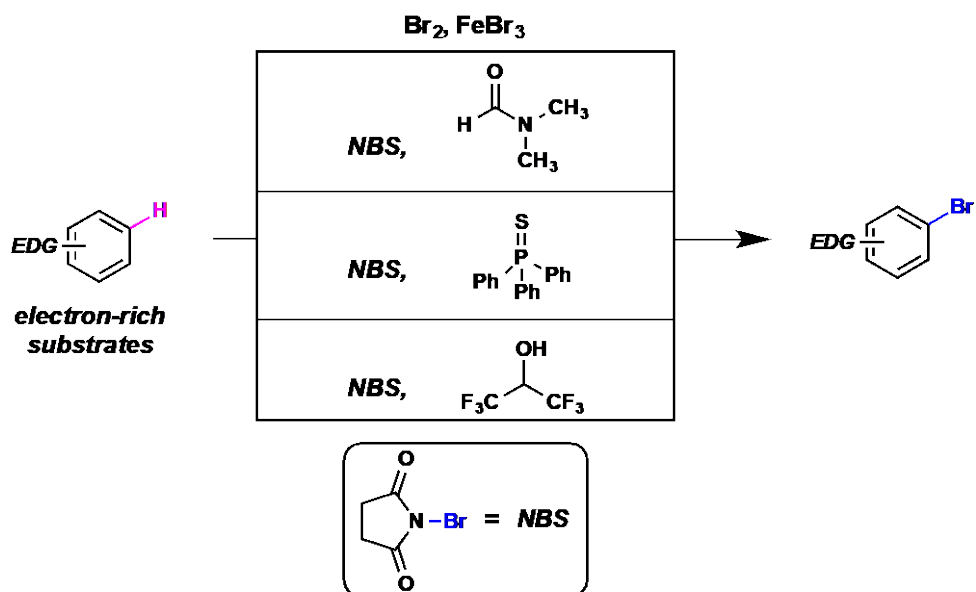
B) Electrophilic Aromatic Bromination using Lactic Acid Derivates (*This Work*)
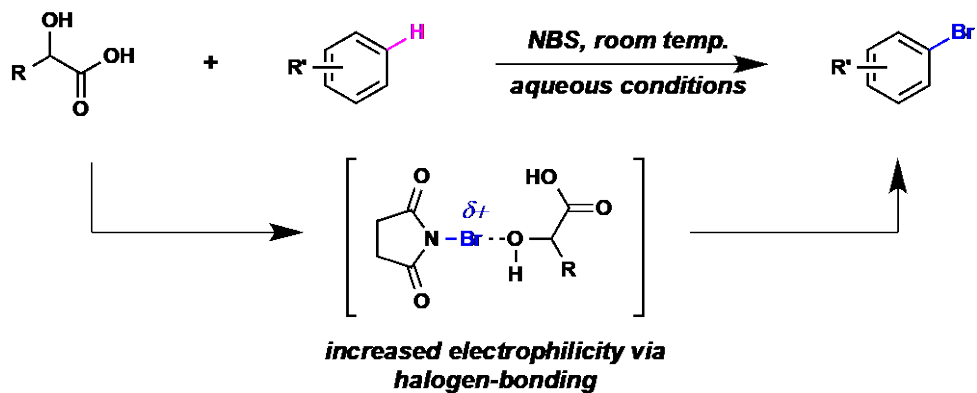
Figure 2.1. Methods for aromatic bromination

2.2 Results and Discussion

2.2.1 Development of Electrophilic Aromatic Bromination

Previously, our lab reported radical benzylic C-H fluorination promoted via [N–F–N]$^+$ halogen bonding between Selectfluor and monosubstituted pyridine additives.[15] We found that halogen bonding between pyridine additives and Selectfluor is required for the reaction. Computational and experimental data showed that the Lewis basicity of the pyridine additive was essential. If the Lewis base were too strong, it would promote unwanted side reactions, but if not strong enough, the reaction would not proceed. Using this idea of [N–X–N] halogen bonding, we set forth to investigate the possibility of halogen bonding between simple monosubstituted pyridine additives and NBS.
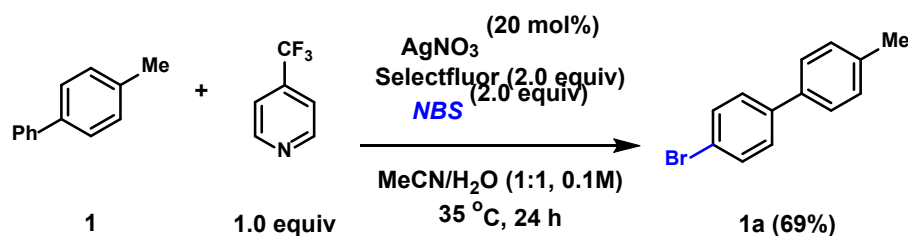
Scheme 2.1 Discovery of selective *para*-bromination

The initial efforts began by adding NBS to our established fluorination reaction conditions. The addition of NBS produced bromination but in the *para*-position, not in the benzylic position as we had hypothesized. Although unexpected, this result makes sense since the C–H abstraction is a fundamental step for benzylic fluorination, and succinimide is not a known C–H abstractor. Based on the results shown in scheme 2.1, we became

interested in studying electrophilic aromatic bromination promoted via halogen bonding between pyridine and NBS.

To investigate what reagents were essential for the reaction, we began by removing reagents from our established reaction conditions. As shown in **Table 2.1**, 4-methylbyphenyl, **1**, could undergo bromination in the presence of 4-trifluoromethyl pyridine, yielding 78% (entry 1). At ambient temperatures, the reaction failed, resulting in no product conversion (entry 2). Entry 3 showed an apparent additive effect when 4-(trifluoromethyl)pyridine was omitted from the reaction. Pyridine additives with various electronic configurations were examined (entries 4-9). The results of the different pyridine additives show a trend similar to the fluorination chemistry, where electron-rich pyridines led to poor product yields (entries 4 and 5). In contrast, electron-withdrawing pyridines afforded modest product yields (entries 6-8).

Next, the sterically hindered electron-withdrawing pyridine, ethyl-2,6-diisopropyl nicotinate, was used. The steric hindrance dominated the electronics of the pyridine resulting in a low yield (entry 9). Varying the pyridine additive's concentration caused the reaction to decrease drastically (entries 10 and 11). Water was determined essential for the reaction to proceed (entry 12). Although bromination was effective in multiple organic co-solvents, ethyl lactate appeared optimal (entries 12-20). Bromination without any pyridine additive is still efficient using aqueous ethyl lactate, demonstrating an apparent solvent effect under these conditions (entry 21). Because ethyl lactate is known to hydrolyze into lactic acid and ethanol under aqueous conditions,[17] we were interested in studying how ethyl lactate or its constituents may interact with NBS to promote bromination.

Reaction scheme: Compound **1** (4-methylbiphenyl with H labeled) + 4-(trifluoromethyl)pyridine (CF₃ at 4-position) (1.0 equiv), with NBS (2.0 equiv), MeCN/H₂O (1:1, 0.1M), 35 °C, 24 h → **1a** (4'-bromo-4-methylbiphenyl, Br labeled).
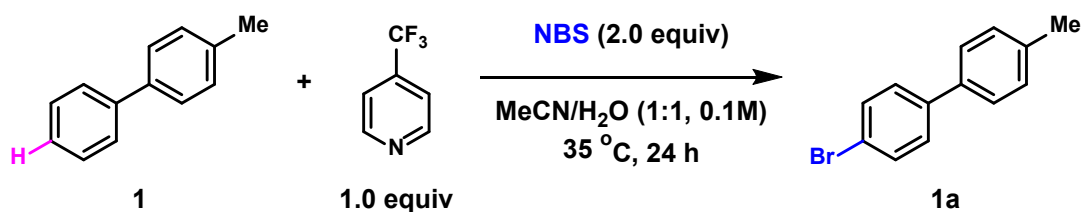
entry	deviation from standard conditions	yield
1	none	78
2	room temperature	0
3	without 4-CF$_3$-pyridine	60
4	4-methoxypyridine	0
5	pyridine	*trace*
6	ethyl isonicotinate	62
7	4-(trifluoro)methylpyridine	78
8	4-cyanopyridine	68
9	2,6-diacetylpyridine	27
10	4-(trifluoro)methyl pyridine (0.5 equiv)	33
11	4-(trifluoro)methyl pyridine (2.0 equiv)	55
12	acetonitrile only	0
13	acetone	30
14	methanol	62
15	ethanol	0
16	tetrahydrofuran	0
17	Dimethylformamide	0
18	methyl-tetrahydrofuran	0
19	diactone alcohol	73
20	ethyl lactate	91
21	NBS only in ethyl lactate/H2O	77

Table 2.1 Development of selective bromination

Using this idea, we began to assess if the hydrolysis of ethyl lactate to form lactic acid was a crucial component in our reaction. To do this, we investigated substrates with better solubility so that we could perform *in-situ* measurements. As shown in Table 2.2, the

bromination of 4′-methoxyacetophenone was explored to determine the effect lactic acid derivatives may have on the reaction efficacy. A catalytic amount of lactic acid promoted aromatic bromination at room temperature in aqueous acetonitrile (entry 1). The formation of the brominated product was not observed in the absence of lactic acid (entry 2). A stoichiometric amount of lactic acid did not provide an increase in the yield (entry 3). Since NBS can oxidize secondary alcohols,[18] pyruvic acid (entry 4) was also explored as a potential additive and produced a higher yield of the brominated product. Replacing lactic acid with unprotected amino acids led to comparable results (entries 5 and 6). However, we did observe oxidative degradation of amino acids[18] in our reaction, which is later discussed in this dissertation. The absence of the α-substituent caused a drastic decrease in yield, suggesting substitution in this position is essential (entries 7 and 9). Mandelic acid was shown to be superior to lactic acid (entry 8). Since increased product yield was observed when replacing lactic acid with pyruvic acid, benzoylformic acid was used. The reaction with benzoylformic acid produced a similar yield to mandelic acid (entry 10). Trifluoroacetic acid (TFA) was used to determine if a Brønsted acid additive with a pKa lower than 4.00 would be a sufficient catalyst to enhance NBS reactivity (entry 11). Although TFA enabled bromination, the reaction yield diminished. Based on these results and the easy handling of mandelic acid, we studied the interaction between mandelic acid and NBS.

Table 2.2 Optimization of lactic acid derivatives

entry	deviation from standard conditions	yield
1	none	54
2	without lactic acid	0
3	lactic acid (1.0 equiv)	59
4	pyruvic acid instead of lactic acid	62
5	alanine instead of lactic acid	56
6	2-phenylglycine instead of lactic acid	71
7	phenylacetic acid instead of lactic acid	0
8	mandelic acid instead of lactic acid	85
9	benzoic acid instead of lactic acid	0
10	benzoylformic acid instead of lactic acid	86
11	trifluoroacetic acid instead of lactic acid	58

After determining mandelic acid was the superior lactic acid derivative, we set further to determine the most optimal reaction conditions to promote electrophilic aromatic bromination (**Table 2.3**). At elevated temperatures, the reaction yielded slightly higher product yields (entry 3). Increasing the amount of mandelic acid caused a drastic decrease in yield (entries 4 and 5), while further decreasing the catalytic amount of additive also hindered the reaction (entry 6). Increasing the amount of NBS caused an increase in the brominated product (entry 7). Entries 8 and 9 showed the relative reaction rate. Since there

is no clear trend between pKa and reactivity, we turned to our colleagues in the Hratchian

theoretical group to evaluate the possibility of *in situ* interactions with NBS and the

additives to produce the reactive brominating species (Section 2.2.4).
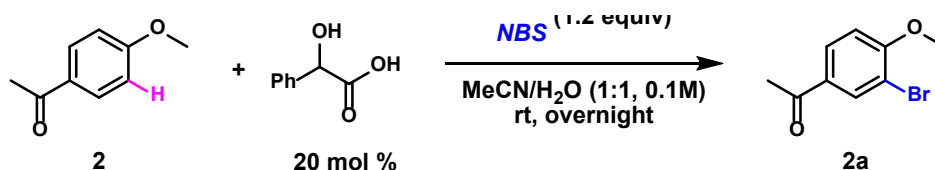
entry	deviation from standard conditions	yield
1	none	85
2	without mandelic acid	0
3	at 35 °C	91
4	mandelic acid (1.0 equiv)	51
5	mandelic acid (50 mol%)	71
6	mandelic acid (10 mol %)	64
7	NBS (1.5 equiv)	90
8	t= 30 minutes	trace
9	t= 4 hours	52
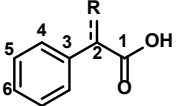
Table 2.3 Optimization of reaction conditions using Mandelic acid as the additive.

2.2.2 NMR study of additives with *N*-bromosuccinimide

To better understand how mandelic acid and benzoylformic acid were halogen-

bonding with NBS, ^{1}H NMR, and ^{13}C NMR spectroscopy were considered. Our *in situ* [1]H

NMR spectroscopy studies for mandelic acid showed negligible differences. We were able

to observe slight shifts in our ^{13}C NMR spectroscopy. The *in situ* NMR studies for

benzoylformic acid showed the degradation to form benzoic acid. For both additives
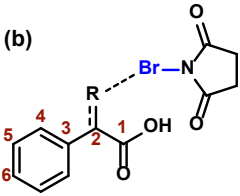
studied, the ^{13}C signals shifted to more upfield in the presence of NBS, with a more considerable shifting noted near sites of proposed halogen bonding.

(a)

	^{13}C NMR for C1 (ppm)	^{13}C NMR for C2 (ppm)	^{13}C NMR for C3 (ppm)	^{13}C NMR for C4 (ppm)	^{13}C NMR for C5 (ppm)	^{13}C NMR for C6 (ppm)
R = O	165.94	188.72	131.84	129.74	128.94	135.17
OH	175.04	72.38	138.44	126.63	128.50	128.32

(b)

	^{13}C NMR for C1 (ppm)	^{13}C NMR for C2 (ppm)	^{13}C NMR for C3 (ppm)	^{13}C NMR for C4 (ppm)	^{13}C NMR for C5 (ppm)	^{13}C NMR for C6 (ppm)
R = O	165.78	188.55	131.77	129.73	128.94	135.20
OH	174.98	72.34	138.40	126.59	128.47	128.29

Table 2.4 NMR study of additives with *N*-bromosuccinimide (a) ^{13}C NMR chemical shifts for additives. (b) ^{13}C NMR chemical shifts for additives in the presence of *N*-bromosuccinimide

2.2.3 Degradation of Amino acids investigation

As we contemplated how the structure of the lactic acid was important, we sought to explore the oxidative decarboxylation of amino acids in our reaction. We suspected that the amino acid acids were interacting with the NBS, as it is known that *N*-halosuccinimides can promote oxidative decarboxylation reactions in aqueous solvents.[18] A reaction was run under standard conditions replacing solvents with the deuterated versions and replacing lactic acid with phenylglycine; then, the reaction was monitored via 1H-NMR over the

course of 24 hours (**Figure 2.2**). The results of this ^{1}H-NMR study showed the reaction plateaued within less than two hours, and the degradation begins to interfere with the reaction almost immediately (see appendix B).
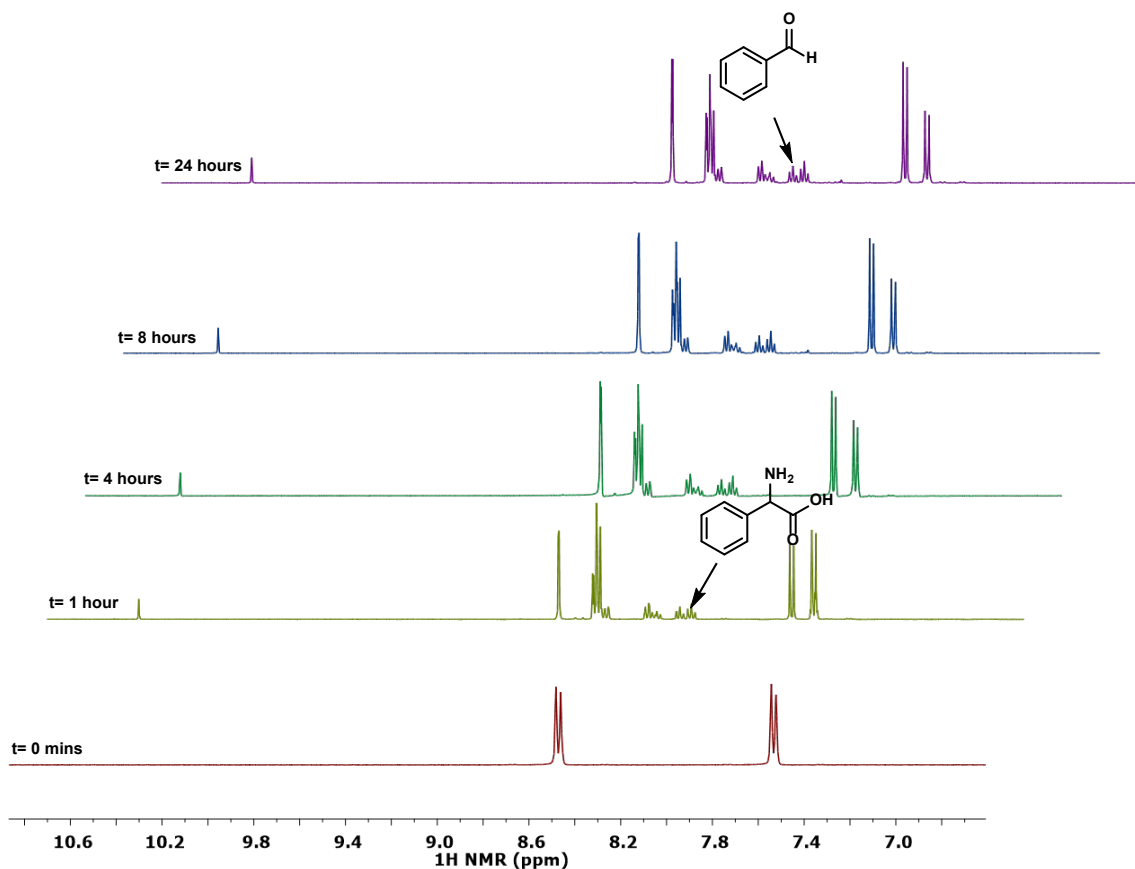
Figure 2.2 Processed kinetic NMR data for the degradation of phenylglycine in the presence of NBS. 4-methoxyacetophenone (0.2 mmol), NBS (0.24 mmol) with phenylglycine (0.04 mmol) in 1.0 mL CH_3CN and 1.0 mL D_2O over the course of 24h.

In order to prove the degradation was occurring as a side reaction when amino acids were used as the additives, we ran a ^{1}H-NMR study of phenylglycine and NBS under the same conditions. The results of this study showed the degradation of the amino acid phenylglycine almost immediately (Figure 2.2), indicating that an oxidative

decarboxylation was occurring on the timescale of a productive reaction causing the decrease in the brominated product.

2.2.4 Computational investigation

Our colleagues in the Hratchian lab undertook a thorough computation study to explore the electronic structure details responsible for enhancing reactivity. We hypothesized the formation of a halogen-bound complex, where the charge dipole influences the electronic characteristics of the bromine. Initial geometry optimizations of the NBS-additive complex using the B3PW91/6-311G(d) model chemistry that accounted for implicit solvation by acetonitrile using a local development version of Gaussian. The energetically favored geometries of the halogen-bound complexes for mandelic acid and NBS are presented below (**Figure 2.2**). We consider the NBS and the additives electrostatically bound for each of these complexes.
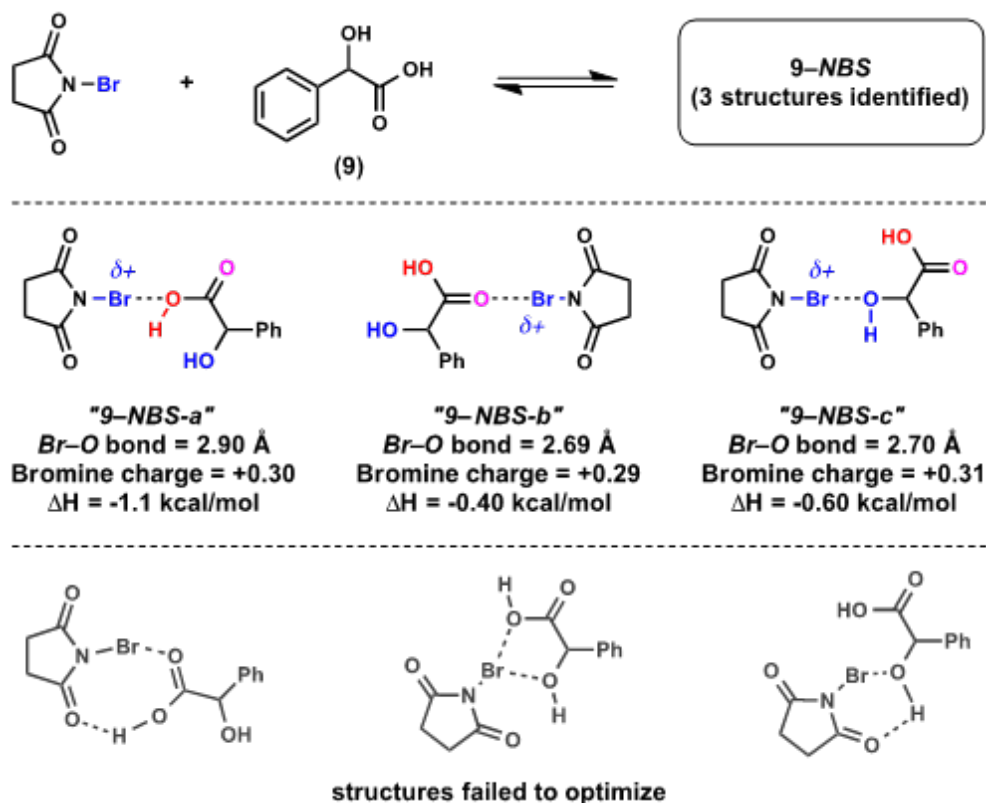
Figure 2.3 Computed values for halogen-bound structures of mandelic acid and NBS

Experimentally, the carboxylate and the α-alcohol were essential for the reaction to proceed. However, the calculations determined the optimized geometry did not utilize both positions for a halogen/hydrogen-bound species. The protonation of NBS via mandelic acid was determined to be unfavorable—the energetically favored geometries were calculated (**Figure 2.3**), presenting partial charges on bromine of approximately 0.30. The ΔHs of formation for each of these complexes are favorable and within 0.61 kcal/ mol. Similar calculations were run for benzoylformic acid–NBS halogen-bound species (**Figure 2.4**). The ΔHs of formation for each benzoylformic acid-NBS complex were determined to be favorable and within 0.60 kcal/mol
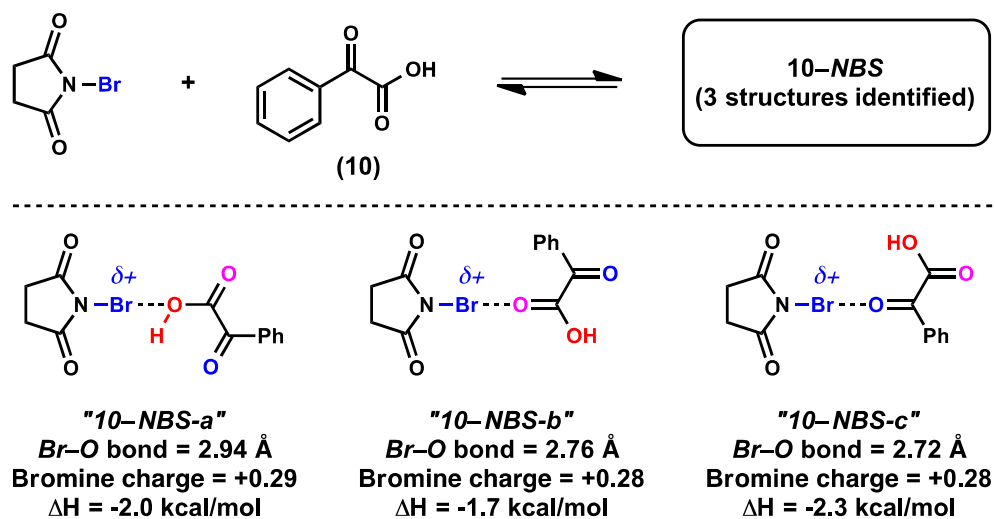
Figure 2.4 Computed values for halogen-bound structures of benzoylformic acid and NBS

Consistent with experimental results discussed in Table 2.3, computational data suggests the thermodynamically favorable formation of halogen-bound species of NBS can be with either mandelic or benzoylformic acid. Calculations suggest the halogen-bound species may enhance the reactivity of NBS due to the increase in electropositive characteristics at the bromine. Although calculations did not conclude the relevance of the α-groups, the NMR study in Section 2.2.2 and optimization proved otherwise.

2.2.5 Kinetics Investigation

To further understand the role of Lewis basic additives in bromination, we experimentally explored the kinetic effect catalytic additives had on reaction efficiency. It was previously mentioned secondary alcohols can be oxidized in the presence of NBS. To eliminate the possibility of mandelic acid being oxidized to benzoylformic acid *in-situ* NMR studies were conducted. ^{1}H NMR of bromination under standard reaction conditions was taken as the reaction progressed to track the formation of benzoylformic acid from mandelic acid. The ^{1}H NMR showed trace amounts of benzoylformic acid being formed, similar to our initial reaction predicted (**Figure 2.5**). These findings further confirm that any kinetic differences observed between mandelic acid and benzoylformic acid are not due to the oxidation of mandelic acid.
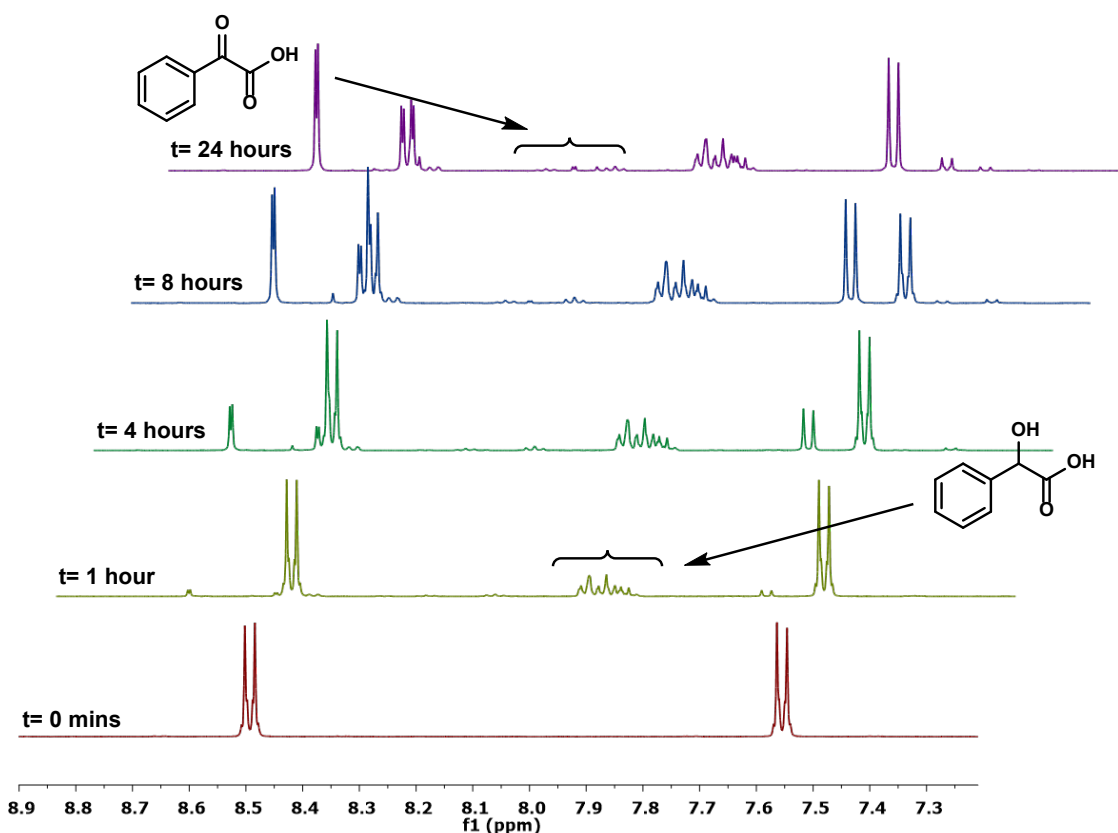
Figure 2.5 Processed kinetic NMR data for the formation of benzoylformic acid from mandelic acid. 4-methoxyacetophenone (0.2 mmol), *N*-bromosuccinimide (0.24 mmol) with mandelic acid (0.04 mmol) in 1.0 mL CH₃CN and 1.0 mL D₂O over the course of 24 h.

As shown in Figure 2.6, the rates of bromination for 4-methoxyacetophenone were compared at room temperature using either mandelic (red data) or benzoylformic acid (blue data) as catalytic additives. Although both reactions produce a high yield of the brominated product over the course of several hours (**Table 2.2, entries 8 and 10**), a significant (>2×) kinetic advantage is observed when using benzoylformic acid as the catalytic additive. Given the theoretical calculations determined the electropositive character of the bromine to be very similar, this was surprising. Further suggesting the bromination is not only dependent on the halogen-bound species but also the kinetics of the bromine transfer.

Based on reactivity alone, benzoylformic acid is the optimum catalytic additive to promote aromatic bromination under mild conditions. However, the high cost of benzoylformic acid compared to mandelic acid limits its use in large-scale applications ($460/mol vs. $21/mol, respectively). Because both additives generally produced similar conversions overall, we selected mandelic acid as our additive of choice due to its lower cost.
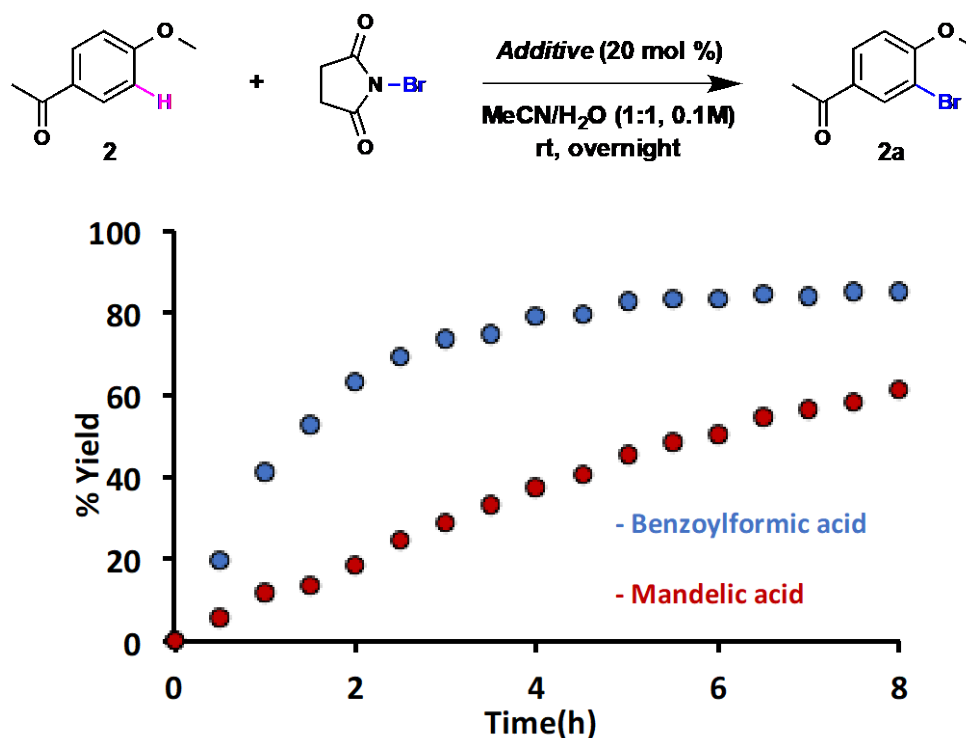
Figure 2.6 Rate comparison for the bromination of 4'-methoxyacetophenone in the presence of catalytic benzoylformic acid (blue data points) and mandelic acid (red data points).

2.2.6 Substrate Scope

Having optimized conditions in hand, we started exploring the bromination of various aromatic compounds. Substrates 1– 11 require catalytic mandelic acid to yield any brominated products at room temperature, with no reactivity observed using NBS alone (Scheme 2.2). It was also determined that the bromination was selective and only favored the formation of one product.
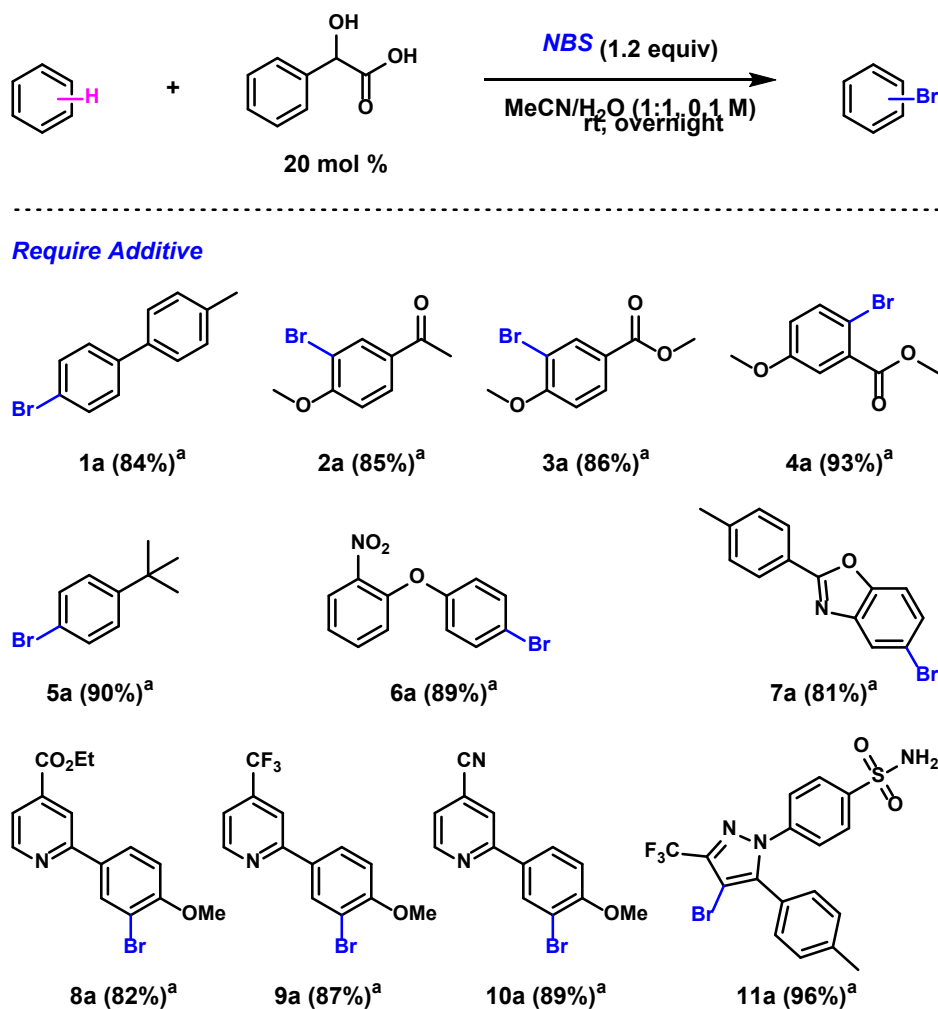
Scheme 2.2 Aromatic bromination of substrates that require mandelic acid. [a] General reaction conditions: (a) starting material (0.2 mmol), NBS (0.24 mmol), mandelic acid (0.04 mmol), and 2 mL of CAN/H$_2$O (1:1), rt for 24 h, yields reported as chromatography pure material.

Substrates 12−24 yield brominated products in the absence of mandelic acid, although increased reactivity is generally noted when catalytic mandelic acid is present (Scheme 2.3). It is worth noting these substrates are considered electron-rich and electron-rich substrates favor bromination without the addition of a catalyst. For these substrates, reaction conversion at 30 min under standard conditions is reported with and without mandelic acid for comparison.
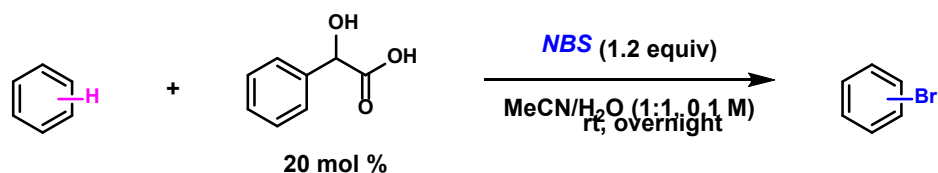
Work With & Without Additive

12a (96%)[a]
(15%)[b]
(0%)[c]

13a (86%)[a]
(96%)[b]
(41%)[c]

14a (92%)[a]
(100%)[b]
(100%)[c]

15a (92%)[a]
(100%)[b]
(100%)[c]

16a (87%)[a]
(93%)[b]
(93%)[c]

17a (85%)[a]
(85%)[b]
(85%)[c]

18a (83%)[a]
(90%)[b]
(90%)[c]

19a (72%)[a]
(17%)[b]
(0%)[c]

20a (85%)[a]
(28%)[b]
(28%)[c]

21a (82%)[a]
(100%)[b]
(100%)[c]

22a (85%)[a]
(100%)[b]
(100%)[c]

23a (85%)[a]
(100%)[b]
(100%)[c]

Scheme 2.3 Aromatic bromination of substrates that work with and without mandelic acid. General reaction conditions: (a) starting material (0.2 mmol), *NBS* (0.24 mmol), mandelic

acid (0.04 mmol), 2 mL ACN: H$_2$O (1:1), r.t. for up to 24 hours. Isolated yields are reported unless otherwise noted. (b) starting material (0.2 mmol), *NBS* (0.24 mmol), mandelic acid (0.04 mmol), 2 mL ACN: H$_2$O (1:1), r.t. for 30 minutes. (c) starting material (0.2 mmol), *NBS* (0.24 mmol), 2 mL ACN: H$_2$O (1:1), r.t. for 30- minutes. Crude conversions were determined for those working with and without additive within 30 minutes by crude 1H NMR.

Anisole derivatives with electron-withdrawing groups such as ketones and esters afforded the corresponding brominated compounds (2a−4a) in high yields. Alkyl substitutions are well-tolerated (5a, 13a), as are su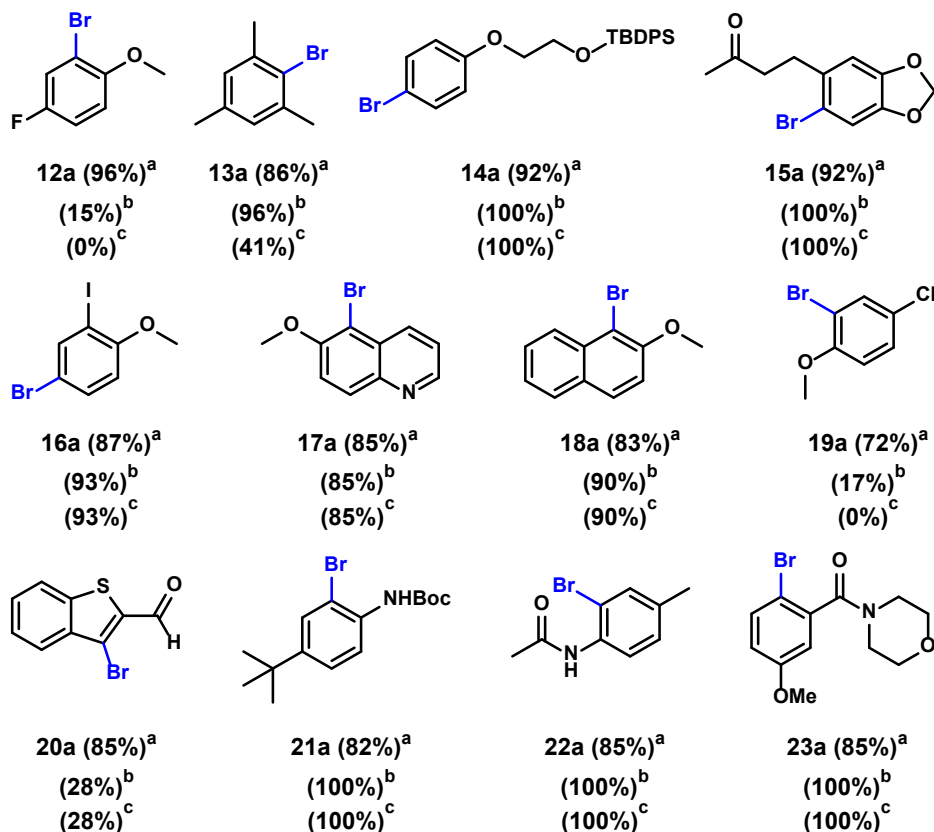bstrates with pre-installed halogens (12a, 16a, 19a). We were pleased to find that more substituted heterocyclic structures were tolerated (7a−10a, 20a), although an interesting reaction feature was noted. Pyridines substituted in the 4-position with electron-withdrawing groups (8-10) were brominated in excellent yields. Substrates containing electron-rich pyridine additives were not, suggesting the electron-rich pyridine hindered the reaction. These results are similar to the data discussed in section 2.2.1, whereby more Lewis basic pyridines react with NBS unproductively, preventing aromatic bromination (Table 2.1, entries 4−5). Similar results to the electron-rich pyridines were obtained when strongly Lewis basic substrates such as unprotected alcohols and amines, although protected primary alcohols (14a) and amides (21a−23a), participate in aromatic bromination to produce high yields. Electrophilic bromination was evaluated for the complex drug molecule, Celecoxib (11), resulting in high product yield. No reactivity is observed for the bromination of Celecoxib in the absence of catalytic mandelic acid. Suggesting when nitrogens are delocalized and no longer considered Lewis basic, they do not participate in halogen bonding. We believe the pyrazole and sulfonamide functional groups are well-tolerated because they do not interfere

with the halogen bonding interaction between NBS and mandelic acid. To date, we were pleased to find half of our substrates required mandelic acid for aromatic bromination. However, half of the substrates examined in (**Scheme 2.3**) produced brominated products by subjecting them to NBS at room temperature. We noted substrate-dependent variations in reaction efficiency when using catalytic amounts of mandelic acid.

2.2.7 NMR Rate Comparison study for 4-fluoroanisole

After our initial investigation of reaction efficiency when using catalytic amounts of mandelic acid, we investigated how substrate 12 tolerated the reaction. Only trace amounts of 12a were observed via thin-layer chromatography (TLC) over the course of several hours when subjected to NBS alone, but a significant amount of product was formed in the same period of time when using 20 mol % mandelic acid at room temperature. Time-course studies via ^{1}H NMR under synthetic conditions further measured this effect (**Figure 2.7**). In the duration of 4 h, when 12 was subjected to the reaction in the presence of a catalytic amount of mandelic acid or benzoylformic acid, the reaction was nearly complete. In comparison, only ~20% conversion was noted during the same timeframe with no additive present. An induction period is observed for the reaction without an additive and the reaction with mandelic acid (**Figure 2.7**). The induction period appears to be substrate dependent, as no initiation period was observed in figure 2.6. The data compiled between Figures 2.6 and 2.7 supports our hypothesis that the presence of mandelic acid yields a more reactive brominating species regardless of the identity of the arene substrate.

55
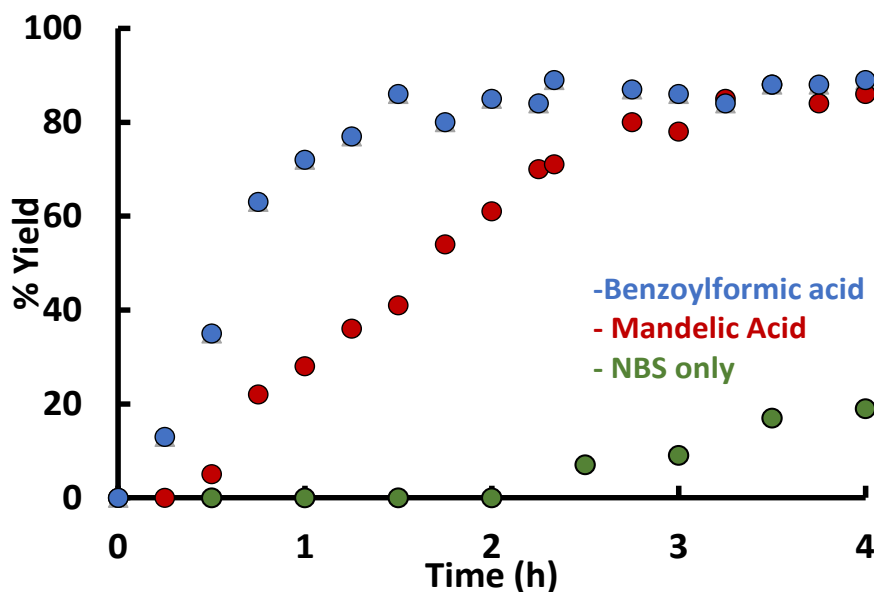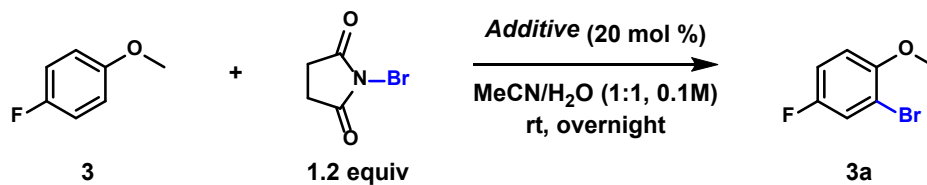
Figure 2.7 Kinetic rate comparison of 4-fluoroanisole with and without additives. Conditions: **a.** 100 uL aliquot of 4-methoxyacetophenone (0.2 mmol), *N*-bromosuccinimide (0.24 mmol) in 1.0 mL CH3CN and 1.0 mL D2O over the course of 4 h; (green) **b.** 100 uL aliquot of 4-methoxyacetophenone (0.2 mmol), *N*-bromosuccinimide (0.24 mmol) with mandelic acid (0.04 mmol) in 1.0 mL CH3CN and 1.0 mL D2O over the course of 4 h; (red) **c.** 100 uL aliquot of 4-methoxyacetophenone (0.2 mmol), *N*-bromosuccinimide (0.24 mmol) with benzoylformic acid (0.04 mmol) in 1.0 mL CH3CN and 1.0 mL D2O over the course of 4 h; (blue)

2.3 Summary Electrophilic Aromatic Bromination

In summary, we have developed a simple method for aromatic bromination under mid conditions. Catalytic amounts of lactic acid derivatives were shown to enable or increase the efficacy of bromination depending on the inherent reactivity of the aromatic substrate.

We have experimental and computational data to support the halogen bonding interaction of NBS with lactic acid derivatives. Calculations show increased electrophilicity of the bromine source due to halogen bonding. Experimental data demonstrate a direct example of amino acids undergoing degradation in the presence of NBS and eliminate the question of secondary alcohols undergoing oxidation. Kinetic comparisons showed that catalytic additives promote bromination via enhanced reaction rates. Mandelic acid was chosen as the additive based on enhanced reactivity and cost-effectiveness when considering large-scale reactions.

This work inspired us to investigate the bromohydrin formation of olefins by invoking halogen bonding between NBS and mandelic acid. Chapter three of this dissertation explores our goals and preliminary data on this topic.

2.4 References

(1) (a) Ruiz-Castillo, P.; Buchwald, S. *Chem. Rev.,* **2016**, *116*, 12564. (b) Wilcken, R.; Zimmermann, M.; Lange, A.; Joerger, *J. Med. Chem.,* **2013**, *56*, 4, 1363–1388. (c) Jeschke, P. *Pest Manag. Sci.,* **2017**, *73*, 1053-1066 (d) Fuge, R. *Environ. Geochem. Health*, **1988**, *10*, 51–61.

(2) Datta, R.; Chatterjee, N. Halogenation. XIV. *J. Am. Chem. Soc.,* **1916**, *38*, 11, 2545–2552.

(3) (a) Djerassi, C. *Chem. Rev.,* **1948**, *43*, 2, 271–317. (b) Robert, I.; Kimball, G. The Halogenation of ethylenes. *J. Am. Chem. Soc.,* **1937**, *59*, 5, 947–948.

(4) Mitchell, R.; Lai, Y.; Williams, R. *J. Org. Chem.,* **1979**, *44*, 25, 4733–4735. (b) Rogers, D.; Brown, R.; Brandeburg, Z.; Ko, E.; Hopkins, M.; LeBlanc, G.; Lamar, A. *ACS Omega*, **2018**, *3*, 12868–12877. (c) Stilinovic, V.; Horvat, G.; Hrenar, T.; Nemec, V.; Cincic, D. *Chem Eur. J.*, **2017**, *23*, 5244–5257. (d) Pramanick, P.; Hou, Z.; Yao, B. *Tetrahedron,* **2017**, *73*, 7105–7114.

(5) (a) Zhang, Y.; Shibatomi, K.; Yamamoto, H. *Synlett,* **2005**, *18*, 2837–2842. (b) Firouzabadi, H.; Iranpoor, N.; Jafarpour, M. *Tetrahedron Lett.,* **2004**, *45*, 7451. (c) Shi, L.; Zhang, D.; Lin, R.; Zhang, C.; Li, X.; Jiao, N. *Tetrahedron Lett.,* **2014**, *55*, 2243–2245.

(6) (a) Bulfield, D.; Huber, S. M. *Chem. Eur. J.* **2016**, *22*, 14434. (b) Guha, S.; Kazi, I.; Nandy, A.; Sekar, G. *Eur. J. Org. Chem.,* **2017**, 5497–5518. (c) Samanta, R.; Yamamoto, H. *Chem. Eur. J.,* **2015**, *21*, 11976–11979. (d) Lorpaiboon, W.; Bovonsombat, P.; *Org. Biomol. Chem.,* **2021***, 19,* 7518–7534*.

(7) (a) Bovonsombat, P.; Sophanpanichkul, P.; Pandey, A.; Tungsirisurp, S.; Limthavornlit, P.; Chobtumskul, K.; Kuhataparuk, P.; Sathityatiwat, S.; Teecomegaet, P. *Tetrahedron Lett.,* **2015**, *56*, 2193–2196. (b) Jakab, G.; Hosseini, A.; Hausmann, H.; Schreiner, P. R. *Synthesis,* **2013**, *45*, 1635–1640. (c) Bovonsombat, P.; Stone, S.; Rossi, M.; Caruso, F. *Struct. Chem.,* **2019**, *30*, 2205–2215.

(8) Maddox, S. M.; Nalbandian, C. J.; Smith, D. E.; Gustafson, J. L. *Org. Lett.,* **2015**, *17*, 1042–1045.

(9) Xiong, X.; Tan, F.; Yeung, Y. *Org. Lett.,* **2017**, *19*, 4243–4246.

(10) Hirose, Y.; Yamazaki, M.; Nogata, M.; Nakamura, A.; Maegawa, T. *J. Org. Chem.,* **2019**, *84*, 7405–7410.

(11) Iida, K.; Ishida, S.; Watanabe, T.; Arai, T. *J. Org. Chem.,* **2019**, *84*. 7411–7417.

(12) Nishii, Y.; Ikeda, M.; Hayashi, Y.; Kawauchi, S.; Miura, M. *J. Am. Chem. Soc.,* **2020**, *142*, 1621–1629.

(13) Tang, R. J.; Milcent, T.; Crousse, B. *J. Org. Chem.,* **2018**, *83*, 930–938.

(14) "*1,1,1,3,3,3-Hexafluoroisopropanol*" MSDS No. AC293410000; ThermoFisher Scientific: Fair Lawn, NJ, March 21, 2011.

https://www.fishersci.com/shop/msdsproxy?storeId=10652&productName=AC293410500

(15) Hua, A. M.; Bidwell, S. L.; Baker, S. I.; H. Hratchian, H. P.; Baxter, R. D. *ACS Catal.,* **2018**, *9*, 3322–3326.

(16) Cavallo, G.; Metrangolo, P.; Milani, R.; Pilati, T.; Priimagi, A.; Resnati, G.; Terraneo, G. *Chem. Rev.,* **2016**, *116*, 4, 2478–2601.

(17) Pereira, C.; Silva, V.; Rodrigues, A. *Green Chem.,* **2011**, *13*, 2658–2671.

(18) Venkatasubramnian, N.; Thiagarajan, V. *Can. J. Chem.,* **1969**, *47*, 694–697. (a) Ramachandran, M.S.; Easwaramoorthy, D.; Rajasingh, V.; Vivekanadam, T.S. *Bull. Chem. Soc. Jpn.,* **1990**, *63*, 2397–2403. (b) Gopalakrishnan, G.; Hogg, J. *J. Org. Chem.,* **1985**, *50*, 1206–1212. (c) Chappelee, E. W.; Luck, J. M. *J. Biol. Chem.,* **1957**, *229*, 1, 171-179. (d) Konigsberg, N.; Stevenson, G.; Luck, J. *J. Biol. Chem*., **1960**, *235*, 5, 1341–1345.

Chapter 3

Halohydrin Formation of Alkenes Using Various Brominating Reagents

3.1 Introduction

Halohydrins are valuable tools, consisting of a hydroxyl and halogen group bonded to adjacent carbons. [1] Its unique structure makes it synthetically useful for various applications. Halohydrins can be used in organometallics to form new carbon-carbon bonds, synthesis of pharmaceuticals, track the kinetic resolution of epoxides, and can be utilized in the degradation of halogenated environmental pollutants. [2,3]

Traditionally, undergraduate students learn about the formation of halohydrins during the first semester of organic chemistry. When introduced, the textbook teaches students that the halohydrin mechanism proceeds when a nucleophilic alkene attacks the halogen source (Br_2 or Cl_2), creating an induced dipole on the diatomic halogen. The partial positive on the halogen forms the electrophile, and now it can add to the sp^2 carbon of the alkene.[4] The addition of the electrophilic halogen generates an unstable bridged intermediate, and an electrophilic solvent, such as water, adds to the unstable intermediate, producing the halohydrin product **(Figure 3.1)**. Students are usually unaware of alternative electrophilic halogen sources that exist.
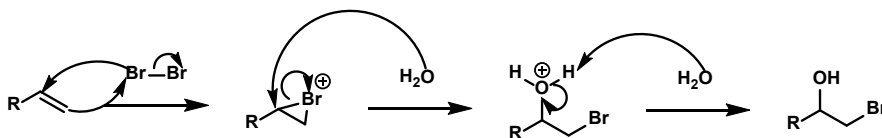

**Figure 3.1.** Mechanism for bromohydrin using bromine.

In 1952, chemists began utilizing *N*-bromosuccinimide as an alternative electrophilic bromine source for halohydrin formation. [5] Previously, scientists studied the use of NBS for electrophilic aromatic and allylic bromination. [6] Ziegler concluded the bromine of the NBS had a slightly positive charge making it an ideal electrophile.[7] Following this discovery, Guss and Rosenthal published the first example of bromohydrins from olefins using NBS in water.[8] Using methodology previously developed for bromohydrin formation with *N*-bromoacetamide, NBS showed useful as a more stable alternative **(scheme 3.1)**.

Scheme 3.1. Bromohydrin formation in H_2O
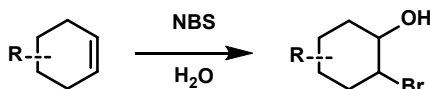
A similar methodology was later developed by Jones and co-workers to promote the bromohydrin formation of unsymmetrical alkene derivatives in DMSO.[9] Labeling experiments were conducted to determine if the bridged halogen intermediate still exists when using NBS as the bromine source. The results of this experiment were unable to conclude the exact mechanism but did demonstrate that highly hindered olefins produce the bromohydrin on the most stable carbonium ion **(scheme 3.2)**. This methodology proved tolerant to unsymmetrical alkenes but had little success when the alkene contained electron-withdrawing substituents and when the alkene was semi-symmetrical or if it contained neighboring carbons with the same hybridization.

Scheme 3.2. Bromohydrin formation investigation in DMSO

note: the ratio of i:ii is 42:57.
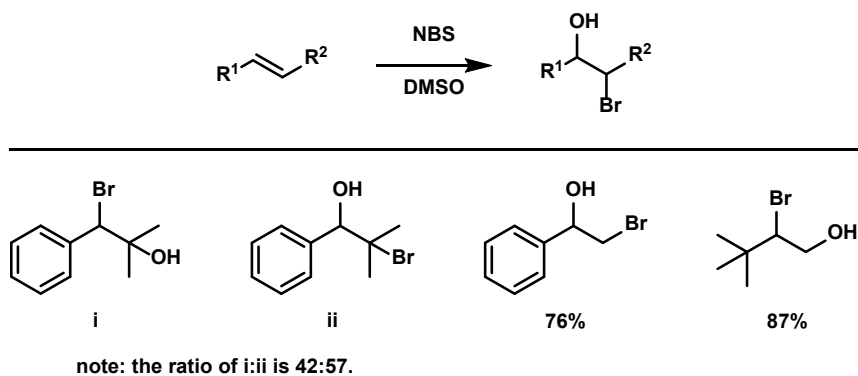
A considerable amount of literature has been published on the formation of bromohydrin compounds. These studies have reported different methods for synthesizing bromohydrins using various reagents such as elemental halogen catalysts[10], metal catalysts[11], and organic solvents.[12] In our recent work demonstrating electrophilic aromatic bromination, we investigated the halogen bonding interaction between lactic acid derivatives and *N*-bromosuccinimide.[13] We identified a simple strategy to enhance bromination using NBS when using catalytic amounts of lactic acid derivatives. We sought to expand this strategy to include the asymmetric formation of alkenes using NBS and mandelic acid.

Currently, there are very few examples of asymmetric halohydrin formation of olefins, and the published methodologies use exotic metal catalysts and alternative toxic halogen sources.[14] The most recent methodology for asymmetric bromohydrin formation from Karmakar and co-workers tests a variety of Lewis acid catalysts with *N*-halosuccinimide.[15]

Scheme 3.3 Lewis acid catalyzed asymmetric bromohydrin formation
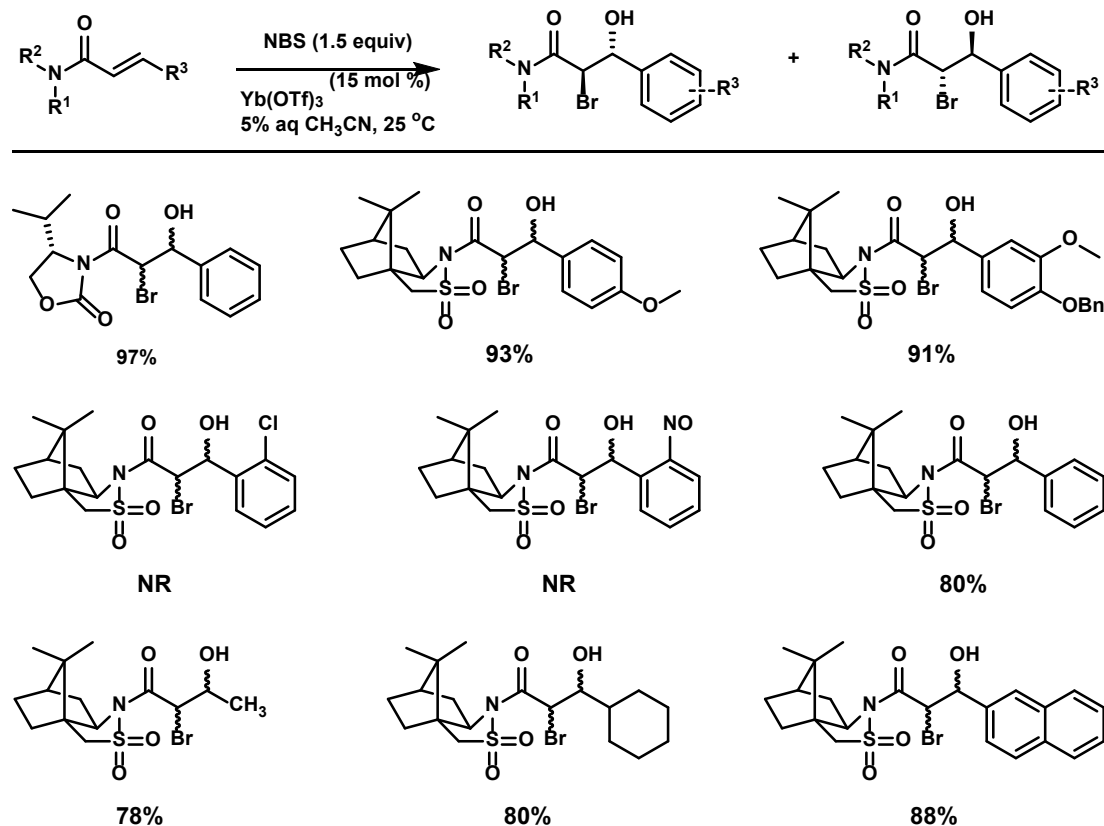
Using knowledge previously gained by Rancourt and co-workers,[16] α,β-unsaturated carbonyls underwent halohydrin formation in the presence of NBS/NIS and H_2SO_4. The asymmetric bromohydrin reaction of chiral α,β-unsaturated carboxylic acid derivatives using *N*-halosuccinimide as halogen sources found using the Lewis acid, Ytterbium triflate, $Yb(OTf)_3$ to catalyze the reaction was the most efficient **(scheme 3.3)**. The methodology tolerated electron-rich cinnamoyl substrates but found highly electron-rich substrates

favored electrophilic aromatic bromination over the bromohydrin formation. Under these specific reaction conditions, the reaction yielded 100% regio-selective product distribution.

3.2 Results and Discussion

3.2.1 Preliminary Results of NBS

As discussed in section 2.1, our group had recently expanded upon the current methodology for the bromination of aromatic compounds. In an effort to continue the development of halogen–bonding with NBS, we began to investigate if the conditions from our aromatic bromination could be applied to alkenes to form asymmetric bromohydrins. Trans-β-methylstyrene was used as the alkene for our investigation (Table 3.1). To begin, we ran the experiment with our standard conditions without any deviation (entry 1). We found the reaction yielded a di-brominated product without any formation of the bromohydrin. The reaction proceeded without the addition of mandelic acid, but clearly, there is an additive effect when it is present (entry 2). These results are similar to our aromatic bromination. Our goal of bromohydrin was not possible when NBS was in excess, so we lowered the equivalency of NBS (entry 3). We found that the di-brominated trans-β-methylstyrene was still the major product, so we set out to see if we could manipulate the reaction to get our desired outcome.

Table 3.1 Investigation of NBS with olefin. Yields are determined where NBS is the limiting reactant.
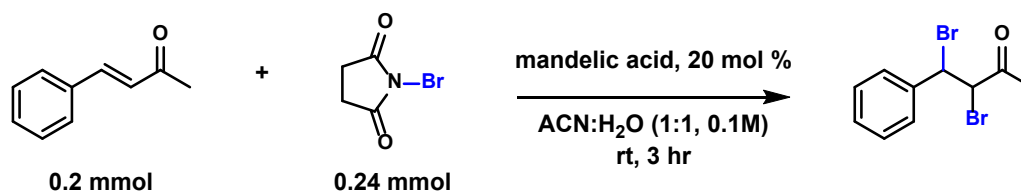
entry	deviation from standard conditions	Yield
1	none	94
2	without mandelic acid	45
3	1.0 equiv of NBS	78
4	0 °C	89
5	in the dark	85
6	recrystallized NBS	93
7	no water	trace
8	TEMPO as a radical trap	0

We began by running the reaction at 0 °C, to see if the temperature was responsible (entry 4). To avoid the reaction being catalyzed by light, it was run in an amber reaction vial and covered with foil (entry 5). Ziegler documented that NBS is usually contaminated with trace amounts of hydrobromic acid (HBr) when left out at room temperature.[6] If HBr is present, it could promote bromination via a radical process. The NBS was recrystallized and used immediately in the reaction to determine if the HBr was responsible for catalyzing di-bromination. Entry 6 demonstrates the presence of trace HBr did not affect the outcome of the reaction. Water can also result in the presence of HBr, but the removal of water completely shuts down the reaction (entry 7). We ran a reaction with TEMPO, the radical trap, and as expected, the reaction resulted in zero conversion (entry 8). No matter the conditions with NBS, the di-brominated product was yielded and proceeded via a radical

mechanism, making it challenging to install chirality. Since our standard reaction conditions using NBS did not form the desired outcome, we began examining the use of other brominating reagents.

3.2.2 Preliminary Results of the Different Brominating Reagent *N*-bromosultam

Recently our lab published and designed a new reagent used for nitrosation under mild conditions.[17] This unique reagent is stable to air and moisture and can be used in various solvents. The design and structural features of the reagent had us curious if we could use a derivative of it containing bromine as a brominating reagent. In 1993, Saveant et al. published a paper in which they investigated controlling factors of stepwise and concerted reductive cleavages using aromatic *N*-halosultams.[18] This work explores the electrochemical reduction of the N-Halogen bond in saccharin halosultams. Saveant found the saccharin halosultams undergo a two-electron process and found it challenging to reproduce the work for the bromine and chlorine derivatives. Given their findings, we set out to see if this new brominating reagent could be employed in our research (table 3.2).

Table 3.2 Investigation of *N*-bromosultam reagent
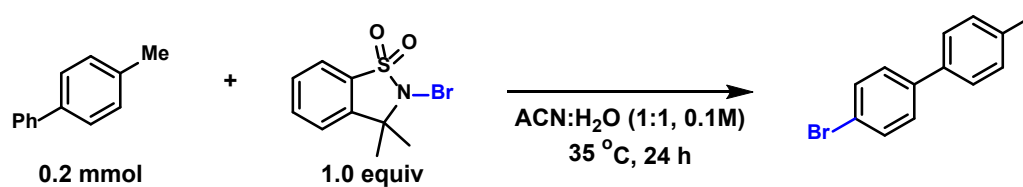
| entry	deviation from standard conditions	Yield
1	none	39
2	room temp	0
3	with mandelic acid (20 mol %)	60
4	with TFA (20 mol %)	82
5	with saccharin (20 mol %)	77

Our initial findings determined that the reaction was unfavorable at room temperature (entry 2). If the reaction was completed at a slightly elevated room temperature, we obtained an increase in yield (entry 1). Following these low-yield reactions, we subjected the reagent to our traditional brominating conditions where mandelic acid is used as an additive (entry 3). To our luck, the additive mandelic acid caused a 20% increase in product conversion. Mandelic acid has a pKa of 3.4, making it a relatively weak acid. To see if the strength of the acid could induce a higher product conversion, we replaced mandelic acid with trifluoroacetic acid (TFA). TFA has a known pKa of 0.52, making it a significantly stronger acid than mandelic acid but not as strong as hydrochloric acid (HCl). The change in acid from mandelic acid to TFA caused an increase in yield (entry 4). As previously mentioned, *N*-bromosultam is a derivative of saccharin, and saccharin is considered acidic with a pKa of 1.6, which is not as strong as TFA but is

not as weak as mandelic acid. Entry 5 reveals a boost in reactivity when TFA is replaced with saccharin. What is interesting in this data is that the saccharin had an additive effect; this result also suggests the possibility of trans-bromination occurring between our *N*-bromosultam and saccharin. Comparing the three reagents would establish the probability of which reagent is best for the halohydrin formation. The findings from table 3.2 suggest an alternative brominating reagent, such as *N*-bromosaccharin, may be responsible for product conversion. To determine the reagent responsible for bromination in our reaction with saccharin, we had to first understand the electrophilicity of each reagent.

### 3.2.3 Comparing the Electrophilicity

  N-bromosaccharin was synthesized using the method detailed in scheme 3.4.[19] To compare the electrophilicity of the three different reagents, we tested each in previously established aromatic bromination conditions without mandelic acid. We determined the electrophilicity of NBS is enhanced by replacing one carbonyl group with a sulfonyl group.

Scheme 3.4 Established synthesis for *N*-bromosaccharin
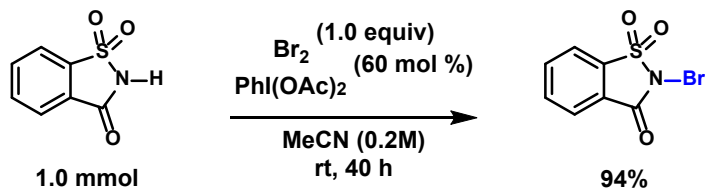
During our investigation, we found that NBS was the least electrophilic, as it yielded 0% of the product when the reaction was unheated. We attempted the same reaction

but heated it to a slightly elevated room temperature of 35 °C (Table 3.3, 2). The same reactions were run with *N*-bromosultam and *N*-bromosaccharin. The reactions with *N*-bromosultam yielded similar results at room temperature. The elevated temperature reaction increased product conversions more than NBS alone, yielding 39%. The most impressive finding was the drastic increase in product conversion when *N*-bromosaccharin was used. We found that the reaction yielded 85% at room temperature, and when the temperature was increased to 35 °C, it improved to 94%.
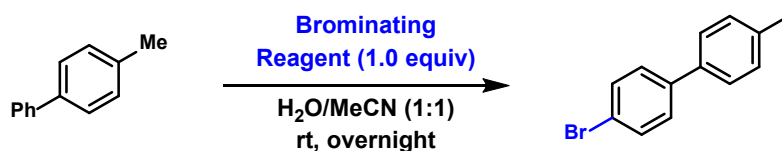
entry	deviation from standard conditions	Yield
1	*N*-bromosuccinimide	0
2	*N*-bromosuccinimide at 35 °C	26
3	*N*-bromosultam	0
4	*N*-bromosultam at 35 °C	39
5	*N*-bromosaccharin	85
6	*N*-bromosaccharin at 35 °C	94

**Table 3.3.** Results from various brominating reagents

3.2.4 Halohydrin Formation

Given the instability of the *N*-bromosultam and its complex synthesis, we suspected that the bromohydrin formation across an alkene may be unfavorable and likely result in the di-brominated product similar to NBS due to its lower electrophilicity. We continued our research using *N*-bromosaccharin, hoping the increase in electrophilicity would

facilitate the desired product. Current literature search demonstrates bromohydrin formation is possible under certain conditions when using *N*-bromosaccharin.

The first discussion and analyses of *N*-bromosaccharin (NBSa) emerged in 1976.[20] After the successful synthesis, Sanchez demonstrated the reagent's ability to work for benzylic bromination of toluene. Following this innovation, various groups have used NBSa for a variety of applications, such as the oxidation of aldehydes, ketones, and alcohols, for the halogenation of aromatic compounds, the cleavage of oximes and the conversion of alcohols to bromides. [23] In 2003, de Mattos' lab found that NBSa could also be used for bromohydrin formation using alkenes. Following this advancement, the Dolenc lab found that NBSa works to brominate deactivated alkenes. [24] Currently, these two methods are the only examples of halohydrin formation using this reagent. Inspired by the literature search and our recent work using lactic acid derivatives to activate NBS via halogen bonding, we contemplated invoking this strategy to install an asymmetric bromohydrin.

Scheme 3.5 Results from NBSa with benzalacetone

| 0.2 mmol | 1.0 equiv | | 97% |
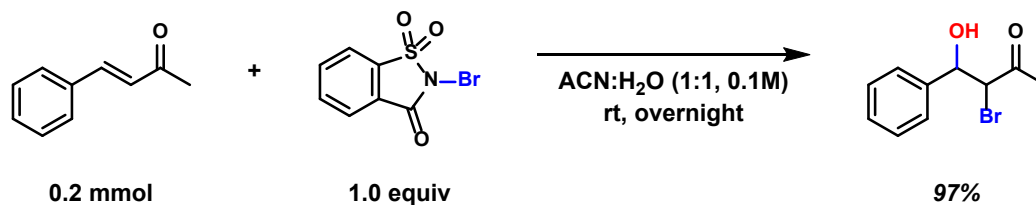
An initial objective of the project was to identify if NBSa could form the bromohydrin product in our set reaction conditions. **Scheme 3.5** demonstrates our reaction conditions using benzalacetone as the olefin, which produced the desired product with a yield of 97%. Our next goal was to determine if mandelic acid could have an additive effect similar to the aromatic project. To do this, we chose a substrate that failed for aromatic bromination, p-Anisaldehyde. The results of this study did not show any significant increase in aromatic bromination (Scheme 3.6). Suggesting mandelic acid will not have an additive effect with NBSa as it did with NBS.
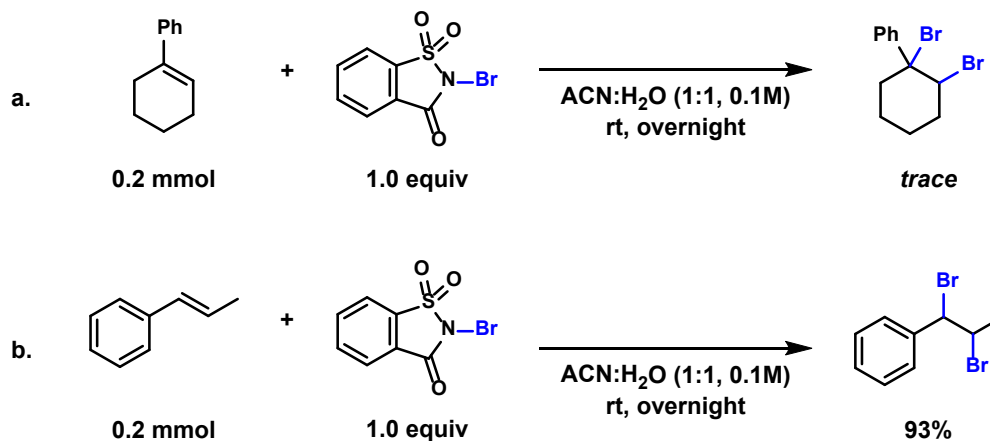
Scheme 3.6 Results from NBSa with p-Anisaldehyde
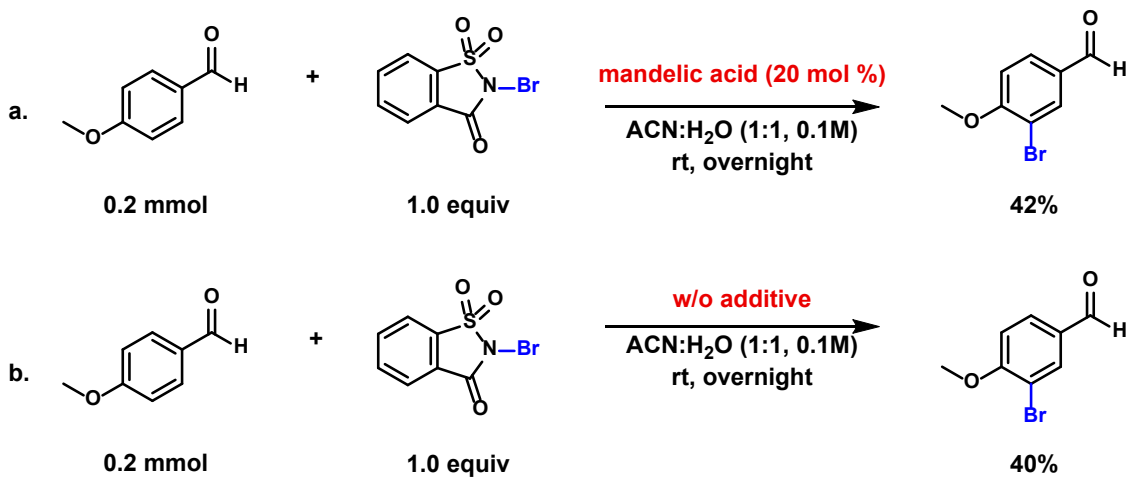
To establish whether the carbonyl group is essential, we substituted benzalacetone with 1-phenyl-1-cyclohexene and trans-β- methylstyrene. The 1-phenyl-1-cyclohexene reaction produced trace amounts of the di-brominated product, suggesting the alkene may be sterically inaccessible (Scheme 3.7a). The results obtained from the preliminary analysis of trans-β-methylstyrene indicate a correlation between the carbonyl group and the

bromohydrin product's formation since the reaction exclusively formed a di-brominated product (scheme 3.7b).

Scheme 3.7 Determination of carbonyl importance

a. 0.2 mmol + 1.0 equiv → ACN:H$_2$O (1:1, 0.1M) rt, overnight → *trace*

b. 0.2 mmol + 1.0 equiv → ACN:H$_2$O (1:1, 0.1M) rt, overnight → 93%

3.3 Summary of Bromohydrin Formation

In summary, we have preliminary data to suggest the bromohydrin formation from *N*-bromosaccharin is more complex than initially thought. Our next step in continuing this project is to determine if the oxygen's electronegativity from the carbonyl dictates the product or if it is possible to protect the oxygen or replace it with other electronegative groups to produce the desired product. After completing this investigation, we can design a catalyst to invoke chirality.

3.4 References

(1) Moss, G. P., Smith, A. S., Tavernier, D. *Pure & Appl. Chem.* **1995**, 67, 1307-1375.
(2) Moschona, F., Savvopoulou, I., Tritopoulou, M., Tataraki, D., Rassias, G. *Catalysts*, **2020**, 10, 1117.
(3) You, Z. Y., Liu, Z. Q., Zheng, Y. G. *Appl. Microbiol Biotechnol.* **2013**, 97, 9-21.
(4) Bruice, P. Y. *Pearson/Prentic Hall*, **2004**, 8, 255-257.
(5) H. L. Slates and N. L. Wendler, J. Amer. Chem. Soc, 1956, 78, 3751.
(6) Djerassi, C. *Chem. Rev.* **1948**, 43, 2, 271 – 317.
(7) Novikov, S. S., Sevost'yanova, V. V., Fainzil'berg, A. A. *Russ. Chem. Rev.* **1962**, 31, 671-681.
(8) Guss, C. O., Rosenthanl, R. *J. Am. Chem. Soc.* **1955**, 77, 9, 2549.
(9) Lodh, R.S., Boran, A. J., Phukan, P. *Ind. J. of Chem.* , **2014**, 53B, 1425-1429
(10) Saikia, I., Borah, A. J., Phukan, P. *Chem. Rev.* **2016**, 116, 6837-7042.
(11) Dalton, D. R., Dutta, V. P., Jones, D. C., *J. Amer. Chem. Soc.,* **1968**, 90, 20, 5498-5501.
(12) Raghavan, S., Rasheed, M. A., Joseph, S. J., Rajender, A. *Chem. Commun.,* **1999**, 1845-1846.
(13) Baker, S. I., Yaghoubi, M., Bidwell, S. L., Pierce, S. L, Hratchian, H. H., Baxter, R. D. *J. Org. Chem.* **2022**, 87, 13, 8492-8502.
(14) Catellanos, A., Fletcher, S.A. *Chem. Eur. J.* **2011**, 17, 5766-5766.
(15) Hajra, S., Bhowmick, M., Karmakar, A. *Tetra. Lett.* **2005**, 3073-3077.
(16) Guindon, Y.; Rancourt, J. J. Org. Chem. **1998**, 63, 6554.
(17) Galloway, J. D., Sarabia, C., Fettinger, J. C., Hratchian, H. P, Baxter, R. D. *Org. Lett.* **2021**, 23, 9, 3253-3258.
(18) Andrieux, C. P., Differding, E., Robert, M., Saveant, J. M. *J. Am. Chem. Soc.* **1993**, 115, 15, 6592-6599.
(19) Dolenc, D.; *Synlett* **2000**, 544.
(20) De Souza, S. P. L.; Da Silva, J. F. M.; De Mattos, M. C. S., *J. Braz. Chem. Soc.* **2003**, *14*, 832.
(21) Kim, Y. *Encyclopedia of Reagents for Organic Synthesis.,* **2012**, 1-3.
(22) De Souza, A. V. A, Mendonca, G., F., Bernini, R. B., De Matto, M. C. S. *J. Braz. Chem. Soc.,* **2007**, 18, 8, 1575-1579.
(23) Urankar, D., Rutar, I., Modec, B., Dolenc, D. *Eur. J. Org. Chem,* **2005**, 2349-2353.

APPENDIX

General Considerations

Reagents and solvents were purchased at the highest commercial quality and used without purification. Yields refer to chromatographically and spectroscopically (1H NMR, 13C NMR, 19F NMR) homogenous material unless otherwise noted. The yields in the Supporting Information describe the result of a single experiment. Reactions were monitored by GCMS (Agilent Technologies 5975 Series MSD GCMS) and thin-layer chromatography using 0.25 mm E. Merck silica gel plates (60F-254) using UV light. NMR spectra were recorded on a Varian-INOVA 400 MHz or 500 MHz spectrometer and calibrated using residual undeuterated solvent as an internal reference (CDCl3 – 1H NMR: 7.26 ppm, 13C NMR: 77.16 ppm; CD3CN – 1H NMR: 1.94 ppm, 13C NMR: 1.32 ppm), whereas for 15N spectra, a sealed capillary filled with nitromethane (0 ppm) was used as an internal standard, and for 19F spectra, a sealed capillary filled with hexafluorobenzene (-164.90 ppm) was used. The following abbreviations were used to explain multiplicities (s – singlet, d – doublet, t – triplet, q – quartet, m – multiplet).

APPENDIX – A

Experimental Set Up: Benzylic C–H Fluorination promoted by $[N–F–N]^+$ Halogen Bonding

General Procedure

The threads of a 3 mL borosilicate scintillation vial were thoroughly taped with Teflon tape. To this vial containing a stir bar was added Selectfluor (142 mg, 0.4 mmol, 2 equiv), and arene (0.2 mmol, 1 equiv). Acetonitrile (1 mL) and H2O (0.9 mL) were then added and stirred for approximately 1 min at room temperature. A solution of AgNO3 (0.1 mL of a 0.4 M solution in H2O, 0.04 mmol) was added in one portion and stirred at 35 °C for approximately 10 minutes before the pyridine additive (0.2 mmol, 1 equiv) was added. The reaction was capped with a teflon screw cap and rubber septum (24/40). The reaction was heated to 35 °C until reaction was completed as judged by GCMS (up to 24 hours).

Upon completion, the reaction was diluted with ethyl acetate (1 mL) and transferred to a test tube containing saturated NaHCO3 (3 mL). The aqueous phase was extracted with ethyl acetate (3 x 3 mL) and the combined organic layers were dried over MgSO4, filtered and carefully concentrated *en vacuo* due to product volatility. The crude material was purified by silica gel chromatography (ethyl acetate:hexanes) to yield the desired fluorinated products.

The reaction was diluted with ethyl acetate (1 mL) and transferred to a test tube containing saturated NaHCO3 (3 mL) and 1,3,5-trimethoxybenzene (16.8 mg, 0.1 mmol) as an internal standard. The aqueous phase was extracted with ethyl acetate (3 x 3 mL) and the combined organic layers were dried over MgSO4, filtered and carefully concentrated *en vacuo*. NMR yields were then determined from 1H NMR spectroscopic

High Resolution Mass Spectroscopy (HRMS)

General Procedure

An aliquot (~70 uL) of the reaction mixture was diluted with HPLC grade CH3CN/H2O (1:1) to approximately 2 mL. The resulting solution was then filtered and injected onto the HRMS. Data collection was done using factory default parameters for positive ion ESI-MS.

Cyclic Voltammetry Experiments

General Procedure

In a borosilicate scintillation cell, tetrabutylammonium tetrafluoroborate supporting electrolyte solution was added (5ml, 0.1 M in CH3CN). The glassy carbon working electrode, platinum counter electrode, and platinum pseudo reference electrode were positioned in the cell with ~0.5 cm of the electrode tips submerged in the electrolyte solution. All chemical components of CV experiments used were added in at 0.1 M (0.5 mmol), unless otherwise noted. All spectra were collected with Gamry Instruments Framework, version 6.25, build 3318. All spectral analyses were performed with Gamry Echem Analyst, version 6.25. Experiment set-up is shown in Figure S1.

Cyclic Voltammetry Parameters:

initialE (V): 0.5 vs. Eref
scan limit 1 (V): 3 vs. Eref
scan limit 2 (V): 0.4 vs. Eref
finalE (V): 0.4 vs. Eref
scan rate (mV/s): 200
electrode area (cm2): 1
equil. Time (s): 0
I/E range mode: auto I/E range
max. current (mA): 5
cycles (#): 3
open circuit (V): 0
sampling mode: Noise reject
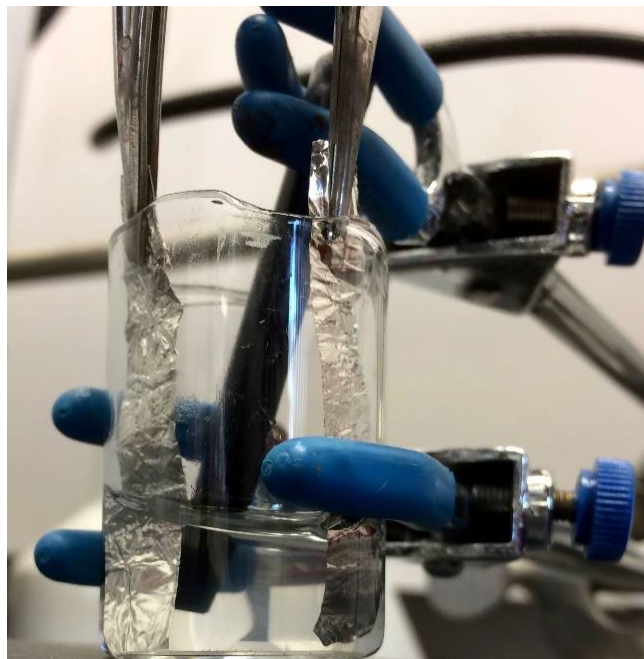
ReactIR Experiments

Experimental Procedure

In a 3 mL borosilicate scintillation vial containing a stir bar, Selectfluor (142 mg, 0.4 mmol, 2 equiv), *p*-tolyl acetate (29 uL, 0.2 mmol, 1 equiv), and 2 mL CH3CN:H2O (0.1 M, 1:1). The resulting mixture was stirred for approximately 1 minute at room temperature. A bored-through 14/20 rubber septum was fitted firmly over the opening of the vial. The ReactIR probe was inserted through the opening of the septum. A solution of AgNO3 (0.1 mL of a 0.4 M solution in H2O, 0.04 mmol) was added in one portion. The reaction mixture was stirred at 35 °C for approximately 10 minutes before the pyridine additive (0.2 mmol, 1 equiv) was added. Data acquisition was initiated. Data was collected for approximately 24 hours or until reaction was complete, as evidenced by consumption of Selectfluor. Data was acquired using a Mettler Toledo ReactIR 15 instrument and analyzed with the Mettler Toledo iC IR 7.0 software package. Graphical analysis was performed using Excel.

ReactIR Parameters:
Detector: MCT
Apodization: HappGenzel
Probe: DiComp (Diamond)
Interface: AgX 6 mm x 1.5 m fiber
(Silver Halide)
Sampling: 3000 to 650 cm-1
Resolution: 8
Scan Option: AutoSelect
Gain: 1x
Time Interval: Data collected every
2 minutes for the entire duration
of experiment
Spectrum Math: Second Derivative
Baseline: One-point baseline
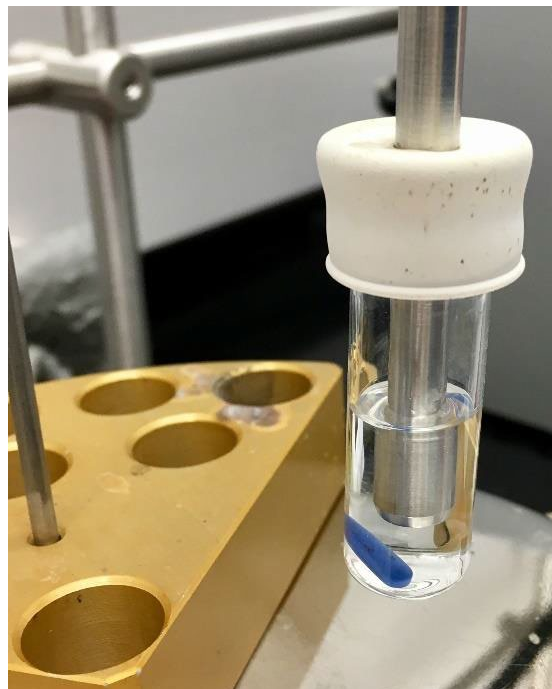
^{19}F NMR Experiment

General Procedure
In each 19F NMR experiment, 0.4 mmol of Selectfluor and 0.4 mmol of 4-R-pyridine (R= CF3, CO2Et, H, OCH3) was used. To an NMR tube, Selectfluor and 1.00 mL of CD3CN was added, then inverted several times until Selectfluor was dissolved, then a sealed capillary of hexafluorobenzene as an internal standard was placed in the NMR tube. An NMR of the Selectfluor with the standard was taken, immediately following 0.4 mmol of the 4-R-pyridine additive was added. The NMR tube was then gently inverted several times and an 19F NMR was immediately taken.

1H/15N HMBC Experiment

General Procedure
In each HMBC experiment, 0.1 mmol of 4-R-pyridine (R = OCH3, H, CO2Et, CF3) and 0.1 mmol of Selectfluor (when applicable) was used. To a test tube, the compound(s) under investigation was added and diluted with 700 uL of CD3CN, vigorously stirred, and transferred to an NMR tube containing a sealed capillary of nitromethane. Experimental parameters were adjusted from the default settings for 1H/13C HMBC found in VnmrJ (version 4.2 Revision A). The multiple bond coupling constant (*multiple bond jnxh*) was left at the default value of 8 Hz for all experiments except for the mixture of pyridine and Selectfluor. When *multiple bond jnxh* = 8 Hz, no correlation signals were detected for 1H/15N of pyridine upon interaction with Selectfluor. It was critical to set *multiple bond jnxh* = 12 Hz. For the HMBC studies that showed 1H/15N correlation when *multiple bond*

jnxh = 8 Hz, the coupling constants were calculated to be at least 10 Hz, which is on the higher end of the instrument's limitations when the protocol is looking for bonds with coupling constants around 8 Hz. HMBC spectral data processing was done using MestReNova. It should be noted that the *default* processing method varies between the software versions for Mac and Windows PC.

<u>HMBC Parameters</u>
f1 Nucelus: N15
N15 spec width: -400 to 400 ppm
t1 increments: 200
2-step J1xh x filter: No
Scans: 4 (up to 32)
Multiple bond jnxh: 8 Hz (12 Hz for pyridine + Selectfluor mixture)

<u>HMBC Spectral Data Processing Method Parameters</u>

***Mac** (MestReNova version 10.0.2-15465)*

<u>f2 - Time Domain</u>   <u>f2 - Frequency Domain</u>
FID Shift: not selected   Phase Correction: selected
Truncate: not selected   Method: Magnitude
Apodization: not selected   Baseline Correction: not selected
Zero Filling and LP   Smoothing: not selected
     Spectrum Size: 2048 (2K)   Reverse: not selected
         Backward LP: not selected   Cuts: not selected
         Forward LP: not selected
     LP Options
         Method: Zhu-Bax
         Basis Points: 1191
         Coefficients: 10
     Fourier Transform
         Protocol: none
         Swap Halves: on
         Mirror Image: on

<u>f1 - Time Domain</u>   <u>f1 - Frequency Domain</u>
     Truncate: not selected   Phase Correction: selected
     Apodization: selected   Method: NoPC
         Gaussian: 39.33 GB(Hz)   Baseline Correction: not selected
     Zero Filling and LP   Smoothing: not selected
         Spectrum Size: 2048 (2K)   Reverse: not selected
         Backward LP: not selected   Cuts: not selected
         Forward LP: not selected
     LP Options

Method: Zhu-Bax
Basis Points: 189
Coefficients: 10
Fourier Transform
Protocol: Echo-Antiecho
Swap Halves: on
Mirror Image: on

Windows PC *(MestReNova version 6.0.2-5475)*

f2 - Time Domain
FID Shift: not selected
Truncate: not selected
Apodization: selected
Sine Bell: 90.00 Deg
Zero Filling and LP
Spectrum Size: 2048 (2K)
Backward LP: not selected
Forward LP: not selected
LP Options
Method: Toeplitz
Basis Points: 1177
Coefficients: 24
Fourier Transform
Protocol: none
Swap Halves: on
Mirror Image: on

f2 - Frequency Domain
Phase Correction: selected
Method: Manual
PH0: 171.34 PH1: 0.00
Baseline Correction: not selected
Smoothing: not selected
Reverse: not selected
Cuts: not selected

f1 - Time Domain
Truncate: not selected
Apodization: selected
Sine Square: 90.00 Deg
First Point: 0.50
Zero Filling and LP
Spectrum Size: 2048 (2K)
Backward LP: not selected
Forward LP: not selected
LP Options
Method: Toeplitz
Basis Points: 187
Coefficients: 12
Fourier Transform
Protocol: Echo-Antiecho
Swap Halves: on
Mirror Image: on

f1 - Frequency Domain
Phase Correction: not selected
Baseline Correction: not selected
Smoothing: not selected
Reverse: not selected
Cuts: not selected

Experimental Procedures and Characterization Data
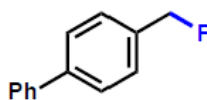
3a

4-(fluoromethyl)-1,1'-biphenyl (3a): The general procedure was employed using 4- methyl-1,1'-biphenyl (33.7 mg, 0.2 mmol), Selectfluor (141.7 mg, 0.4 mmol), and 4-(trifluoromethyl)pyridine (23.2 μL, 0.2 mmol) in acetonitrile and water, (1:1, 2 mL each, 0.05 M). The reaction afforded quantitative amounts of **3a** (NMR yield). The data matches those previously reported.[A1]
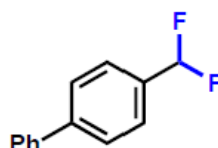
3b

4-(difluoromethyl)-1,1'-biphenyl (3b): The general procedure was employed using 4-methyl-1,1'-biphenyl (33.7 mg, 0.2 mmol), Selectfluor (141.7 mg, 0.4 mmol), and 4-(trifluoromethyl)pyridine (23.2 μL, 0.2 mmol). The reaction afforded **3b** (85%, NMR yield). The data matches those previously reported.[A1]

Appendix-A References
[A1] Xia, J.; Zhu, C.; Chen, C. *J. Am. Chem. Soc.* **2013**, *135*, 17494–17500.
[A2] Mąkoza, M.; Bujok, R. *J. Fluorine Chem.* **2005**, *126*, 209–216.
[A3] Bloom, S.; Pitts, C. R.; Woltornist, R.; Griswold, A.; Holl, M. G.; Lectka, T. *Org. Lett.* **2013**, *15*, 1722–1724.
[A4] Ma, J.; Yi, W.; Lu, G.; Cai, C. *Org. Biomol. Chem.* **2015**, *13*, 2890–2894.
[A5] Champagne, P. A.; Benhassine, Y.; Dessroches, J.; Paquin, J. *Angew. Chem. Int. Ed.* **2014**, *53*, 13835–13839.
[A6] Bloom, S.; McCann, M.; Lectka, T. *Org. Lett.* **2014**, *16*, 6338–6341.

APPENDIX – B

Experimental Set Up: Enhanced Reactivity for Aromatic Bromination via Halogen Bonding with Lactic Acid Derivatives

General Procedure

        The threads of a 4 mL borosilicate scintillation vial were thoroughly taped with Teflon tape. To this vial containing a stir bar was added *N*-bromosuccinimide (43 mg, 0.24 mmol, 1.2 equiv), mandelic acid (6 mg, 0.04 mmol, 20 mol %) and an aromatic compound (0.2 mmol, 1.0 equiv). Acetonitrile (1 mL) and H_2O (1 mL) were then added. The reaction was capped with a Teflon screen cap and rubber septum (24/40). The reaction was then stirred at room temperature until completed as judged by thin-layer chromatography.

        Upon completion, the reaction was diluted with ethyl acetate (1 mL) and transferred to a test tube containing saturated $NaHCO_3$ (3 mL). The aqueous phase was extracted with ethyl acetate (3 x 3 mL) and the combined organic layers were dried over $MgSO_4$, filtered, and carefully concentrated *in vacuo*. The crude material was purified by silica gel chromatography to yield the desired product.

High Resolution Mass Spectroscopy (HRMS) procedure

        The purified product (~10 mg) was diluted with HPLC grade CH_3CN/H_2O (1:1) to approximately 2 mL. The resulting solution was then filtered and injected onto the HRMS. Data collection was done using factory default parameters for positive ion ESI-MS.

General Procedure for NMR Studies:

Determining rate of reaction with mandelic acid

        In the absence of mandelic acid, 4-methoxyacetophenone (30 mg, 0.2 mmol, 1.0 equiv) and *N*-bromosuccinimide (43 mg, 0.24 mmol, 1.2 equiv) in D_2O/CH_3CN (1:1, 0.2 M) was placed in an NMR tube. The first time point (t=0 min) was then collected via NMR. After mandelic acid (6 mg, 0.04 mmol, 20 mol %) was added in one portion directly to NMR tube and NMR time points were taken over the course of 24 h at rt.

Determining rate of reaction with benzoylformic acid

        In the absence of benzoylformic acid, 4-methoxyacetophenone (30 mg, 0.2 mmol, 1.0 equiv) and *N*-bromosuccinimide (43 mg, 0.24 mmol, 1.2 equiv) in D_2O/CH_3CN (1:1, 0.2 M) was placed in an NMR tube. The first time point (t=0 min) was then collected via NMR. After benzoylformic acid (6 mg, 0.04 mmol, 20 mol %) was added in one portion directly to NMR tube and NMR time points were taken over the course of 24 h at rt.

Kinetic NMR study of 4-methoxyacetophenone

General Procedure using mandelic acid

        In each ${}^1H$ NMR experiment, 0.2 mmol of 4-methoxyacetophenone (30 mg) was mixed with *N*-bromosuccinimide (43 mg, 0.24 mmol, 1.2 equiv). 1000 uL of CH_3CN and

1000 uL of D_2O were added to the sample. The sample was then transferred to an NMR tube. The initial time point t=0 was then taken via NMR. After t=0, mandelic acid (6 mg, 0.04 mmol, 20 mol%) was added directly to the NMR tube and inverted several times to ensure the mandelic acid was fully dissolved. An NMR was taken every 15 minutes over the course of 8 hours. The final time point was taken at 24 hours. D_2O was used as the lock solvent (4.79 ppm). The chemical shift for the methoxy peak of the starting material (4.39 ppm) vs the product (4.46 ppm) for each time point were tabulated in excel (Table S3). The NMR conversion was calculated setting the integration of methoxy peak of the starting material to 1 and integrating the product. The integration of the product methoxy peak was then divided by the total of the starting material and product integration combined, then multiplied by 100. To eliminate any discrepancy between whether the reaction must stir, the same experiment was completed where 400uL of the reaction was pipetted into an NMR tube and an NMR was taken. The sample was then carefully poured back into the reaction vial to continue stirring. This was done every 30 minutes to compare the reaction when it was completed in an NMR vs stirring in a reaction vial (Figure S1C).

General Procedure using Benzoylformic acid

In each ^1H NMR experiment, 0.2 mmol of 4-methoxyacetophenone (30 mg) was mixed with *N*-bromosuccinimide (43 mg, 0.24 mmol, 1.2 equiv). 1000 uL of CH_3CN and 1000 uL of D_2O were added to the sample. The sample was then transferred to an NMR tube. The initial time point t=0 was then taken via NMR. After t=0, benzoylformic acid (6 mg, 0.04 mmol, 20 mol%) was added directly to the NMR tube and inverted several times to ensure the mandelic acid was fully dissolved. An NMR was taken every 15 minutes over the course of 8 hours. The final time point was taken at 24 hours. D_2O was used as the lock solvent (4.79 ppm). The chemical shift for the methoxy peak of the starting material (4.39 ppm) vs the product (4.46 ppm) for each time point were tabulated in excel (Table S4). The NMR conversion was calculated setting the integration of methoxy peak of the starting material to 1 and integrating the product. The integration of the product methoxy peak was then divided by the total of the starting material and product integration combined, then multiplied by 100. To eliminate any discrepancy between whether the reaction must stir, the same experiment was completed where 400uL of the reaction was pipetted into an NMR tube and an NMR was taken. The sample was then carefully poured back into the reaction vial to continue stirring. This was done every 30 minutes to compare the reaction when it was completed in an NMR vs stirring in a reaction vial (Figure S2C).

General Procedure using phenylglycine

In each ^1H NMR experiment, 0.2 mmol of 4-methoxyacetophenone (30 mg) was mixed with *N*-bromosuccinimide (43 mg, 0.24 mmol, 1.2 equiv). 1000 uL of CH_3CN and 1000 uL of D_2O were added to the sample. The sample was then transferred to an NMR tube. The initial time point t=0 was then taken via NMR. After t=0, phenylglycine (6 mg,

0.04 mmol, 20 mol%) was added directly to the NMR tube and inverted several times to ensure the phenylglycine was fully dissolved. An NMR was taken every 30 minutes over the course of 8 hours. The final time point was taken at 24 hours. D_2O was used as the lock solvent (4.79 ppm). The chemical shift for the methoxy peak of the starting material (4.39 ppm) vs the product (4.46 ppm) for each time point were tabulated in excel (Table S3). The NMR conversion was calculated setting the integration of methoxy peak of the starting material to 1 and integrating the product. The integration of the product methoxy peak was then divided by the total of the starting material and product integration combined, then multiplied by 100.

Kinetic NMR benzoylformic acid formation

General Procedure

   In each ^{1}H NMR experiment, 0.2 mmol of 4-methoxyacetophenone (30 mg) was mixed with *N*-bromosuccinimide (43 mg, 0.24 mmol, 1.2 equiv). 1000 uL of CH_3CN and 1000 uL of D_2O were added to the sample. The sample was then transferred to an NMR tube. The initial time point t=0 was then taken via NMR. After t=0, mandelic acid (6 mg, 0.04 mmol, 20 mol%) was added directly to the NMR tube and inverted several times to ensure the mandelic acid was fully dissolved. An NMR was taken every 15 minutes over the course of 8 hours. The final time point was taken at 24 hours. D_2O was used as the lock solvent (4.79 ppm). The chemical shift for mandelic acid ranged from 7.87-7.97 ppm and the chemical shift for benzoylformic acid ranged from 8.10-8.25 ppm. The conversion of mandelic acid to benzoylformic acid was monitored over the course of 24 hours.

NMR Study of the degradation of phenylglycine

General Procedure

   In each ^{1}H NMR experiment, 0.04 mmol of phenylglycine and 0.24 mmol of *N*-bromosuccinimide (when applicable) was used. To a test tube, the compound(s) under investigation was added and diluted using a mixture of 600 uL CD_3CN/D_2O, 300 uL of each solvent was used, vigorously stirred, and transferred to an NMR tube. CD_3CN was used as the lock solvent (^{1}H: 1.94, ^{13}C: 118.26 ppm). The chemical shift for phenylglycine was 7.36 ppm for aromatic and 4.60 ppm for the benzlic singlet. To confirm the degradation of phenylglycine into benzyladehyde the mixture of phenylglycine and *N*-bromosuccinimide was spiked with benzaldehyde (8 uL, 0.04 mmol, 20 mol %), causing the peaks for benzaldehyde to grow (δ 9.18 (s, 1H), 7.14 (d, J = 8.3 Hz, 2H), 6.94 (t, J = 7.4 Hz, 1H), 6.82 (t, J = 7.7 Hz, 2H), confirming the degradation of phenylglycine into benzaldehyde.

NMR study of additives with *N*-bromosuccinimide

General Procedure

In each ^{1}H NMR experiment, 0.4 mmol of additive and 0.4 mmol of *N*-bromosuccinimide (when applicable) was used. To a test tube, the compound(s) under investigation was added and diluted using a mixture of 300 CD$_3$CN/D$_2$O, 300 uL of each solvent was used, vigorously stirred, and transferred to an NMR tube.

NMR rate comparison study for 4-fluoroanisole

General Procedure without additive

The threads of a 4 mL borosilicate scintillation vial were thoroughly taped with Teflon tape. To this vial containing a stir bar was added *N*-bromosuccinimide (43 mg, 0.24 mmol, 1.2 equiv) and 4-fluoroanisole (22.6 uL, 0.2 mmol, 1.0 equiv). Acetonitrile (1 mL) and H$_2$O (1 mL) were then added. The reaction was capped with a Teflon screen cap and rubber septum (24/40). The reaction was then stirred at room temperature. Every 30 minutes 100 uL of the reaction solution was pipetted into an NMR and diluted with 400 uL of CD$_3$CN. This continued over the cross of 4 hours to determine the rate of reaction.

General Procedure using additive

The threads of a 4 mL borosilicate scintillation vial were thoroughly taped with Teflon tape. To this vial containing a stir bar was added *N*-bromosuccinimide (43 mg, 0.24 mmol, 1.2 equiv), mandelic acid (6 mg, 0.04 mmol, 20 mol %) or benzoylformic acid (6 mg, 0.04 mmol, 20 mol %) and 4-fluoroanisole (22.6 uL, 0.2 mmol, 1.0 equiv). Acetonitrile (1 mL) and H$_2$O (1 mL) were then added. The reaction was capped with a Teflon screen cap and rubber septum (24/40). The reaction was then stirred at room temperature. Every 15 minutes 100 uL of the reaction solution was pipetted into an NMR and diluted with 400 uL of CD$_3$CN (1.94 ppm). This continued over the cross of 4 hours to determine the rate of reaction. The NMR conversion was calculated setting the integration of methoxy peak of the starting material (3.71 ppm) to 1 and integrating the methoxy peak of the product (3.80 ppm). The integration of the product methoxy peak was then divided by the total of the starting material and product integration combined, then multiplied by 100.

NMR 30-minute rate comparison of product conversion

General Procedure with Mandelic Acid

The threads of a 4 mL borosilicate scintillation vial were thoroughly taped with Teflon tape. To this vial containing a stir bar was added *N*-bromosuccinimide (43 mg, 0.24 mmol, 1.2 equiv), mandelic acid (6 mg, 0.04 mmol, 20 mol %) and an aromatic compound (0.2 mmol, 1.0 equiv). Acetonitrile (1 mL) and H$_2$O (1 mL) were then added. The reaction was capped with a Teflon screen cap and rubber septum (24/40). The reaction was then stirred at room temperature for 30 minutes.

After 30 minutes, the reaction was diluted with ethyl acetate (1 mL) and transferred to a test tube containing saturated $NaHCO_3$ (3 mL). The aqueous phase was extracted with ethyl acetate (3 x 3 mL) and the combined organic layers were dried over $MgSO_4$, filtered, and carefully concentrated *in vacuo.* An NMR of the crude reaction mixture was taken using $CDCl_3$ as the solvent lock. Product conversion was then calculated based on the NMR.

General Procedure without Mandelic Acid

The threads of a 4 mL borosilicate scintillation vial were thoroughly taped with Teflon tape. To this vial containing a stir bar was added *N*-bromosuccinimide (43 mg, 0.24 mmol, 1.2 equiv) and an aromatic compound (0.2 mmol, 1.0 equiv). Acetonitrile (1 mL) and H_2O (1 mL) were then added. The reaction was capped with a Teflon screen cap and rubber septum (24/40). The reaction was then stirred at room temperature for 30 minutes.

After 30 minutes, the reaction was diluted with ethyl acetate (1 mL) and transferred to a test tube containing saturated $NaHCO_3$ (3 mL). The aqueous phase was extracted with ethyl acetate (3 x 3 mL) and the combined organic layers were dried over $MgSO_4$, filtered, and carefully concentrated *in vacuo.* An NMR of the crude reaction mixture was taken using $CDCl_3$ as the solvent lock. Product conversion was then calculated based on the NMR.

Kinetic NMR study of 4-methoxyacetophenone
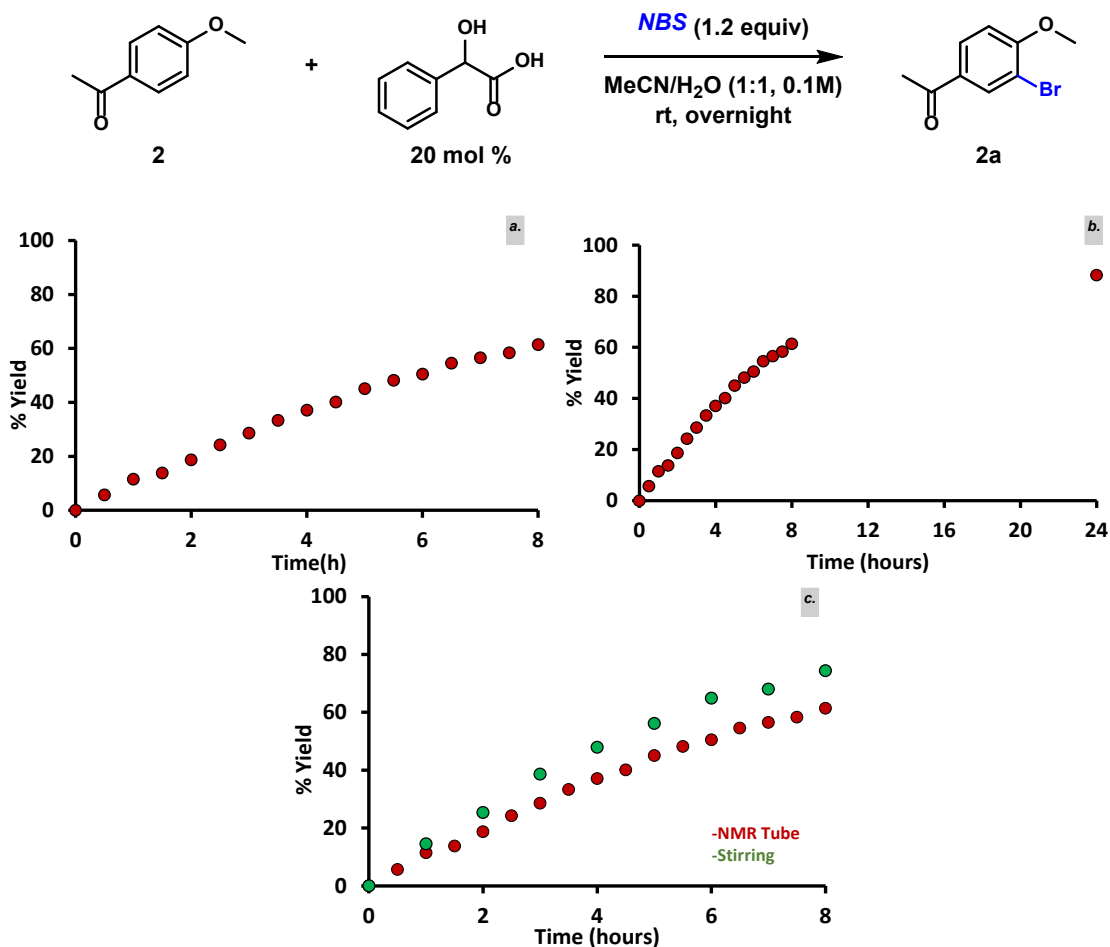
Figure S1

Processed kinetic NMR data for methoxy peak at 4.39 ppm of starting material and 4.46 ppm for product in the presence of mandelic acid. Conditions: **a:** 4-methoxyacetophenone (0.2 mmol), *N*-bromosuccinimide (0.24 mmol) with mandelic acid (0.04 mmol) in 1.0 mL CH_3CN and 1.0 mL D_2O over the course of 8 h; **b.** 4-methoxyacetophenone (0.2 mmol), *N*-bromosuccinimide (0.24 mmol) with mandelic acid (0.04 mmol) in 1.0 mL CH_3CN and 1.0 mL D_2O over the course of 24 h; **c.** 4-methoxyacetophenone (0.2 mmol), *N*-bromosuccinimide (0.24 mmol) with mandelic acid (0.04 mmol) in 1.0 mL CH_3CN and 1.0 mL D_2O over the course of 8 h (reaction stirring in a reaction vial shown in green for reference).
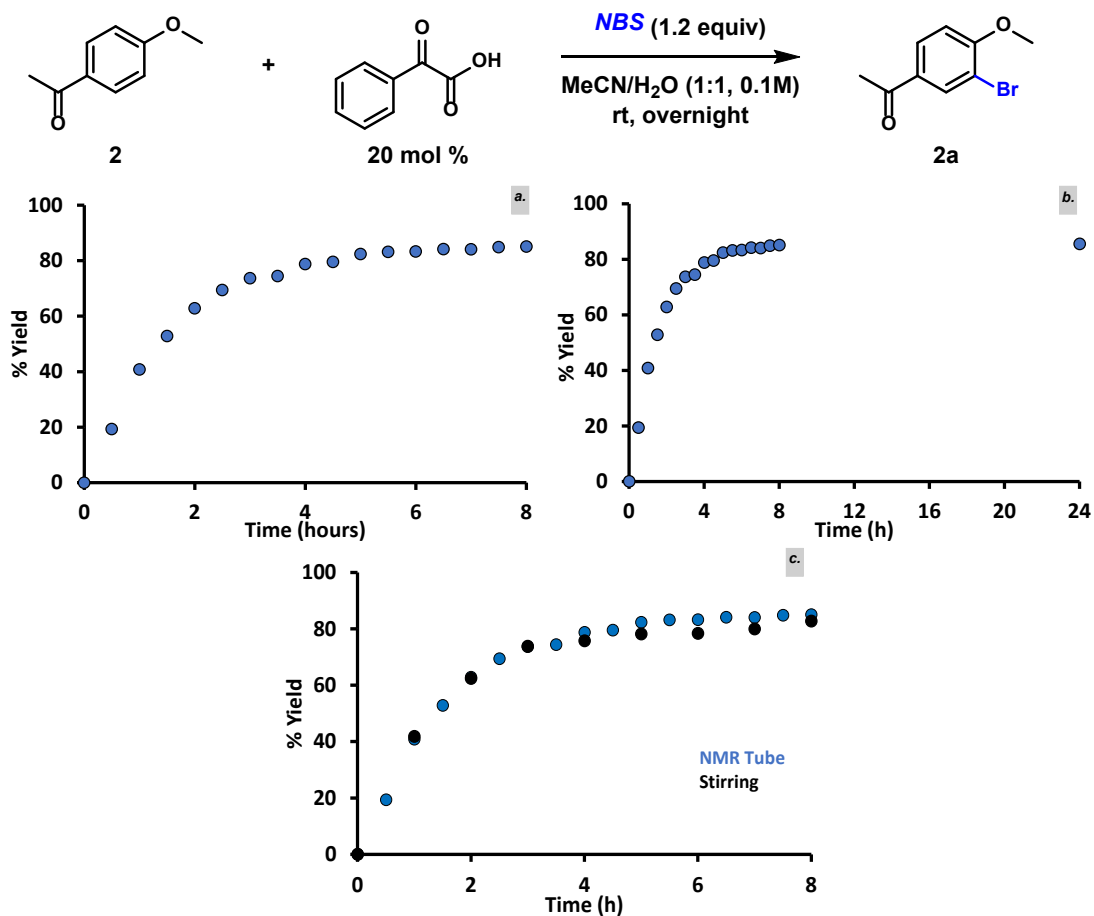
Figure S2   **Processed kinetic NMR data for methoxy peak at 4.39 ppm of starting material and 4.46 ppm for product in the presence of benzoylformic acid.** Conditions: **a:** 4-methoxyacetophenone (0.2 mmol), *N*-bromosuccinimide (0.24 mmol) with benzoylformic acid (0.04 mmol) in 1.0 mL CH₃CN and 1.0 mL D₂O over the course of 8 h; **b.** 4-methoxyacetophenone (0.2 mmol), *N*-bromosuccinimide (0.24 mmol) with benzoylformic acid (0.04 mmol) in 1.0 mL CH₃CN and 1.0 mL D₂O over the course of 24 h; **c.** 4-methoxyacetophenone (0.2 mmol), *N*-bromosuccinimide (0.24 mmol) with benzoylformic acid (0.04 mmol) in 1.0 mL CH₃CN and 1.0 mL D₂O over the course of 8 h (reaction stirring in a reaction vial shown in black for reference).
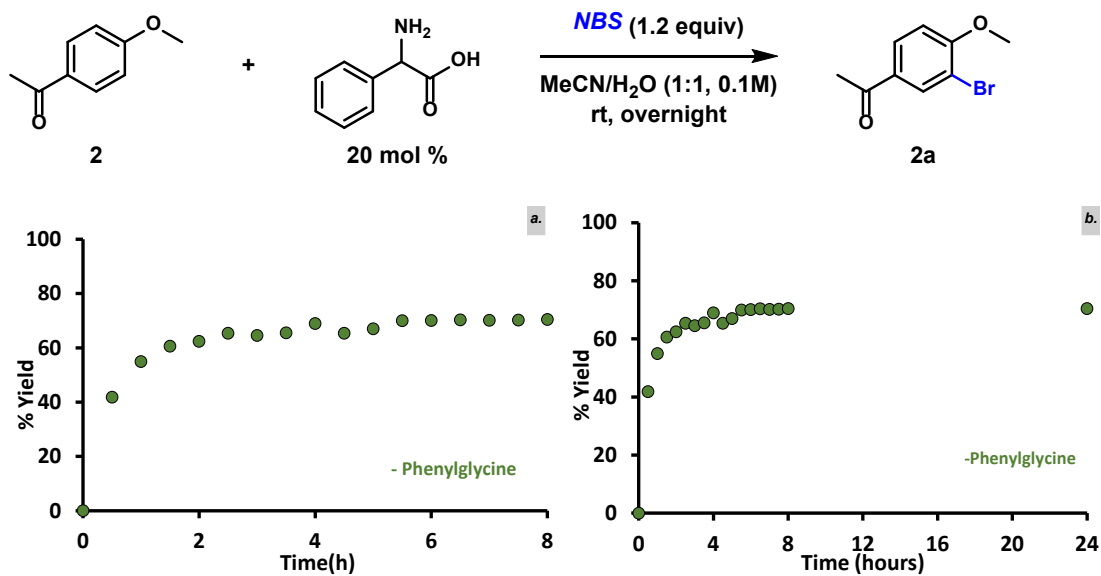
Figure S3 **Processed kinetic NMR data for methoxy peak at 4.39 ppm of starting material and 4.46 ppm for product in the presence of phenylglycine.** Conditions: **a:** 4-methoxyacetophenone (0.2 mmol), *N*-bromosuccinimide (0.24 mmol) with phenylglycine (0.04 mmol) in 1.0 mL CH₃CN and 1.0 mL D₂O over the course of 8 h; **b.** 4-methoxyacetophenone (0.2 mmol), *N*-bromosuccinimide (0.24 mmol) with phenylglycine (0.04 mmol) in 1.0 mL CH₃CN and 1.0 mL D₂O over the course of 24 h.

NMR Study of the Degradation of Phenylglycine
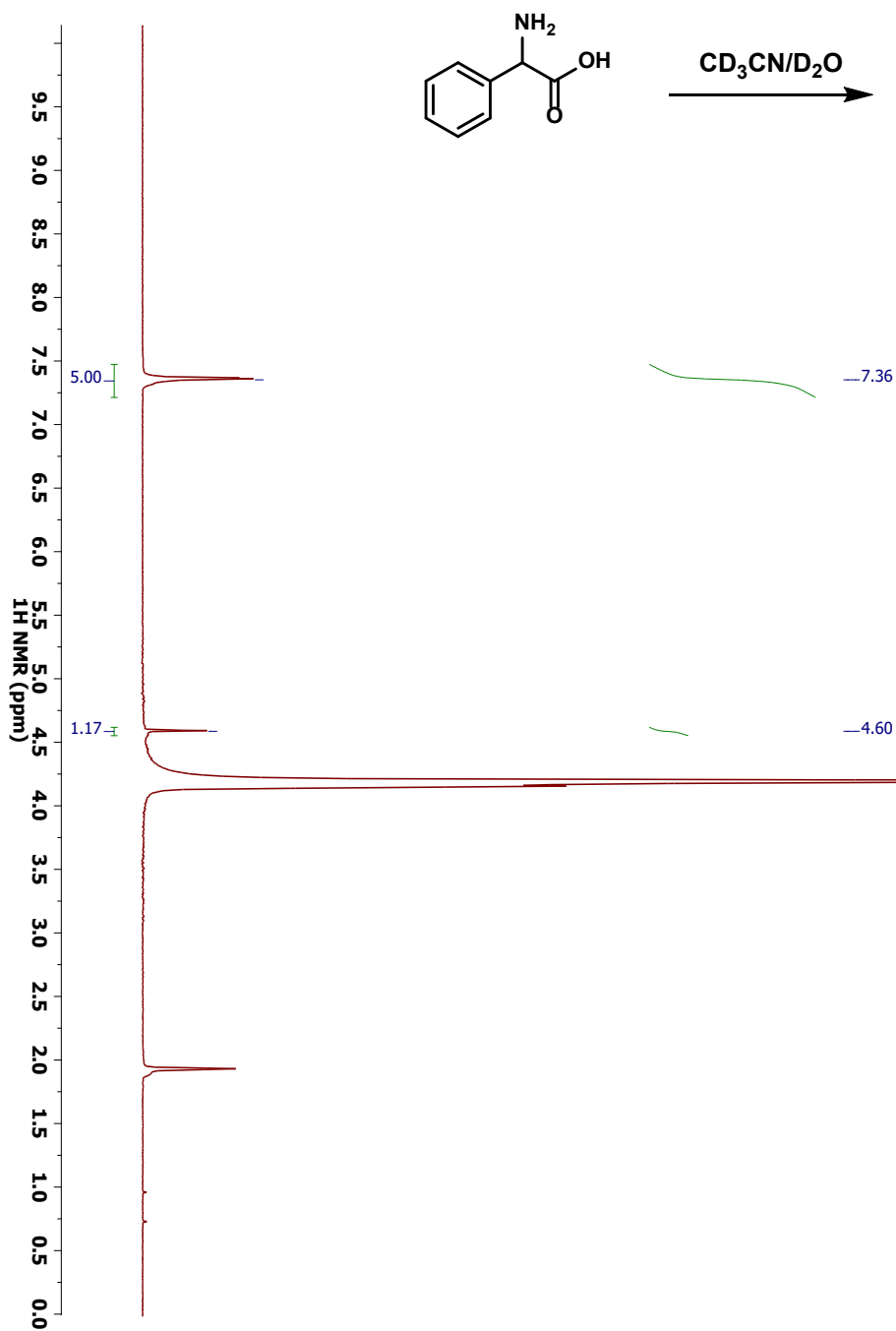
Figure S4 **^{1}H NMR spectra of phenylglycine in CD$_3$Cn/D$_2$O.** Phenylglycine (0.4 mmol), in 1.0 mL CD$_3$CN and 1.0 mL D$_2$O.
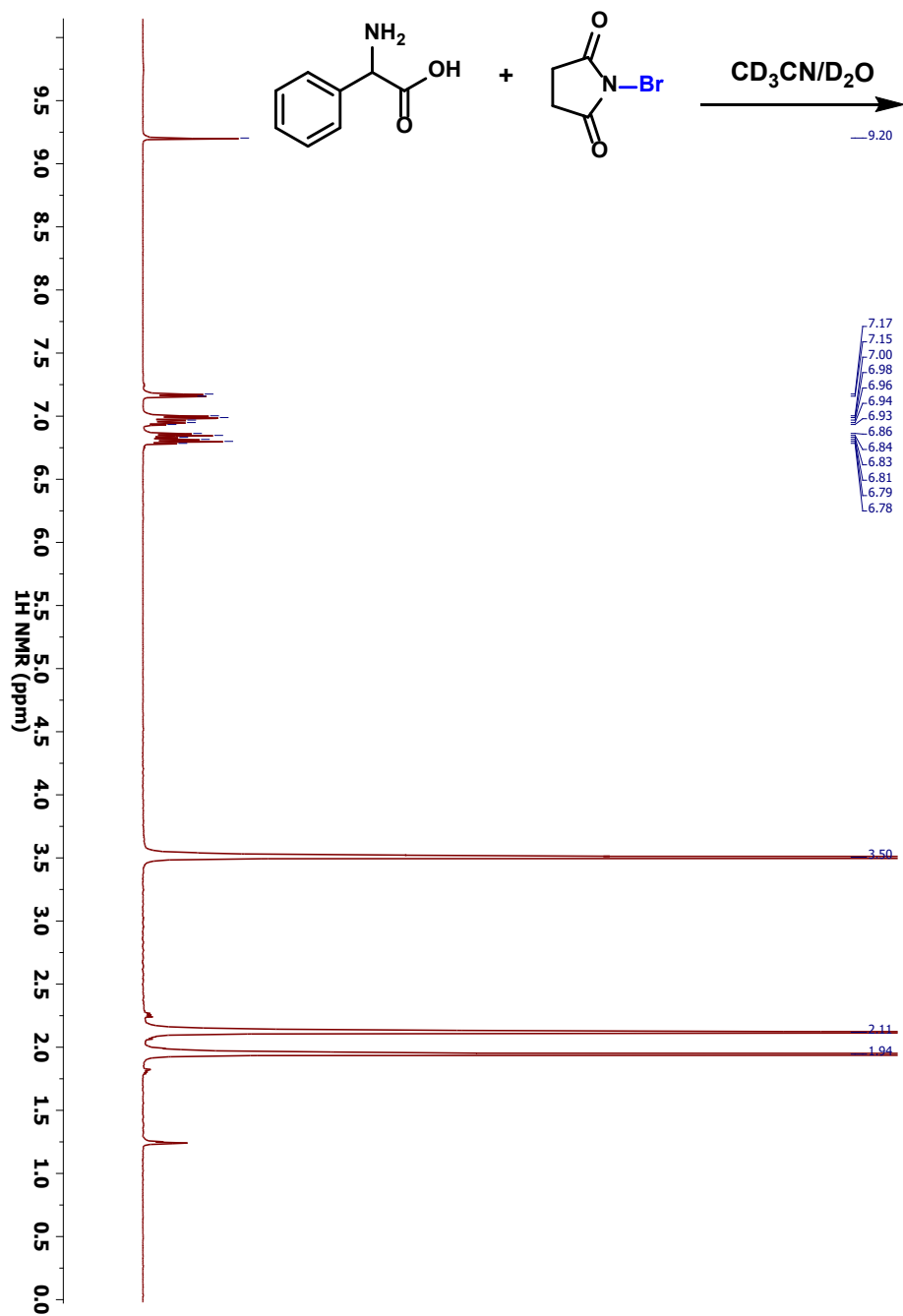
Figure S5 **¹H NMR spectra of phenylglycine with *N*-bromosuccinimide in CD₃Cn/D₂O.** Phenylglycine (0.04 mmol) and *N*-bromosuccinimide (0.24 mmol), in 1.0 mL CD₃CN and 1.0 mL D₂O.
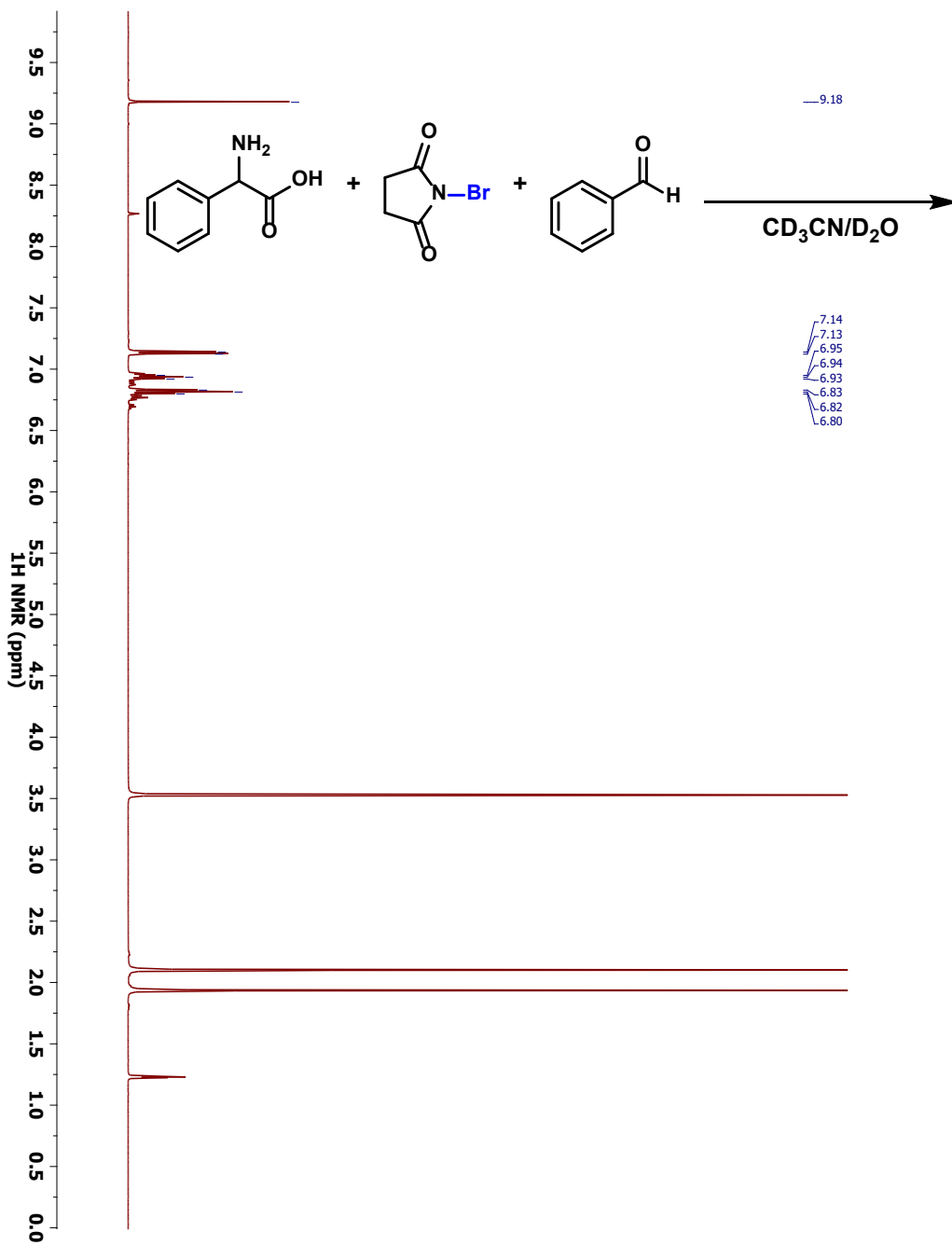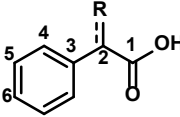
Figure S6 **¹H NMR spectra of phenylglycine with *N*-bromosuccinimide in CD₃Cn/D₂O.** Phenylglycine (0.04 mmol), *N*-bromosuccinimide (0.24 mmol), and benzaldehyde (0.04 mmol) in 1.0 mL CD₃CN and 1.0 mL D₂O.
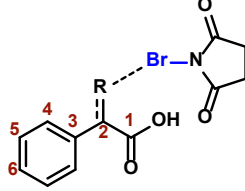
NMR Study of Additives with *N*-bromosuccinimide

Table S1 **¹³C NMR chemical shifts for additives.**

	¹³C NMR for C1 (ppm)	¹³C NMR for C2 (ppm)	¹³C NMR for C3 (ppm)	¹³C NMR for C4 (ppm)	¹³C NMR for C5 (ppm)	¹³C NMR for C6 (ppm)
R = O	165.94	188.72	131.84	129.74	128.94	135.17
OH	175.04	72.38	138.44	126.63	128.50	128.32
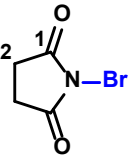
For NMR experiments containing CD_3CN/D_2O (1:1), CD_3CN was used to lock the sample. See Figure S9 and Figure S13.

Table S2 **¹³C NMR chemical shifts for additives in the presence of *N*-bromosuccinimide.**
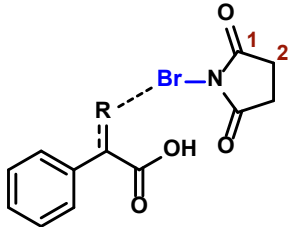
	¹³C NMR for C1 (ppm)	¹³C NMR for C2 (ppm)	¹³C NMR for C3 (ppm)	¹³C NMR for C4 (ppm)	¹³C NMR for C5 (ppm)	¹³C NMR for C6 (ppm)
R = O	165.78	188.55	131.77	129.73	128.94	135.20
OH	174.98	72.34	138.40	126.59	128.47	128.29

For NMR experiments containing CD_3CN/D_2O (1:1), CD_3CN was used to lock the sample. *Values represent the shift of peaks observed for the ¹³C NMR experiment, see Figure S11 and Figure S15.

Table S3 **¹³C NMR chemical shifts for *N*-bromosuccinimide.**

	¹³C NMR for C1 (ppm)	¹³C NMR for C2 (ppm)
	177.02	28.34

For NMR experiments containing CD_3CN/D_2O (1:1), CD_3CN was used to lock the sample, see Figure S17.

Table S4 ^{13}C NMR chemical shifts for *N*-bromosuccinimide.

R =	^{13}C NMR for C1 (ppm)	^{13}C NMR for C2 (ppm)
O	176.90	28.42
OH	176.98	28.32

For NMR experiments containing CD$_3$CN/D$_2$O (1:1), CD$_3$CN was used to lock the sample. See Figure S11 and Figure S15.
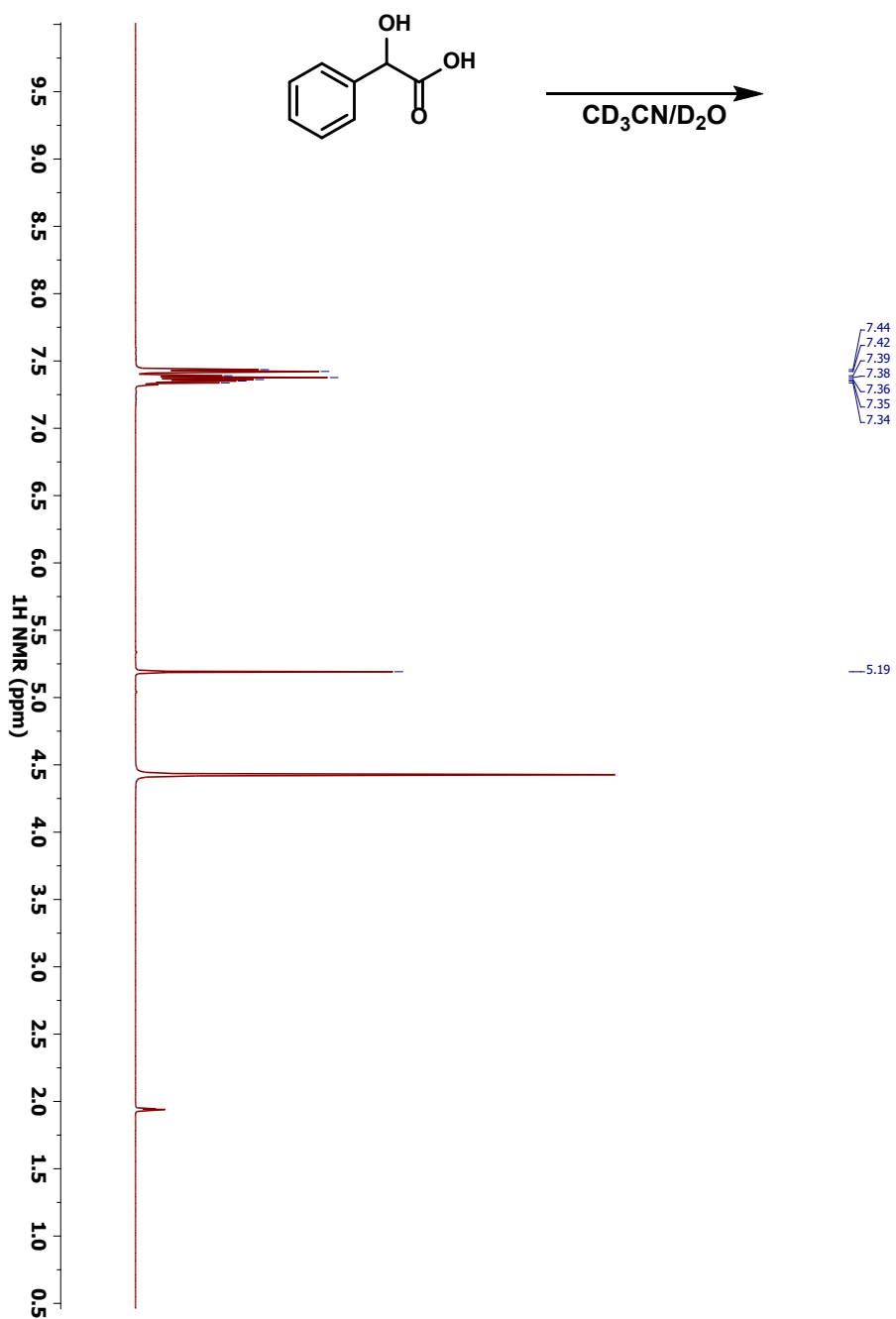
Figure S7   **¹H NMR spectra of Mandelic Acid in CD₃Cn/D₂O.** Mandelic Acid (0.4 mmol), in 300 uL CD₃CN and 300 uL D₂O.
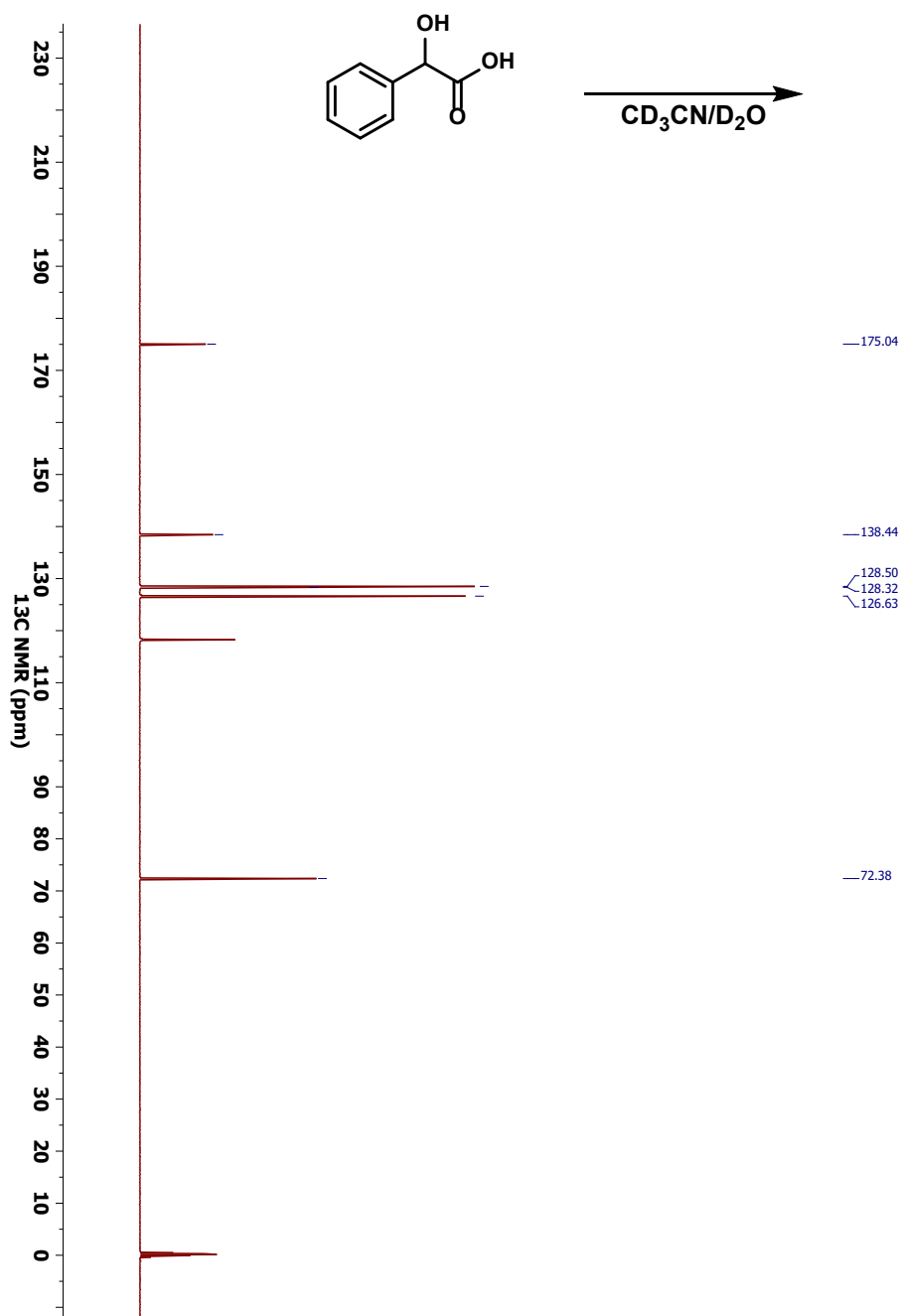
Figure S8 **¹³C NMR spectra of Mandelic Acid in CD₃Cn/D₂O.** Mandelic Acid (0.4 mmol) in 300 uL CD₃CN and 300 uL D₂O.
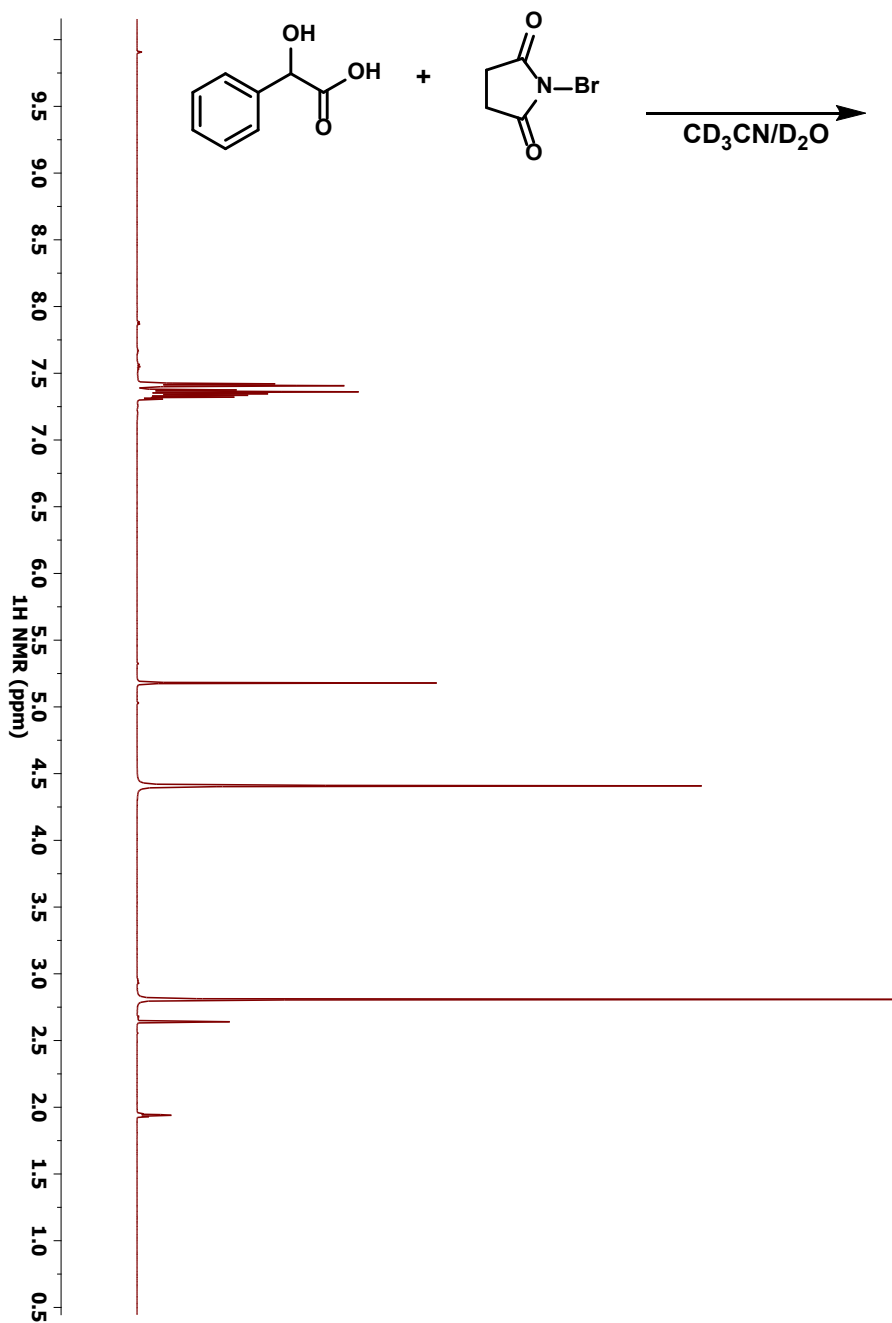
¹H NMR spectra of Mandelic Acid and *N*-bromosuccinimide in CD₃Cn/D₂O.
Figure S9 Mandelic Acid (0.4 mmol) and *N*-bromosuccinimide (0.4 mmol) in 300 uL CD₃CN and 300 uL D₂O.
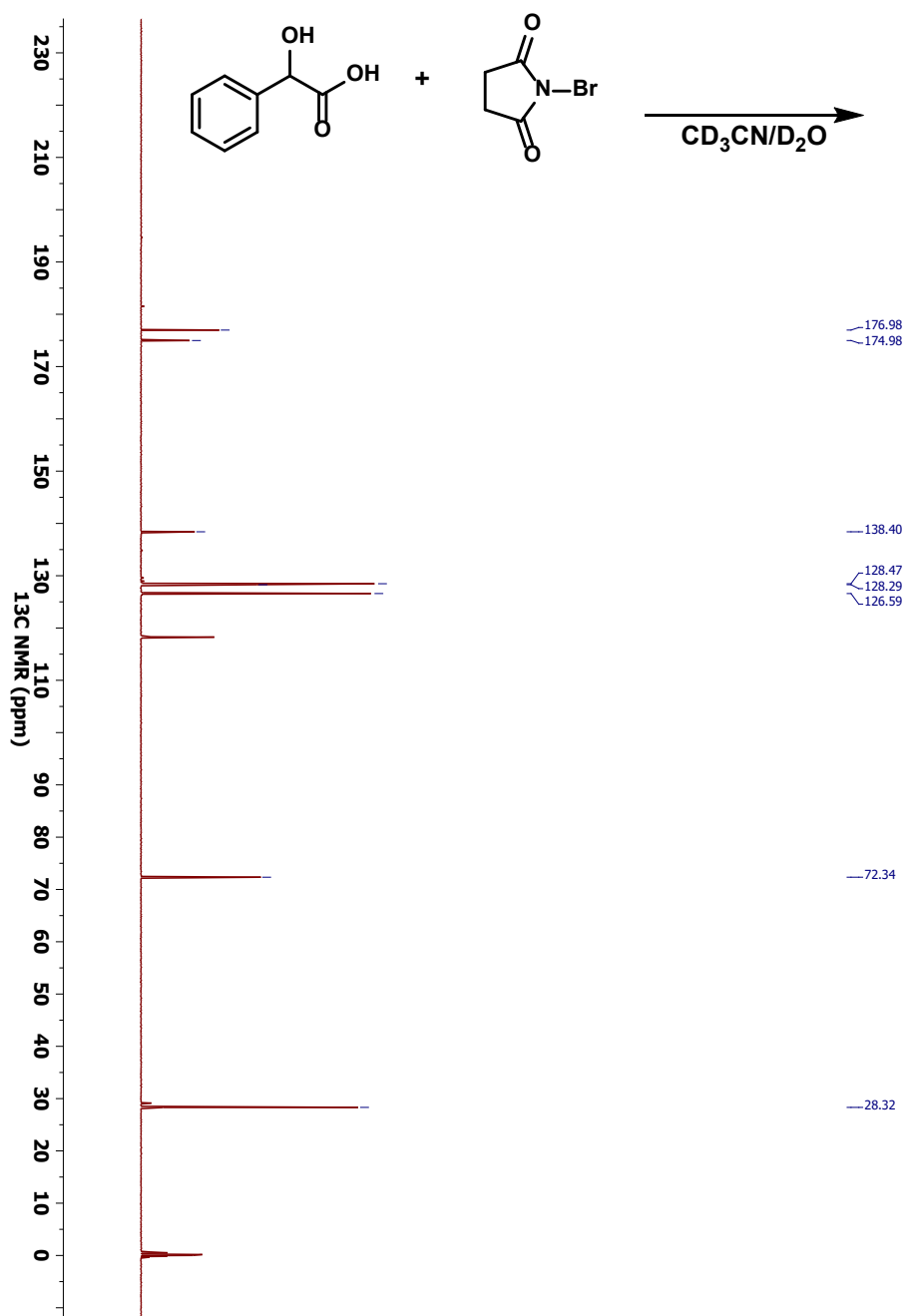
Figure S10 **¹³C NMR spectra of Mandelic Acid and *N*-bromosuccinimide in CD₃Cn/D₂O.**
Mandelic Acid (0.4 mmol) and *N*-bromosuccinimide (0.4 mmol) in 300 uL CD₃CN
and 300 uL D₂O.
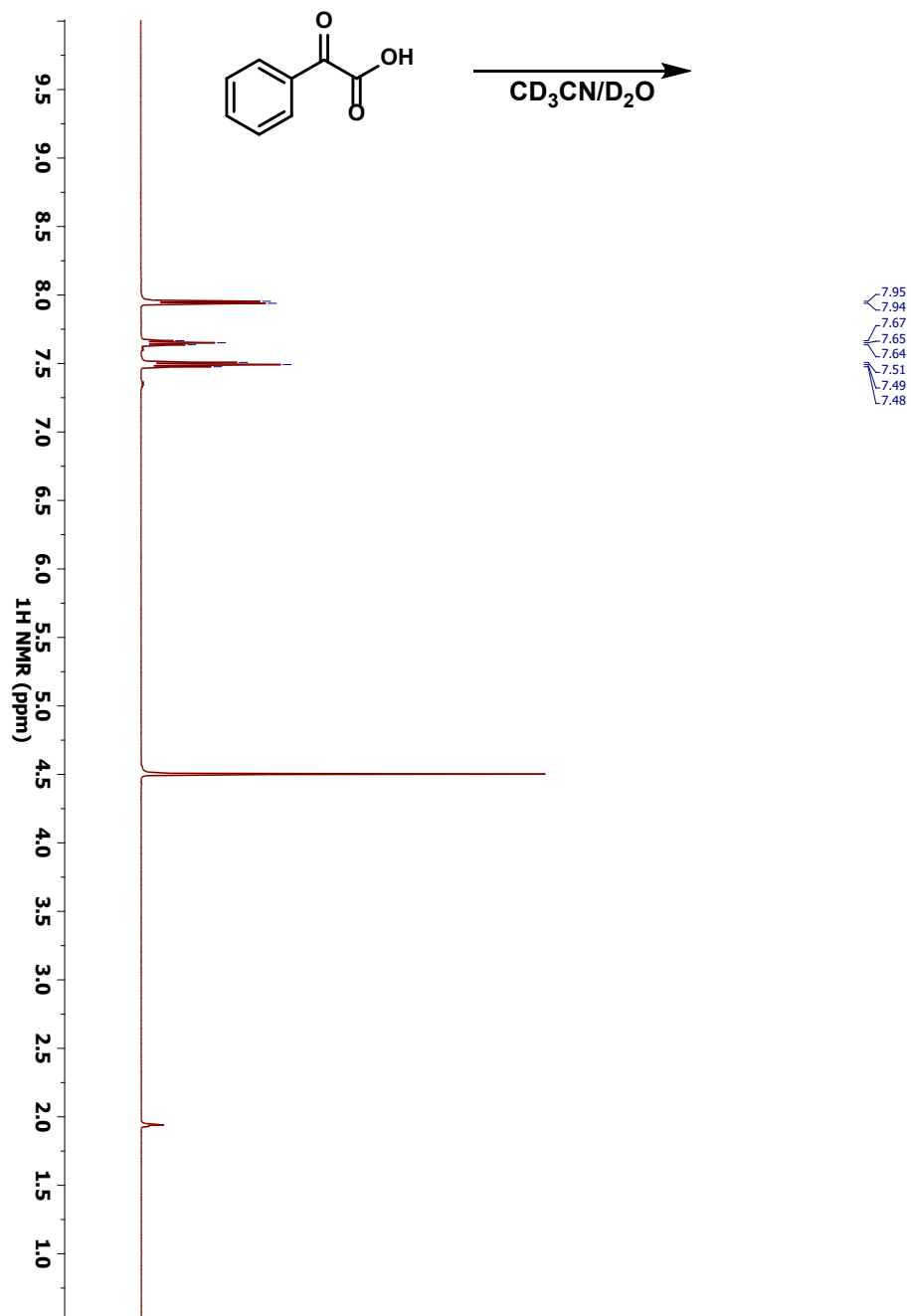
Figure S11 **¹H NMR spectra of Benzoylformic Acid in CD₃Cn/D₂O.** Benzoylformic Acid (0.4 mmol), in 300 uL CD₃CN and 300 uL D₂O.
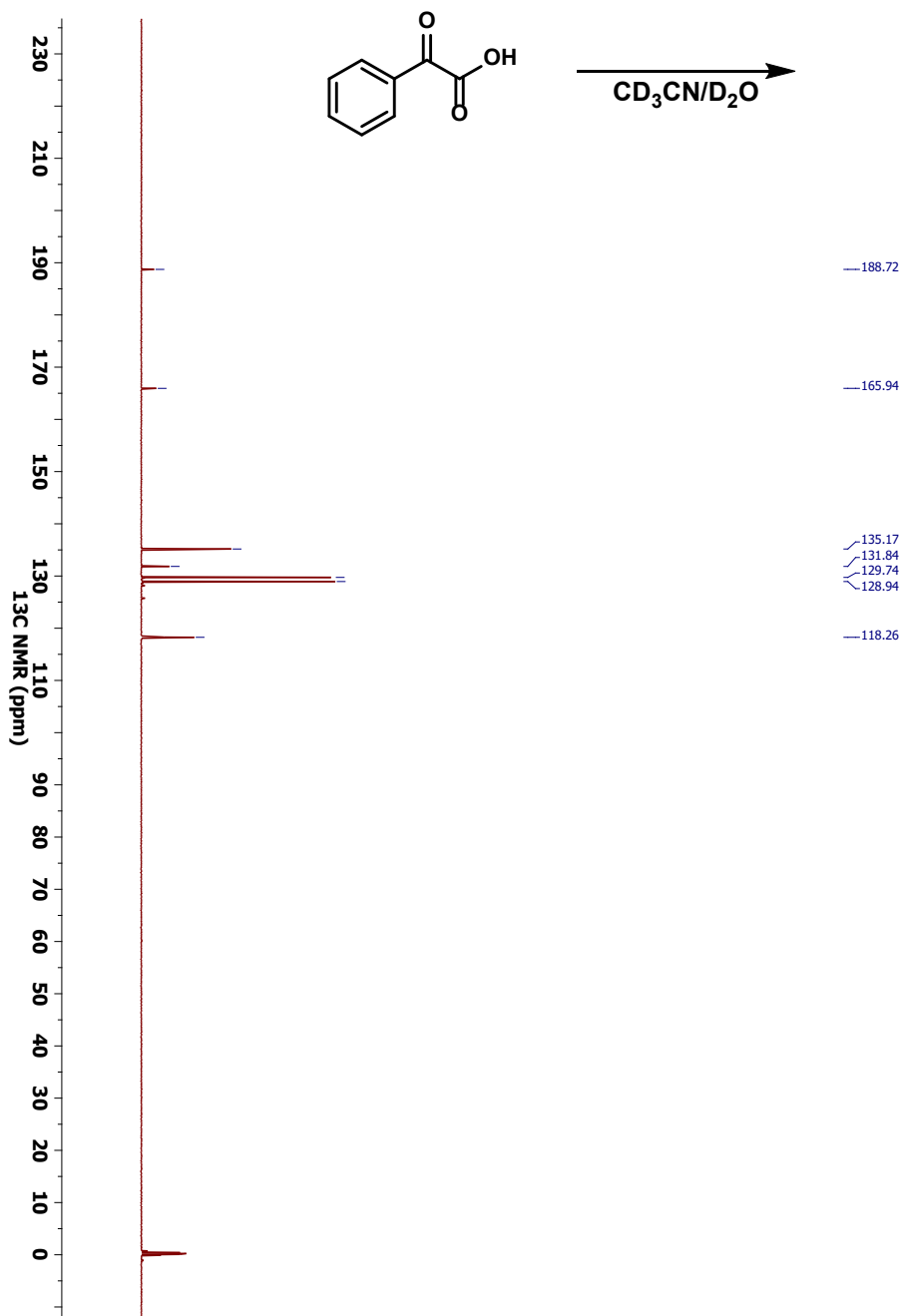
Figure S12 ^{13}**C NMR spectra of Benzoylformic Acid in CD₃Cn/D₂O.** Benzoylformic Acid (0.4 mmol), in 300 uL CD₃CN and 300 uL D₂O.
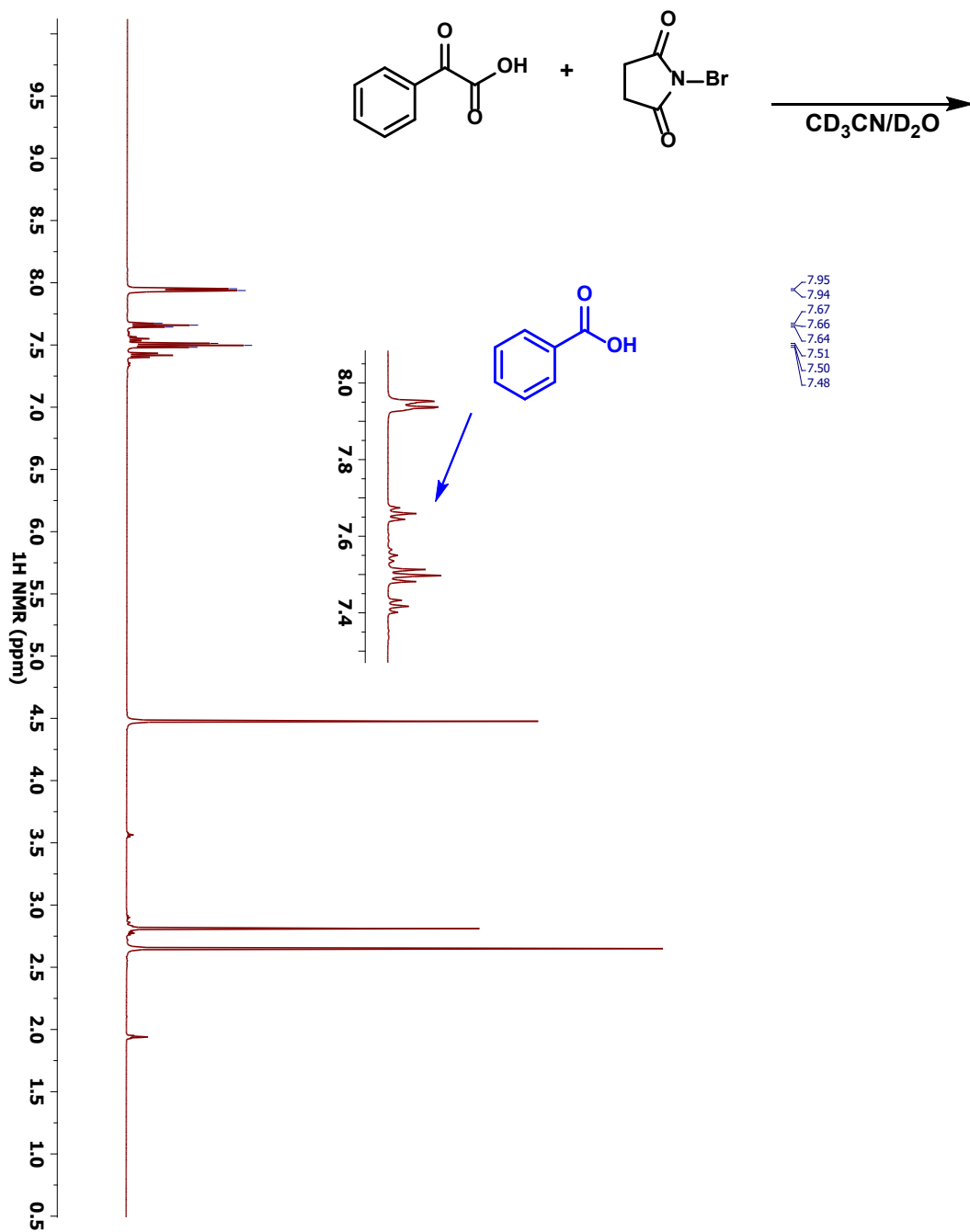
Figure S13   **¹H NMR spectra of Benzoylformic Acid and *N*-bromosuccinimide in CD₃Cn/D₂O.** Benzoylformic Acid (0.4 mmol) and *N*-bromosuccinimide (0.4 mmol), in 300 uL CD₃CN and 300 uL D₂O.
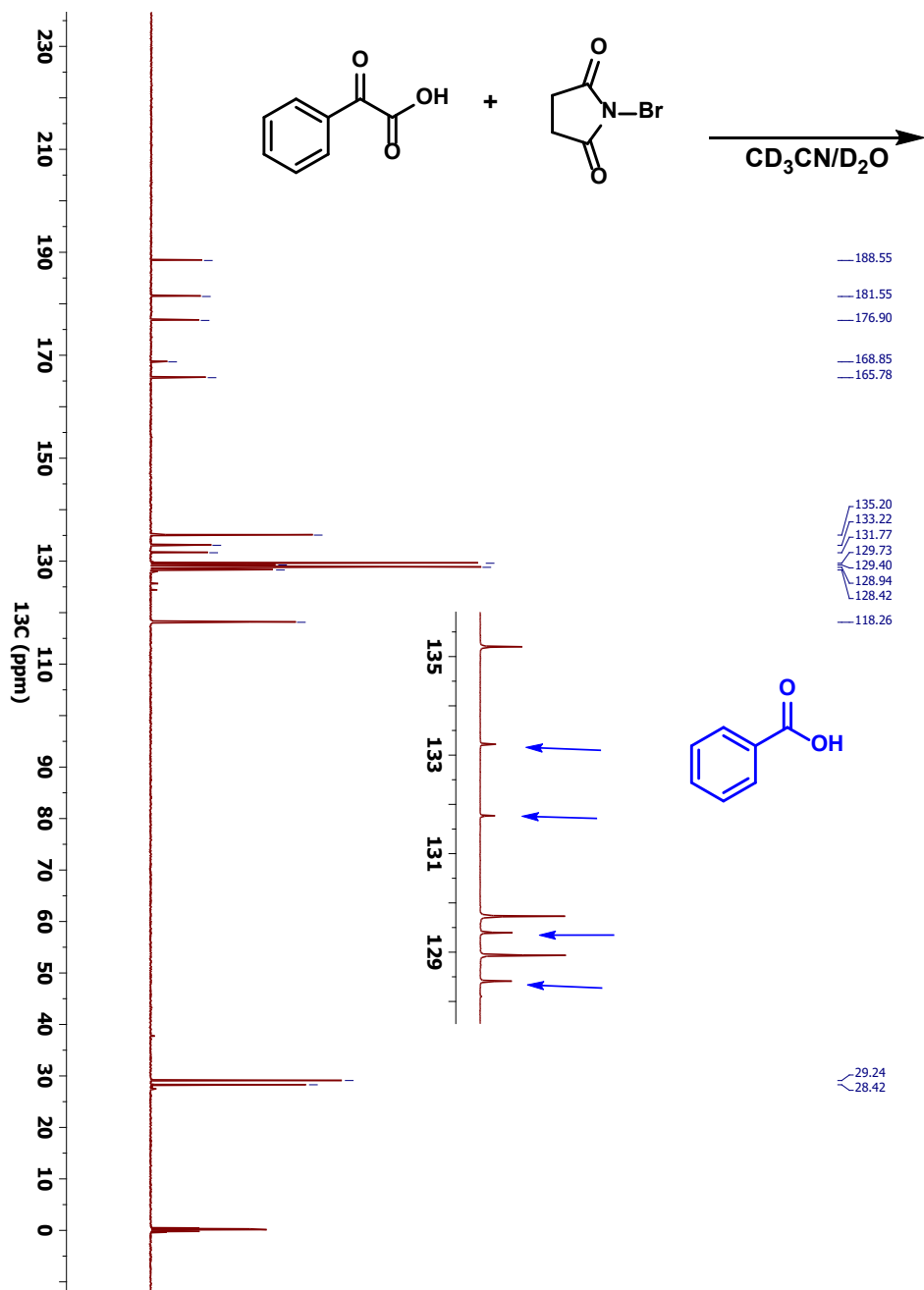
Figure S14 ^{13}C **NMR spectra of Benzoylformic Acid and *N*-bromosuccinimide in CD₃Cn/D₂O.** Benzoylformic Acid (0.4 mmol) and *N*-bromosuccinimide (0.4 mmol), in 300 uL CD₃CN and 300 uL D₂O.
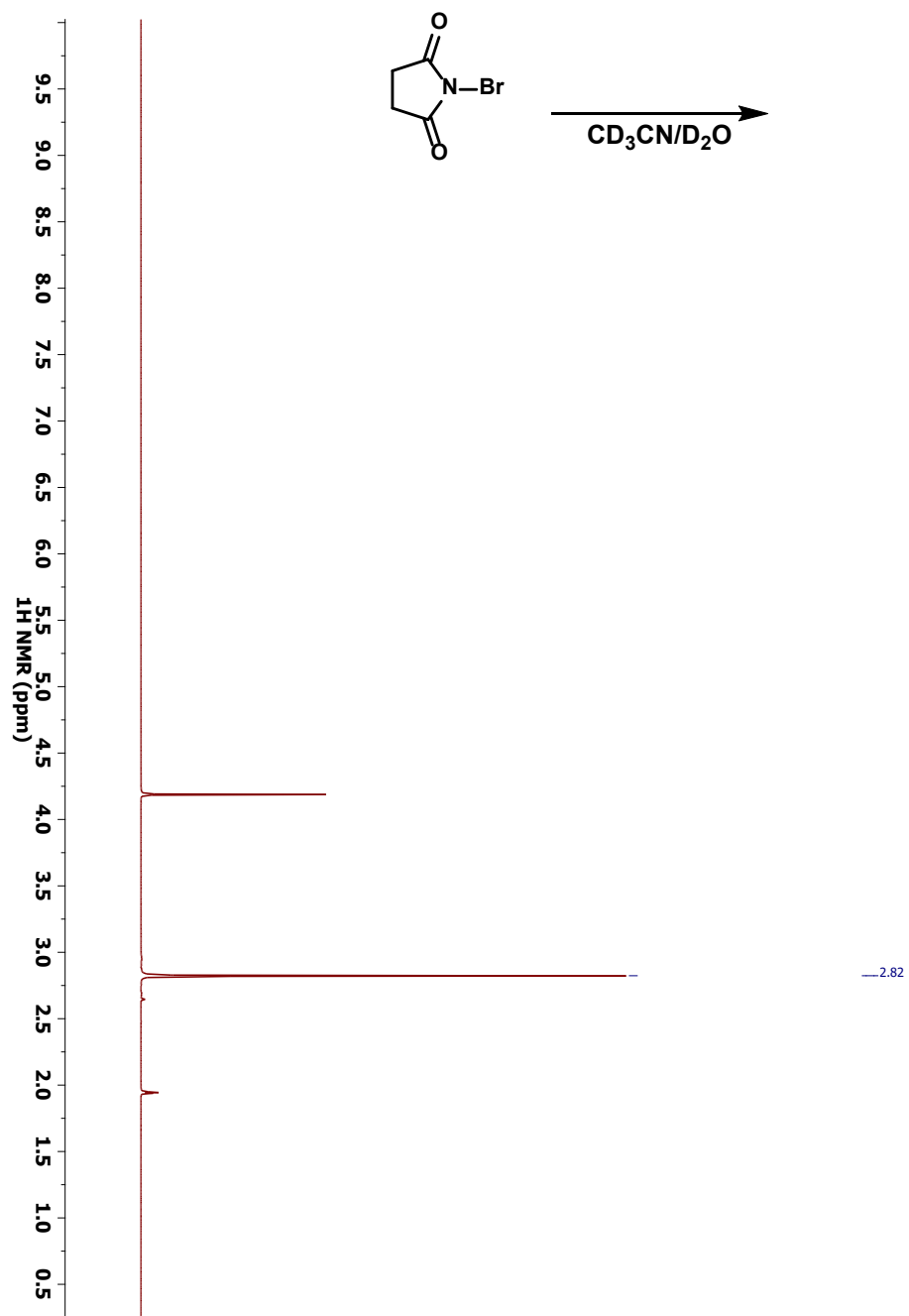
Figure S15 **¹H NMR spectra of *N*-bromosuccinimide in CD₃Cn/D₂O.** *N*-bromosuccinimide (0.4 mmol), in 300 uL CD₃CN and 300 uL D₂O.
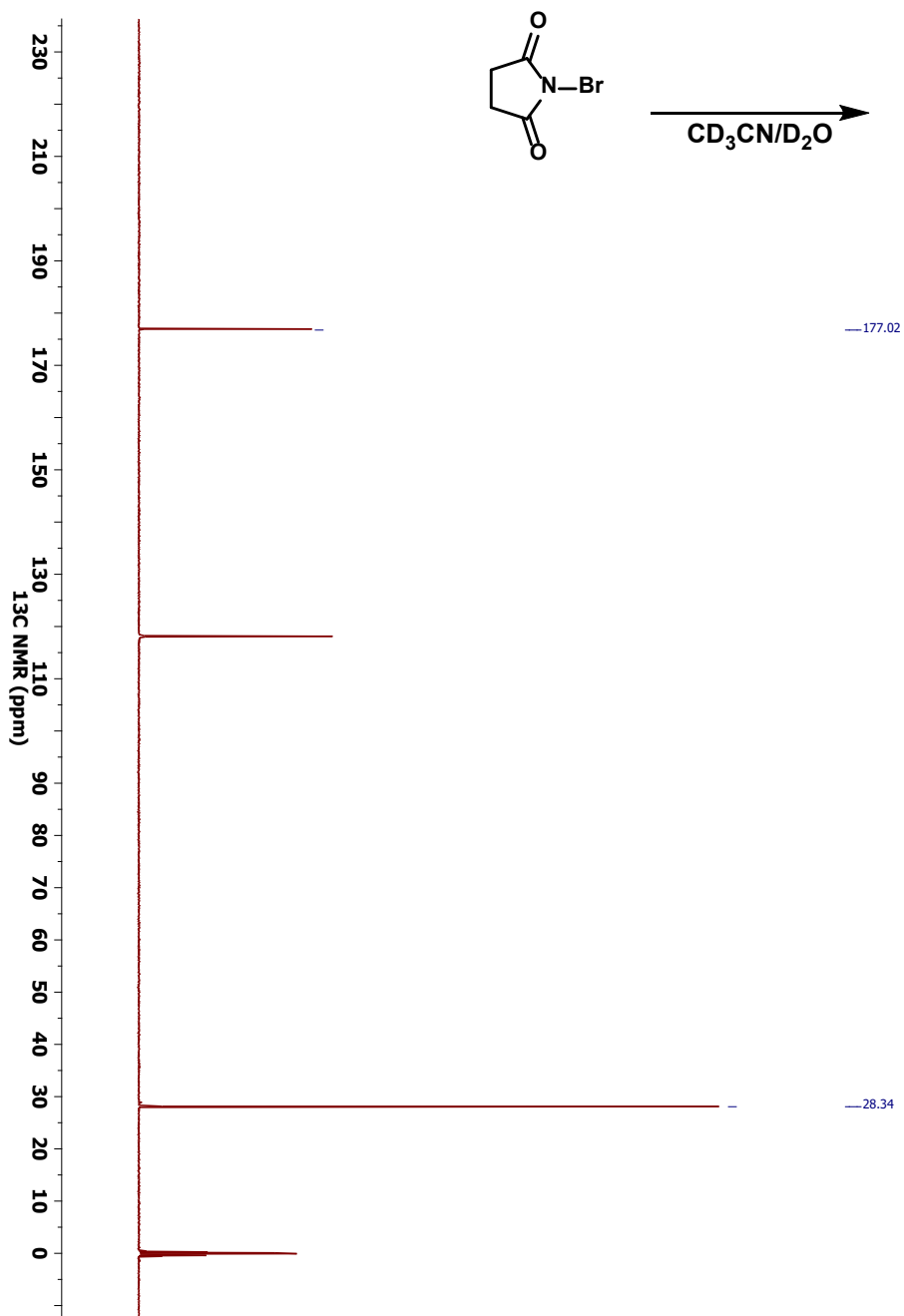
Figure S16   ^13^C NMR spectra of *N*-bromosuccinimide in CD₃Cn/D₂O. *N*-bromosuccinimide (0.4 mmol), in 300 uL CD₃CN and 300 uL D₂O.

NMR rate comparison study for 4-fluoroanisole
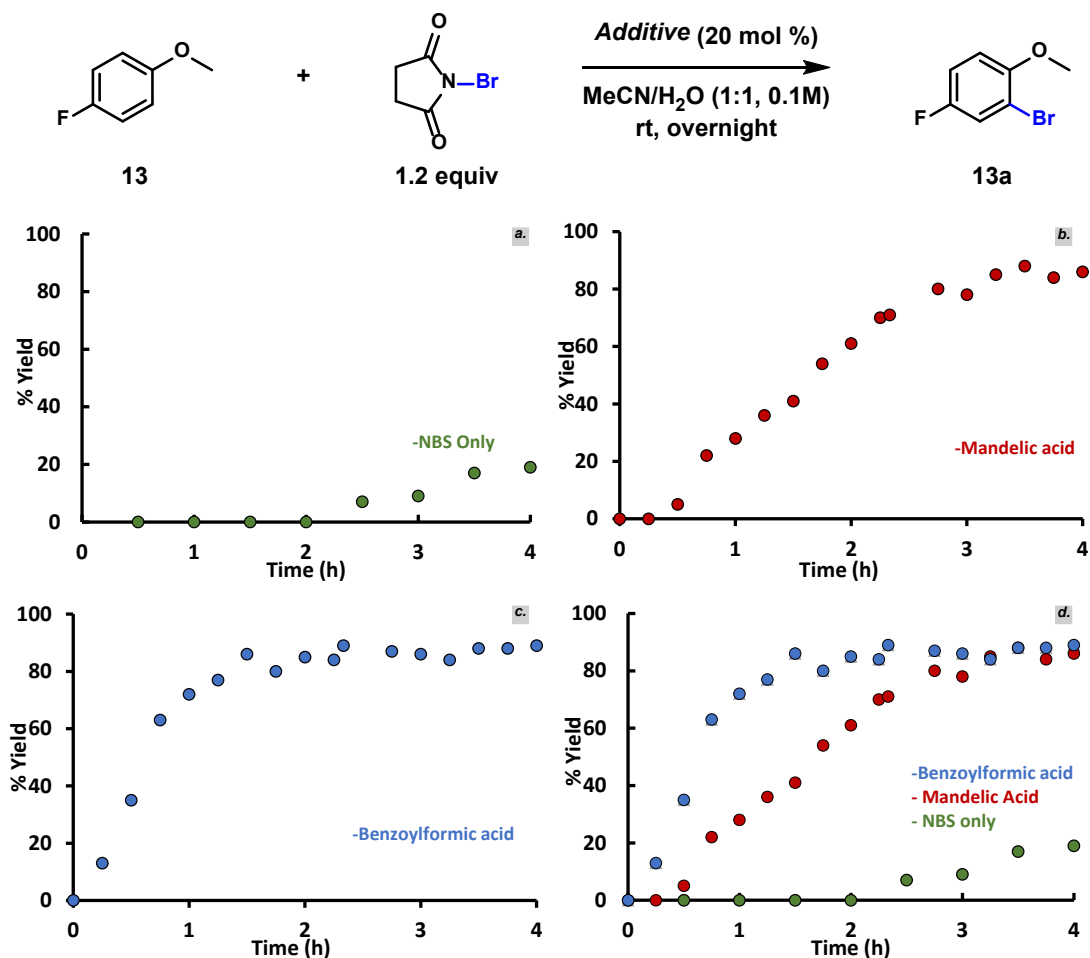
Figure S17   **Processed kinetic NMR data for 4-fluoroanisole methoxy peak at 3.71 ppm of starting material and 3.80 ppm for product in the presence of additives.** Conditions: **a:** 100 uL aliquot of 4-methoxyacetophenone (0.2 mmol), *N*-bromosuccinimide (0.24 mmol) in 1.0 mL CH$_3$CN and 1.0 mL D$_2$O over the course of 4 h; **b.** 100 uL aliquot of 4-methoxyacetophenone (0.2 mmol), *N*-bromosuccinimide (0.24 mmol) with mandelic acid (0.04 mmol) in 1.0 mL CH$_3$CN and 1.0 mL D$_2$O over the course of 4 h; **c.** 100 uL aliquot of 4-methoxyacetophenone (0.2 mmol), *N*-bromosuccinimide (0.24 mmol) with benzoylformic acid (0.04 mmol) in 1.0 mL CH$_3$CN and 1.0 mL D$_2$O over the course of 4 h; **d.** rate comparison of **reaction a** (NBS only) vs **reaction b** (with mandelic acid) vs **reaction c**.

Synthesis of 15, 22 and 24
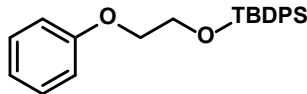
15

2-[[(*tert*-butyl)diphenylsilyl]oxy]ethoxy-benzene (15). Using a modified literature procedure,[1] to a solution of 2-phenoxyethanol (7.2 mmol) in anhydrous dichloromethane (14.4 mL) cooled to 0 °C, imidazole (1.3 eq.) was added, followed by drop wise addition of *tert*-butyl(chloro)diphenylsilane (1.1 eq). The reaction mixture was allowed to warm to room temperature and stirred overnight and then quenched by the addition of water and dichloromethane. The layers were separated, and the organic layer was dried over Na_2SO_4. The solvent was evaporated under reduced pressure to afford the crude product which was purified by column chromatography on silica gel using (9:1) hexanes/EtOAc as the eluent to get the compound **15** in 98% yield as a colorless oil. **^{1}H NMR** (500 MHz, CDCl$_3$): 7.77 – 7.74 (m, 4H), 7.49 – 7.39 (m, 6H), 7.30 (dd, J = 15.4, 7.6 Hz, 2H), 7.00 – 6.95 (m, 1H), 6.92 (d, J = 8.6 Hz, 2H), 4.12 (t, J = 5.2 Hz, 2H), 4.04 (t, J = 5.2 Hz, 2H), 1.11 (s, 9H). **^{13}C{1H} NMR** (125 MHz, CDCl$_3$): 159.2, 135.7, 133.6, 129.7, 129.4, 127.7, 120.7, 114.6, 68.9, 62.7, 26.8, 19.3. **HRMS (ESI-TOF)**: calcd for $C_{24}H_{28}O_2Si$ [M+H]$^+$ 337.1931 found 337.1933.
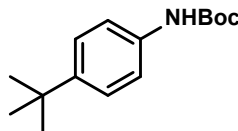

22

1,1-Dimethylethyl N-[4-(1,1-dimethylethyl)phenyl]carbamate (22). Using a modified literature procedure,[2] to a round bottom flask having di-tert-butyl decarbonate (8 mmol) dissolved in glycerol (16 mL) at room temperature, 4-*tert*-butylaniline (1.0 eq.) was added. Let the reaction stir vigorously. The reaction mixture was allowed to stir for 3-4 hours and then quenched by addition water, petroleum ether and ethyl acetate (9:1). The layers were separated, and the organic layer was dried over Na_2SO_4. The solvent was evaporated under reduced pressure to afford 89% isolated yield of **22** as a khaki solid. **^{1}H NMR** (500 MHz, CDCl$_3$): 7.33 – 7.25 (m, 4H), 1.51 (s, 9H), 1.29 (s, 9H). **^{13}C{1H} NMR** (125 MHz, CDCl$_3$): 152.9, 146.0, 135.6, 125.8, 118.5, 34.2, 31.4, 28.3. **HRMS (ESI-TOF)**: calcd for $C_{15}H_{23}NO_2$ [M+H]$^+$ 250.1802 found 250.1789
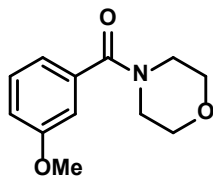
24

(3-methoxyphenyl)-4-morpholinylmethanone (24). Using a modified literature procedure,[3] to a solution of potassium carbonate (2 eq.) in anhydrous dichloromethane (12 mL) cooled to 0 °C, morpholine (2.5 eq.) was added, followed by drop wise addition of 3-methoxybenzoyl chloride (6 mmol). The reaction mixture was allowed to warm to room temperature and stirred overnight and then quenched by the addition of water and dichloromethane. The layers were separated, and the organic layer was dried over Na_2SO_4. The solvent was evaporated under reduced pressure to afford 88% isolated yield of **24** as a colorless oil. **^{1}H NMR** (500 MHz, CDCl$_3$): 7.35 – 7.30 (m, 1H), 6.99 – 6.93 (m, 3H), 3.88 – 3.36 (m, 11H). **^{13}C{1H} NMR** (125 MHz, CDCl$_3$): 170.2, 159.7, 136.4, 129.7, 118.9, 115.6, 112.5, 66.9, 55.4. **HRMS (ESI-TOF)**: calcd for $C_{12}H_{15}NO_3$ [M+H]$^+$ 222.1125 found 222.1117

**Spectral Data of Products**

1a
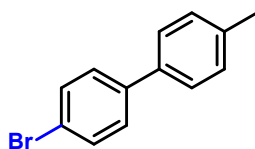
4-Bromo-4'-methylbiphenyl (1a). General procedure **A** was modified using 4-methylbiphenyl **1m** (33.6 mg, 0.2 mmol). The reaction afforded 84% isolated yield as a white solid separated by silica gel (in pentanes). The data matches those previously reported.[4] **1H NMR** (500 MHz, CDCl3) δ 7.53 (d, J = 8.4 Hz, 2H), 7.46-7.40 (m, 4H), 7.24 (d, J = S18 8.0 Hz, 2H), 2.39 (s, 3H). **^{13}C{1H} NMR (125 MHz, CDCl3)** δ 140.2, 137.6, 137.2, 131.9, 129.8, 128.6, 126.9, 121.3, 21.2.
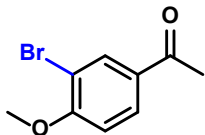
2a

**3-Bromo-4-methoxyacetophenone (2a).** General procedure **A** was employed using 4-methoxyacetophenone **1n** (30 mg, 0.2 mmol). The reaction afforded 85% isolated yield as a white solid separated by silica gel (35% EtOAc in hexanes). The data matches those previously reported.[5] **^{1}H NMR (500 MHz, cdcl$_3$)** δ 8.16, 8.15, 7.91, 7.91, 7.90, 7.89, 6.93, 6.92, 3.96, 2.54. **^{13}C{1H} NMR (125 MHz, CDCl3)** δ 195.6, 159.6, 133.8, 131.2, 129.5, 111.9, 111.1, 56.5, 26.3.
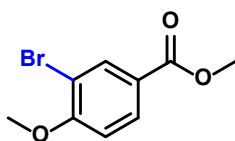

3a

Methyl 3-bromo-4-methoxybenzoate (3a). General procedure **A** was employed using methyl 4-methoxybenzoate **4** (33 mg, 0.2 mmol). The reaction afforded 86% isolated yield of **4a** as a white solid separated by silica gel (15% EtOAc in hexanes). The data matches those previously reported.[5] **^{1}H NMR** (500 MHz, CDCl$_3$): 8.24 (d, J = 2.1 Hz, 1H), 7.99 (dd, J = 8.6, 2.8 Hz, 1H), 6.93 (d, J = 8.6 Hz, 1H), 3.96 (s, 4H), 3.90 (s, 3H). **^{13}C{1H} NMR** (125 MHz, CDCl$_3$): 165.7, 159.5, 134.8, 130.5, 123.8, 111.4, 111.0, 56.5, 56.5, 52.1, 52.1.
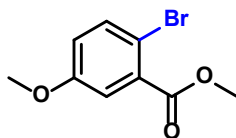

4a

Methyl 2-bromo-5-methoxybenzoate (4a). General procedure **A** was employed using methyl 3-methoxybenzoate **5** (29 μL, 0.2 mmol). The reaction afforded 93% isolated yield of **5a** as a yellow oil separated by silica gel (15% EtOAc in hexanes). The data matches those previously reported.[6] **^{1}H NMR (500 MHz, CDCl$_3$)**: 7.53 (d, J = 8.8 Hz, 1H), 7.32 (d, J = 3.1 Hz, 1H), 6.90 (dd, J = 8.8, 3.1 Hz, 1H), 3.94 (s, 3H), 3.82 (s, 3H). **^{13}C{1H} NMR (126 MHz, CDCl$_3$)**: 166.5, 158.6, 135.0, 132.6, 119.0, 116.2, 111.9, 55.6, 52.5.
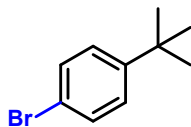
5a

1-Bromo-4-*t*-butylbenzene (5a). General procedure **A** was employed using *t*-butylbenzene **6** (26.8 mg, 0.2 mmol). The reaction afforded 90% isolated yield of **6a** colorless oil separated by silica gel (pentanes). The data matches those previously reported.[7] **^{1}H NMR (500 MHz, cdcl$_3$)** δ 7.39 (d, J = 8.6 Hz, 1H), 7.25 (d, J = 8.6 Hz, 1H), 1.29 (s, 4H). **^{13}C{1H} NMR (126 MHz, CDCl$_3$)** δ 150.3, 131.1, 127.1, 119.3, 34.7, 31.3.
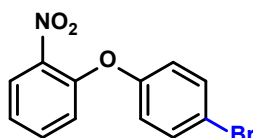

6a

1-(4-Bromophenoxy)-2-nitrobenzene (6a). The general produce was used to procedure **7**.[8] General procedure **A** was employed using 1-Nitro-2-phenoxybenzene **7** (43 mng, 0.2 mmol). The reaction afforded 89% isolated yield of **7a** as yellow oils separated by silica gel (2% to 20% EtOAc in hexanes). **^{1}H NMR (500 MHz, cdcl$_3$)** δ 8.00 (dd, J = 8.2, 1.4 Hz, 1H), 7.60 – 7.54 (m, 1H), 7.51 (d, J = 8.9 Hz, 2H), 7.28 (d, J = 8.3 Hz, 1H), 7.07 (d, J = 8.3 Hz, 1H), 6.96 (d, J = 8.9 Hz, 2H). **^{13}C{1H} NMR (126 MHz, cdcl$_3$)** δ 155.3, 150.1, 141.7, 134.4, 133.2, 126.0, 123.9, 121.0, 120.7, 117.3. **HRMS (ESI-TOF)**: calcd for C$_{12}$H$_8$BrNO$_3$ [M+H]$^+$ 293.9760 found 293.9751
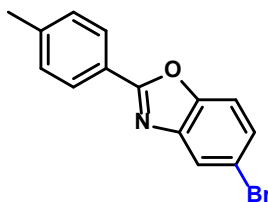

7a

5-Bromo-2-(4-methylphenyl)benzoxazole (7a). General procedure **A** was employed using 2-(4-Methylphenyl)benzoxazole **8** (41.8 mg, 0.2 mmol). The reaction afforded 81% isolated yield of **8a** as pale white solid separated by silica gel (dichloromethane). **^{1}H NMR (500 MHz, cdcl$_3$)** δ 8.08 (d, J = 8.0 Hz, 1H), 7.69 (s, 1H), 7.58 (d, J = 8.4 Hz, 1H), 7.44 (d, J = 8.4 Hz, 1H), 7.30 (d, J = 8.0 Hz, 1H), 2.42 (s, 2H). **^{13}C{1H} NMR (126 MHz, cdcl$_3$)**

δ 163.9, 151.2, 142.5, 141.5, 129.8, 127.9, 127.7, 123.9, 120.8, 117.7, 114.1, 21.8. **HRMS (ESI-TOF)**: calcd for $C_{14}H_{10}BrNO$ $[M+H]^+$ 288.0019 found 288.0011.


8a
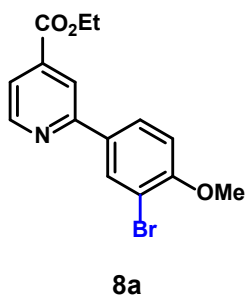
2-(3-Bromo-4-methoxyphenyl)-, ethyl ester-4-Pyridinecarboxylic acid (8a). The general produce was used to procedure **9.**[9] General procedure was employed using 2-(4-methoxyphenyl)-, ethyl ester-4-Pyridinecarboxylic acid **9** (51.5 mg, 0.2 mmol). The reaction afforded 82% isolated yield of **9a** as pale-yellow oils separated by silica gel (20 to 25% EtOAc in hexanes). **^{1}H NMR (500 MHz, cdcl₃)** δ 8.77 (d, J = 5.0 Hz, 1H), 8.29 (d, J = 2.2 Hz, 1H), 8.19 (s, 1H), 7.98 (dd, J = 8.6, 2.2 Hz, 1H), 7.73 (dd, J = 5.0, 1.4 Hz, 1H), 6.99 (d, J = 8.6 Hz, 1H), 4.44 (q, J = 7.1 Hz, 2H), 3.95 (s, 3H), 1.43 (t, J = 7.1 Hz, 3H). **^{13}C{1H} NMR (126 MHz, cdcl₃)** δ 165.3, 157.0, 156.7, 150.4, 138.7, 132.5, 132.0, 127.3, 121.0, 119.1, 112.4, 111.9, 62.0, 56.5, 14.4. **HRMS (ESI-TOF)**: calcd for $C_{15}H_{15}BrNO_3$ $[M+H]^+$ 336.0231 found 336.0223.


9a
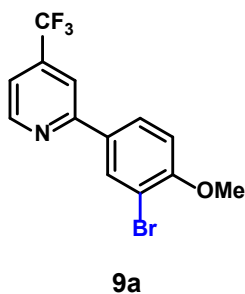
2-(3-Bromo-4-methoxyphenyl)-4-(trifluoromethyl)- pyridine (9a). The general produce was used to procedure **10.**[9] General procedure **A** was employed using 2-(4-methoxyphenyl)-4-(trifluoromethyl)- pyridine **10** (50.6 mg, 0.2 mmol). The reaction afforded 87% isolated yield of **10a** as a yellow oil separated by silica gel (10% EtOAc in hexanes). **^{1}H NMR (500 MHz, cdcl₃)** δ 8.81 (d, J = 5.0 Hz, 1H), 8.27 (d, J = 2.2 Hz, 1H), 7.96 (dd, J = 8.6, 2.2 Hz, 1H), 7.83 (s, 1H), 7.40 (d, J = 5.0 Hz, 1H), 6.99 (d, J = 8.6 Hz, 1H), 3.96 (s, 3H). **^{13}C{1H} NMR (126 MHz, cdcl₃)** δ 157.2, 156.9, 150.6, 139.6, 139.3, 139.0, 138.7, 131.9, 131.8, 127.2, 126.1, 123.9, 121.8, 119.6, 117.3, 117.3, 117.3, 117.2, 115.2, 115.2, 115.2, 112.4,

111.9, 56.4. **19F NMR (470 MHz, cdcl₃)** δ -64.85. **HRMS (ESI-TOF)**: calcd for C₁₃H₉BrF₃NO [M+H]⁺ 331.9892 found 331.9883.
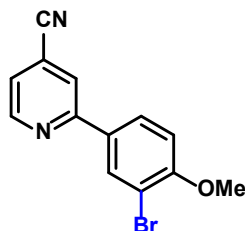

10a

2-(4-methoxyphenyl)-4-pyridinecarbonitrile (10a). The general produce was used to procedure **11.**[9] General procedure **A** was employed using 2-(4-methoxyphenyl)-4-pyridinecarbonitrile **11** (42mg, 0.2 mmol). The reaction afforded 89% isolated yield of **11a** as orange solid separated by silica gel (dichloromethane). **1H NMR (500 MHz, cdcl₃)** δ 8.80 (d, *J* = 4.9 Hz, 1H), 8.24 (d, *J* = 2.2 Hz, 1H), 7.91 (dd, *J* = 8.6, 2.2 Hz, 1H), 7.84 (s, 1H), 7.39 (dd, *J* = 4.9, 1.3 Hz, 1H), 6.99 (d, *J* = 8.6 Hz, 1H), 3.96 (s, 3H). **13C{1H} NMR (126 MHz, cdcl₃)** δ 157.6, 156.9, 150.7, 132.1, 131.1, 127.3, 122.9, 121.4, 121.3, 116.8, 112.6, 112.0, 56.6. **HRMS (ESI-TOF)**: calcd for C₁₃H₉BrN₂O [M+H]⁺ 288.9971 found 288.9963.
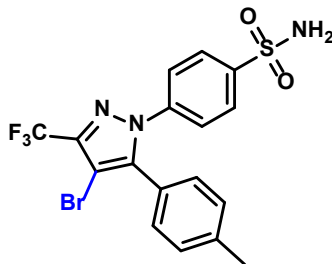

11a

4-[4-bromo-5-(4-methylphenyl)-3-(trifluoromethyl)-1*H*-pyrazol-1-yl]-benzenesulfonamide (11a). General procedure **A** was employed using Celebrex **12** (76 mg, 0.2 mmol). The reaction afforded 96% isolated yield of **12a** as a pale yellow-green solid separated by silica gel (2% methanol in dichloromethane).[10] **1H NMR (500 MHz, cdcl₃)** δ 7.82 (d, *J* = 8.7 Hz, 1H), 7.36 (d, *J* = 8.7 Hz, 1H), 7.22 (d, *J* = 8.0 Hz, 1H), 7.15 (d, *J* = 8.1 Hz, 1H), 5.45 (s, 1H), 2.38 (s, 1H). **13C{1H} NMR (126 MHz, cdcl₃)** δ 143.8, 142.6, 142.3, 142.2, 142.0, 141.7, 141.7, 140.6, 129.95, 129.9, 127.5, 125.2, 123.9, 123.8, 121.6, 119.5, 94.5, 21.5.
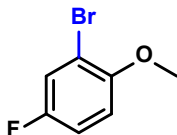
12a

2-Bromo-4-fluoroanisole (12a). General procedure **A** was employed using 4-fluoroanisole **13a** (25mg, 0.2 mmol). The reaction afforded 96% isolated yield of **13a** as yellow oil separated by acid-base extraction (1M HCl in H_2O). The data matches those previously reported.[11] **^{1}H NMR (500 MHz, cdcl3)** δ 7.26 (dd, J = 7.9, 3.0 Hz, 1H), 7.03 – 6.98 (m, 1H), 6.90 (dd, J = 9.1, 4.8 Hz, 1H), 6.72 (s, 1H). **^{13}C{1H} NMR (101 MHz, cdcl3)** δ 157.9, 155.5, 152.7, 120.7, 120.5, 114.9, 114.7, 112.4, 112.3, 111.8, 111.7, 56.9.
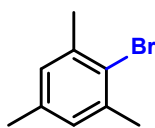

13a

1-Bromomesitylene (13a). General procedure **A** was employed using mesitylene **14** (28 μL, 0.2 mmol). The reaction afforded % isolated yield of **14a** as colorless oil separated by silica gel (*n*-pentane). The data matches those previously reported.[12] **^{1}H NMR** (500 MHz, CDCl3): 6.9 (s, 2H), 2.38 (s, 6H), 2.24 (s, 3H). **^{13}C{1H} NMR** (125 MHz, CDCl3): 138.0, 136.4, 129.2, 124.3, 23.9, 20.8.
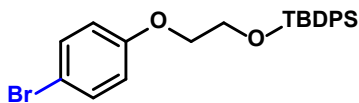

14a

1-Bromo-4-[2-[[(*tert*-butyl)diphenylsilyl]oxy]ethoxy]-benzene (14a). General procedure **A** was employed using 2-[[(1,1-dimethylethyl)diphenylsilyl]oxy]ethoxy]-benzene **15** (75 mg, 0.2 mmol). The reaction afforded 92% isolated yield of **15a** as colorless oil separated by silica gel (only in hexanes). **^{1}H NMR** (400 MHz, CDCl3): 7.74 – 7.69 (m, 4H), 7.48 – 7.33 (m, 8H), 6.79 – 6.72 (m, 2H), 4.06 – 4.04 (m, 2H), 4.01 – 3.98 (m, 2H), 1.08 (s, 9H). **^{13}C{1H} NMR** (100 MHz, CDCl3): 158.1, 135.6, 133.4, 132.2, 129.7, 127.7, 116.4, 112.8, 69.3, 62.6, 26.9, 19.3. **HRMS (ESI-TOF)**: calcd for $C_{24}H_{27}BrO_2Si$ [M+H]$^+$ 455.1036 found 455.1007.
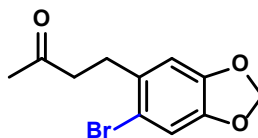
15a

4-(6-Bromo-1,3-benzodioxol-5-yl)-2-butanone (15a). General procedure **A** was employed using 4-(1,3-benzodioxol-5-yl)-2-butanone **16** (38 mg, 0.2 mmol). The reaction afforded 87% isolated yield of **16a** as a yellow oil separated by silica gel (30% EtOAc in hexanes). **^{1}H NMR** (500 MHz, CDCl$_3$): 6.98 (s, 1H), 6.74 (s, 1H), 5.94 (s, 2H), 2.91 (t, J = 7.6 Hz, 2H), 2.72 (t, J = 7.6 Hz, 2H), 2.16 (s, 3H). **^{13}C{1H} NMR** (125 MHz, CDCl$_3$): 207.6, 147.4, 146.9, 133.2, 114.2, 112.7, 110.2, 101.6 , 43.6, 30.2, 30.0. **HRMS (ESI-TOF)**: calcd for C$_{11}$H$_{11}$BrO$_3$ [M+H]$^+$ 270.9964 found 270.9956.
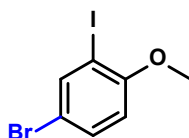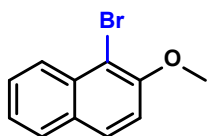

16a

4-Bromo-2-iodoanisole (16a). General procedure **A** was employed using 2-iodoanisole **17** (26 μL, 0.2 mmol). The reaction afforded 87% isolated yield of **17a** separated by silica gel (20% EtOAc in hexanes). The data matches those previously reported.[13] **^{1}H NMR** (500 MHz, CDCl$_3$): 7.89 (d, J = 2.4 Hz, 1H), 7.42 (dd, J = 8.7, 2.4 Hz, 1H), 6.70 (d, J = 8.7 Hz, 1H), 3.87 (s, 3H). **^{13}C{1H} NMR** (125 MHz, CDCl$_3$): 157.4, 140.9, 132.1, 113.5, 112.1, 86.7, 56.6.
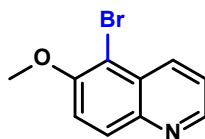

17a

5-Bromo-6-methoxyquinoline (17a). General procedure **A** was employed using 6-methoxyquinoline **18** (28 μL, 0.2 mmol). The reaction afforded 85% isolated yield of **18a** as an off-white solid separated by silica gel (35% EtOAc in hexanes). The data matches those previously reported.[14] **^{1}H NMR** (500 MHz, CDCl$_3$): 8.82 (d, J = 3.2 Hz, 1H), 8.58 (d, J = 8.6 Hz, 1H), 8.17 (d, J = 9.2 Hz, 1H), 7.54 (d, J = 9.3 Hz, 1H), 7.51 (dd, J = 8.6, 4.1 Hz, 1H), 4.08 (s, 3H). **^{13}C{1H} NMR** (125 MHz, CDCl$_3$): 154.2, 148.3, 143.8, 135.2, 129.9, 128.7, 122.4, 116.8, 107.4, 57.1.

18a

1-Bromo-2-methoxynaphthalene (18a). General procedure **A** was employed using 2-methoxynaphthalene **19** (31 mg, 0.2 mmol). The reaction afforded 83% isolated yield of **19a** separated by silica gel (5% EtOAc in hexanes). The data matches those previously reported.[15] **¹H NMR** (500 MHz, CDCl₃): 8.24 (d, J = 8.6 Hz, 1H), 7.83 (d, J = 9.0 Hz, 1H), 7.80 (d, J = 8.2 Hz, 1H), 7.58 (t, J = 8.2 Hz, 1H), 7.41 (t, J = 7.5 Hz, 1H), 7.29 (d, J = 9.0 Hz, 1H), 4.05 (s, 3H). **¹³C{1H} NMR** (125 MHz, CDCl₃): 153.8, 133.0, 129.8, 128.9, 128.0, 127.7, 126.1, 124.3, 113.8, 108.7, 57.1.
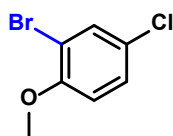

19a

2-Bromo-4-chloroanisole (19a). General procedure **A** was modified using 4-chloroanisole **20** (24 µL, 0.2 mmol). The reaction afforded 72% isolated yield of **20a** as orange-brown oil separated by silica gel (5% EtOAc in hexanes). **¹H NMR** (500 MHz, CDCl₃): 7.54 (s, 1H), 7.25 (d, J = 8.7 Hz, 1H), 6.83 (d, J = 8.7 Hz, 1H), 3.89 (s, 3H). **¹³C{1H} NMR** (125 MHz, CDCl₃): 154.8, 132.8, 128.3, 125.9, 112.5, 112.1, 56.4. **HRMS (ESI-TOF)**: calcd for C_7H_6BrClO [M+H]⁺ 220.9363 found 220.9356
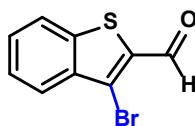

20a

3-Bromobenzo[*b*]thiophene-2-carboxaldehyde (21a). General procedure **A** was employed using benzo[b]thiophene-2-carboxaldehyde **21** (32.4 mg, 0.2 mmol). The reaction afforded 85% isolated yield of **21a** as a yellow solid separated by silica gel (20% EtOAc in hexanes). The data matches those previously reported.[16] **¹H NMR** (500 MHz, CDCl₃): 10.29 (s, 1H), 8.03 (d, J = 7.8 Hz, 1H), 7.88 (d, J = 8.0 Hz, 1H), 7.61 – 7.49 (m, 2H). **¹³C{1H} NMR** (125 MHz, CDCl₃): 184.9, 140.5, 138.2, 136.4, 129.4, 125.9, 125.1, 123.4, 118.8.
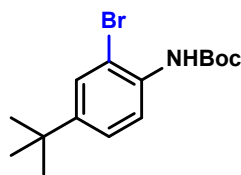
21a

1,1-Dimethylethyl-N-[2-bromo-4-(1,1-dimethylethyl) phenyl] carbamate (21a). General procedure **A** was employed using 1,1-Dimethylethyl-N-[4-(1,1-dimethylethyl) phenyl] carbamate **22** (45 mg, 0.2 mmol). The reaction afforded 82% isolated yield of **22a** as an orange oil separated by silica gel (10% EtOAc in hexanes). **^{1}H NMR** (500 MHz, CDCl$_3$): 8.02 (d, J = 8.6 Hz, 1H), 7.50 (d, J = 2.1 Hz, 1H), 7.31 (dd, J = 8.7, 2.1 Hz, 1H), 6.91 (s, 1H), 1.54 (s, 9H), 1.30 (s, 9H). **^{13}C{1H} NMR** (125 MHz, CDCl$_3$): 152.6, 147.3, 133.6, 129.1, 125.3, 119.9, 112.5, 80.9, 34.3, 31.2, 28.3. **HRMS (ESI-TOF)**: calcd for C$_{15}$H$_{22}$BrNO$_2$ [M+H]$^+$ 328.0907 found 328.0897.
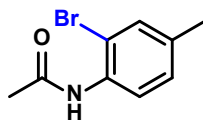
22a

N-(2-Bromo-4-methylphenyl) acetamide (22a). General procedure **A** was employed using 4-methylacetanilide **23** (25 μL, 0.2 mmol). The reaction afforded 85% isolated yield of **23a** as a pale yellow solid separated by silica gel (15% EtOAc in hexanes). The data matches those previously reported.[17] **^{1}H NMR (500 MHz, cdcl$_3$)** δ 8.14 (d, J = 8.3 Hz, 1H), 7.53 (s, 1H), 7.34 (s, 1H), 7.09 (d, J = 8.2 Hz, 1H), 2.28 (s, 3H), 2.21 (s, 3H). **^{13}C{1H} NMR (126 MHz, cdcl$_3$)** δ 168.3, 135.4, 133.2, 132.5, 129.1, 122.1, 113.4, 24.9, 20.6.
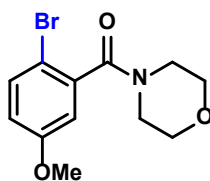
23a

(2-Bromo-5-methoxyphenyl)-4-morpholinylmethanone (23a). General procedure **A** was employed using (3-methoxyphenyl)-4-morpholinylmethanone **24** (42.4 mg, 0.2 mmol)). The reaction afforded 85% isolated yield of **24a** as a yellow oil separated by silica gel (30% Acetone in hexanes). **^{1}H NMR** (500 MHz, CDCl$_3$): 7.48 – 7.42 (m, 1H), 6.81 (m, 2H), 3.91 – 3.70 (m, 8H), 3.59 (m, 1H), 3.31 (m, 1H), 3.21 (m, 1H). **^{13}C{1H} NMR** (125 MHz, CDCl$_3$): 167.51, 159.18, 138.17, 133.73, 116.64, 113.10, 109.27, 66.74, 66.62, 55.68, 47.12, 41.98. **HRMS (ESI-TOF)**: calcd for C$_{12}$H$_{14}$BrNO$_3$ [M+H]$^+$ 300.0230 found 300.0234

Appendix – B References

[1] Yalla, R.; Rghavan, S. *Org. Biomol. Chem*. **2019**, *17*, 4572–4592.

[2] Ingale, A.; More, V. K.; Gangarde, U. S.; Shinde, S. V. *New J. Chem*. **2018**, *42*, 10142–10147.

[3] Cederbalk, A.; Lysen, M.; Kehler, J.; Kristensen, J. L. *Tetrahedron*, **2017**, *73*,1576–1582.

[4] Diehl, C. J.; Scattolin, T.; Englert, U.; Schoenebeck, F. *Angew. Chem. Int. Ed*. **2019**, *58*, 211 –215.

[5] Hirose, Y.; Yamazaki, M.; Nogata, M.; Nakamura, A.; Maegawa, T. *J. Org. Chem*. **2019**, *84*, 7405–7410.

[6] Pramanick, P. K.; Hou, Z.-L.; Yao, B. *Tetrahedron*, **2017**, *73*, 7105−7114.

[7] Tang, R.-J.; Milcent, T.; Crousse, B. *J. Org. Chem*. **2018**, *83*, 930−938.

[8] Wen, F.; Jin, H.; Tao, K.; Hou, T. *European Journal of Medicinal Chemistry.* **2016**, 120, 244-251.

[9] Galloway, J.; Mai, D.; Baxter, R. *Org. Lett*. **2017**, *19*, 5772–5775.

[10] Muzelevskiy, V.; Nenajdenko, V. *Org. Biomol. Chem.,* **2018**, 16, 7935-7946.

[11] Iwanaga, K.; Kobayashi, J.; Kawashima, T. *Tetrahedron*, **2007**, *63*, 10127–10132.

[12] Fricke, C.; Deckers, K.; Schoenebeck, F. *Angew. Chem. Int. Ed*. **2020**, *59*, 18717–18722.

[13] Perry, G. J. P.; Quibell, J. M.; Panigrahi, A.; Larrosa, I. *J. Am. Chem. Soc*. **2017**, *139*, 11527−11536.

[14] Cakmak, O.; Okten, S. *Tetrahedron*, **2017**,*73*, 5389–5396.

[15] Shi, Y.; Ke, Z.; Yeung, Y.-Y. *Green Chem*., **2018**, *20*, 4448−4452.

[16] Shigeno, M.; Fujii, Y.; Kajima, A.; NozawaKumada, K.; Kondo, Y. *Org. Process Res. Dev*. **2019**, *23*, 443–451.

[17] Shi, C.; Miao, Q.; Ma, L.; Lu, T.; Yang, D.; Chen, J.; Li, Z. *ChemistrySelect,* **2019**, *4*, 6043-6045.

ChenShi, Q. Miao, L. F. Ma, T. Lu, D. Yang, J. M.

APPENDIX – C

Experimental Set Up: Halohydrin Formation of Alkenes Using Various Brominating Reagents

General NBS Procedure (a)

      The threads of a 4 mL borosilicate scintillation vial were thoroughly taped with Teflon tape. To this vial containing a stir bar was added *N*-bromosuccinimide (35 mg, 0.20 mmol, 1.0 equiv), mandelic acid (6 mg, 0.04 mmol, 20 mol %) and an aromatic compound (0.2 mmol, 1.0 equiv). Acetonitrile (1 mL) and H_2O (1 mL) were then added. The reaction was capped with a Teflon screen cap and rubber septum (24/40). The reaction was then stirred at room temperature until completed as judged by thin-layer chromatography.

      Upon completion, the reaction was diluted with ethyl acetate (1 mL) and transferred to a test tube containing saturated $NaHCO_3$ (3 mL). The aqueous phase was extracted with ethyl acetate (3 x 3 mL) and the combined organic layers were dried over $MgSO_4$, filtered, and carefully concentrated *in vacuo.* The crude material was purified by silica gel chromatography to yield the desired product.

General N-bromosultam Procedure (b)

      The threads of a 4 mL borosilicate scintillation vial were thoroughly taped with Teflon tape. To this vial containing a stir bar was added *N*-bromosultam (55 mg, 0.20 mmol, 1.0 equiv), mandelic acid (6 mg, 0.04 mmol, 20 mol %) and an aromatic compound (0.2 mmol, 1.0 equiv). Acetonitrile (1 mL) and H_2O (1 mL) were then added. The reaction was capped with a Teflon screen cap and rubber septum (24/40). The reaction was then stirred at 35 °C until completed as judged by thin-layer chromatography.

      Upon completion, the reaction was diluted with ethyl acetate (1 mL) and transferred to a test tube containing saturated $NaHCO_3$ (3 mL). The aqueous phase was extracted with ethyl acetate (3 x 3 mL) and the combined organic layers were dried over $MgSO_4$, filtered, and carefully concentrated *in vacuo.* The crude material was purified by silica gel chromatography to yield the desired product.

General N-bromosaccharin Procedure (c)

      The threads of a 4 mL borosilicate scintillation vial were thoroughly taped with Teflon tape. To this vial containing a stir bar was added *N*-bromosaccharin (52 mg, 0.20 mmol, 1.0 equiv), mandelic acid (6 mg, 0.04 mmol, 20 mol %) and an aromatic compound (0.2 mmol, 1.0 equiv). Acetonitrile (1 mL) and H_2O (1 mL) were then added. The reaction was capped with a Teflon screen cap and rubber septum (24/40). The reaction was then stirred at 35 °C until completed as judged by thin-layer chromatography.

      Upon completion, the reaction was diluted with ethyl acetate (1 mL) and transferred to a test tube containing saturated $NaHCO_3$ (3 mL). The aqueous phase was extracted with ethyl acetate (3 x 3 mL) and the combined organic layers were dried over $MgSO_4$, filtered, and carefully concentrated *in vacuo.* The crude material was purified by silica gel chromatography to yield the desired product.

# Experimental Procedures and Characterization Data
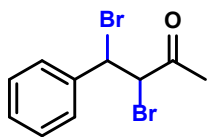
1a

3,4-dibromo-4-phenylbutan-2-one (1a). General procedure **a and b** was modified using (E)-4-phenylbut-3-en-2-one **1** (29.0 mg, 0.2 mmol). The reaction afforded 93% isolated yield as a white solid separated by silica gel (15% EtOAc in hexanes). The data matches those previously reported.[1] **1H NMR** (500 MHz, cdcl$_3$) δ 7.47 – 7.31 (m, 2H), 5.07 (d, J = 8.5 Hz, 1H), 4.40 (d, J = 8.5 Hz, 1H), 2.41 (s, 1H).
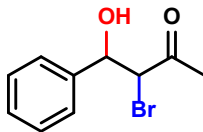

3-bromo-4-hydroxy-4-phenylbutan-2-one (2a). General procedure **c** was modified using (E)-4-phenylbut-3-en-2-one **1** (29.0 mg, 0.2 mmol). The reaction afforded 93% isolated yield as a white solid separated by silica gel (15% EtOAc in hexanes). The data matches those previously reported.[1] **1H NMR** (500 MHz, cdcl$_3$) δ 7.43 – 7.31 (m, 1H), 5.06 (d, J = 8.6 Hz, 1H), 4.39 (t, J = 7.0 Hz, 1H), 2.41 (s, J = 4.1 Hz, 1H).
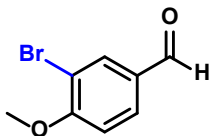
3a

3-Bromo-4-methoxy-benzaldehyde (3a). General procedure **a and b** was employed using 4-methoxy-benzaldehyde **3** (24 μL, 0.2 mmol). The reaction afforded 40% isolated yield of **3a** separated by silica gel (20% EtOAc in hexanes). The data matches those previously reported.[3] **1H NMR** (500 MHz, CDCl$_3$): 9.86 (s, 1H), 8.10 (d, J = 2.0 Hz, 1H), 7.84 (dd, J = 8.5, 2.0 Hz, 1H), 7.03 (d, J = 8.5 Hz, 1H), 4.01 (s, 3H). **13C{1H} NMR** (125 MHz, CDCl$_3$): 189.6, 160.6, 134.7, 131.1, 130.8, 112.8, 111.6, 56.6.

4a
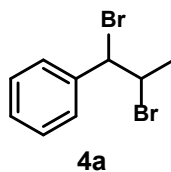
(1,2-dibromopropyl)benzene (4a) General procedure **c** was employed using (E)-prop-1-en-1-ylbenzene **4** (26 µL, 0.2 mmol). The reaction afforded 27% isolated yield of **3a** separated by silica gel (20% EtOAc in hexanes). The data matches those previously reported.[4] **¹H NMR** (400 MHz, CDCl$_3$) 7.37-7.26 (m, 5H), 5.00 (d, J = 10.4 Hz, 1H), 4.45–4.40 (m, 1H, C*H*), 1.55 (d, J = 6.4 Hz, 3H).

Appendix–C References

(1) Kim, K. M., Park. I. H. *Synthesis*. **2004**, 16, 2641-2644.
(2) Wang, Y., Wang, J., Xiong, Y., Liu, Z. Q. *Tetrahedron Lett.* **2014**, 55, 2734-2737.
(3) Pramanick, P. K.; Hou, Z.-L.; Yao, B. *Tetrahedron*, **2017**, *73*, 7105−7114.
(4) Mendoza, F., Ruiz-Guerrero, R., Hernandez-Fuentes, C., Molina, P., Norzagaray-Campos, M., Reguera, E. *Tetrahedron Lett.* **2016**, 57, 50, 5644-5648.